CANADIAN THESES

THÈSES CANADIENNES

NOTICE

The quality of this microfiche is heavily dependent upon the quality of the original thesis submitted for microfilming. Every effort has been made to ensure the highest quality of reproduction possible.

If pages are missing, contact the university which granted the degree.

Some pages may have indistinct print especially if the original pages were typed with a poor typewriter ribbon or if the university sent us an inferior photocopy.

Previously copyrighted materials (journal articles, published tests, etc.) are not filmed.

AVIS

La qualité de cette microfiche dépend grandement de la qualité de la thèse soumise au microfilmage. Nous avons tout fait pour assurer une qualité supérieure de reproduction

S'il manque des pages, veuillez communiquer avec l'université qui a conféré le grade.

La qualité d'impression de certaines pages peut laisser à désirer, surtout si les pages originales ont été dactylographiées à l'aide d'un ruban usé ou si l'université nous a fait parvenir une photocopie de qualité inférieure.

Les documents qui font déjà l'objet d'un droit d'auteur (articles de revue, examens publiés, etc.) ne sont pas microfilmés.

THIS DISSERTATION HAS BEEN MICROFILMED EXACTLY AS RECEIVED

LA THÈSE A ÉTÉ MICROFILMÉE TELLE QUE NOUS L'AVONS REÇUE

FLOW DISTRIBUTION IN ADJACENT SUBCHANNELS
OF UNEQUAL SIZE

by

James Donald Bugg

Submitted to the Faculty of Science and Engineering
of the University of Ottawa
in partial fulfillment of the requirements for the degree of
MASTER OF APPLIED SCIENCE
in
Mechanical Engineering

ISBN 0-315-30990-3

ABSTRACT

This thesis describes an experimental and analytic investigation of the single phase flow distribution in subchannel geometries. It was intended as an investigation of fundamental transport mechanisms and therefore concentrated on simple geometries with two interconnected subchannels. The experimental phase consisted of detailed measurements of the fluid velocity in a geometry representing two communicating subchannels of different sizes. These measurements were made at three axial locations along the test section. The size of one of the subchannels was varied to give subchannel area ratios of 1.0, 0.68, 0.50 and 0.32. Two Reynolds numbers (108 000 and 180 000) were investigated. Axial pressure gradient data for all of these cases was also taken. The analytic phase concentrated on applying a three dimensional finite difference fluid flow code to subchannel geometries. The code was applied to the cases studied in the experiment as well as other investigator's results. It used the two equation k-ε turbulence model. The performance of this model was assessed. Unique features of the subchannel flows were identified and discussed. Conclusions regarding the transport mechanisms involved and the ability of a multidimensional code to predict the flow fields reliably were presented.

ACKNOWLEDGEMENTS

The author would like to thank his research director at the University of Ottawa, Dr. Y. Lee, for his supervision and guidance throughout the course of this work. The advice and suggestions of Mr. M.B. Carver and Mr. A. Tahir are gratefully acknowledged. I am indebted to Mr. J.H. Woodall for the many hours spent fabricating the test section. Mr. J.R. Nickerson's help and encouragement with the experiment is also appreciated. Mr A. Banas and Mr. J.C. Kiteley patiently reviewed the manuscript and their efforts are very much appreciated. This work was funded by the Chalk River Nuclear Laboratories/ University of Ottawa M.A.Sc. Fellowship program.

TABLE OF CONTENTS

LIST OF FIGURES

LIST OF TABLES

NOMENCLATURE

Symbol	Description	Units
A	Control Volume Face Area	m^2
a	Neighbor Coefficient	-
C	Convective Flux	$kg/m^2/s$
C_1	Empirical Constant in k-ε Model	-
C_2	Empirical Constant in k-ε Model	-
C_μ	Empirical Constant in k-ε Model	-
D	Diffusion Flux	$kg/m^2/s$
E	Surface Roughness Parameter	-
f_i	Body Force Vector	N/kg
k	Turbulent Kinetic Energy	J/kg
n	Index for Neighboring Control Volumes	-
$\hat{n}$	Unit Vector Normal to Control Volume	-
P	Instantaneous Pressure	Pa
$\bar{P}$	Mean Pressure	Pa
p	Fluctuating Pressure	Pa
Pe	Peclet Number	-
R	Reynolds Number	-
R_ϕ	Residual of Variable ϕ	-

S	Source Term	-
S_p	Linear Coefficient of Source Term	-
S_u	Constant Coefficient of Source Term	-
t	Time	sec
U_i	Instantaneous Velocity	m/s
$\bar{U}_i$	Mean Velocity	m/s
u_i	Fluctuating Velocity	m/s
U	x-component of mean velocity	m/s
V	y-component of mean velocity	m/s
W	z-component of mean velocity	m/s
W2/W1	Subchannel Area Ratio	-
x_i	Cartesian Coordinate System	-
y^+	Normalized distance from the wall (See Eqn. IV.24)	-

Greek

α	Relaxation Factor	-
δy, δx	Distances to solid surfaces.	m
Γ	General Diffusion Coefficient	-
ε	Dissipation rate of turbulent kinetic energy	J/kg/s
κ	Von Karman's Constant	-
ϕ	General Field Variable	-
ρ	Density	kg/m^3
σ_k	Empirical Diffusion Constant for k	-
σ_ε	Empirical Diffusion Constant for ε	-
τ	Shear Stress	Pa
μ	Dynamic Viscosity	$N.s/m^2$
μ_t	Turbulent Viscosity	$N.s/m^2$
μ_{eff}	Effective Viscosity	$N.s/m^2$
ν	Kinematic Viscosity	m^2/s

Subscripts

ave	average value
D	value at down face of control volume
d	value at downward neighbor
E	value at east face of control volume
e	value at eastern neighbor
l	laminar
N	value at north face of control volume
n	value at northern neighbor
p	evaluated at point "p"
S	value at south face of control volume
s	value at southern neighbor
t	turbulent
U	value at up face of control volume
u	value at upward neighbor
W	value at west face of control volume
w	value at western neighbor

Superscripts

o	value during previous iteration
'	correction to velocity or pressure

I. INTRODUCTION

The accurate measurement and prediction of the fluid flow within various forms of engineering equipment has long been the goal of many researchers. Refinements in measurement and prediction techniques are slowly progressing from the prediction of one dimensional bulk average conditions to a more refined picture of the flow field's details. The increased detail is sought because many situations arise where the important features of an engineering fluid flow are manifested by the fine details of the flow field. The overall nature of the flow may not provide the information required to determine the actual safe operating limit of some equipment since the limiting conditions may occur in a localized region long before the bulk conditions indicate any danger. The cooling of a nuclear reactor fuel channel is a prime example of a flow phenomenon where such detail is of vital importance. If only a small portion of the fuel overheats due to the inability of the coolant to carry heat away from the fuel sheath, a serious accident may develop. Detailed analyses are required to identify regions where this might occur.

In addition to safety considerations, a large economic incentive exists to thoroughly understand the flow field. A detailed knowledge of the flow field is invaluable in accurately predicting the thermal performance of heat exchange equipment or the performance and power requirements of process equipment in general. The ability to make accurate predictions can greatly aid in optimization during the design phase. Potential sites susceptible to fouling and corrosion due to unacceptably low fluid velocities could be readily identified. Also, high velocity regions likely to cause excessive vibration or erosion could be located.

Recognizing the importance of the detailed flow field, and the ability to predict it in advance, a lot of work has been done in recent years on the development of multidimensional computer codes. Several very desirable advantages exist in developing efficient, reliable codes. This has only become possible with the rapid advances in computer speeds and storage capabilities. They can make predictions very quickly at a cost which is generally minimal compared to full scale experiments. Moreover, sensitivity analyses can be easily carried out since the effect of altering various geometrical features can be determined. Another advantage provided by this feature is that conditions beyond the nominal operating limits of the device can be safely investigated. This is a major benefit for the investigation of accident conditions in nuclear reactors.

Before such a thermalhydraulic code can be used with any confidence it must first endure the validation process. Code validation is the final test to establish the credibility of the mathematical model. This process consists of comparing code predictions with actual experimental results. Different sets of experimental results are required covering a wide range of conditions to give the code a greater range of validity. If the code predictions are within acceptable limits of the experiment, some confidence can be gained in using the code for predictions in other situations of interest. However, care must be taken that the code is not extended to phenomena far outside the range of validation. For example, in a nuclear reactor fuel channel, several distinct mechanisms have been identified which govern the distribution of flow within the rod bundle. If a thermalhydraulic code is successful in modelling one of these mechanisms there is no guarantee that it will be valid for a case were other mechanisms dominate the flow distribution. Such a case could be beyond the scope of the code. This highlights the need for a thorough code validation process and care in applying the model to new situations.

The current study is concerned with modelling the flow distribution in CANDU fuel channels. The geometry is depicted in Figure I.1 and consists of axial flow along a 37-element bundle. The first problem that becomes apparent when formulating a numerical scheme for this problem is the complexity of the geometry and the resulting difficulty of developing a suitable computational grid. There are basically two approachs to this problem. Each will now be described in turn and their complementary nature outlined.

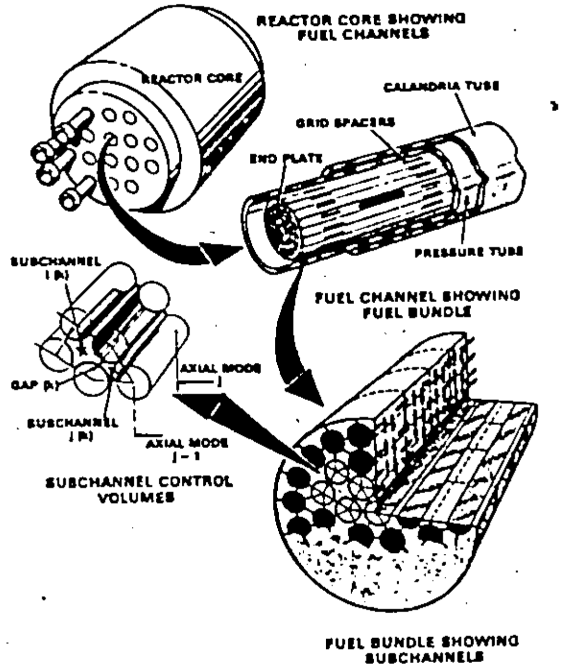

Figure I.1 CANDU Fuel Channel Geometry

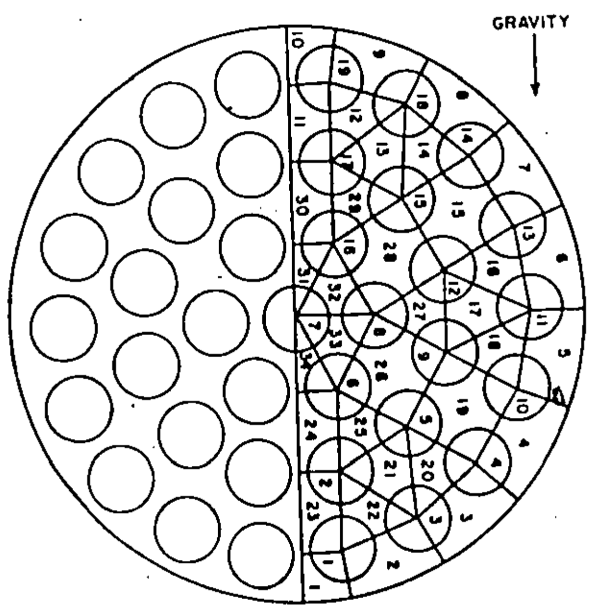

Figure I.2 Subchannel Discretization Scheme

The first subdivision scheme uses the pin boundaries and lines joining the pin centers to define the control volume boundaries. This is shown in Figure I.2. The whole fuel channel is divided axially into a convenient number of nodes to complete the grid definition. Codes that employ such a subdivision scheme are termed subchannel codes (eg. ASSERT, Carver et. al. [1984]). Since ~~this~~ results in a rather coarse geometrical subdivision of the flow field, they are relatively inexpensive to run. However, because of the highly simplified grid, a high degree of empiricism is required to predict the transfer of heat and momentum between adjacent subchannels. Also, the coarse grid makes it difficult to identify localized areas of unacceptably high or low fluid velocity or wall temperature.

In order to provide the finer detail required, a second scheme called fine subdivision can be employed. The scale of the control volumes is greatly reduced from that of a typical subchannel code. Since the number of control volumes quickly becomes very large, these codes can typically be used only to model small portions of the geometry. A useful compromise can be attained by applying subchannel codes to compute average properties within the subchannels and using fine subdivision codes to study localized phenomena and the detailed mechanisms of transfer between the channels. The process is complementary since the average conditions computed by a subchannel code can be used as boundary conditions for a fine subdivision study. In a complementary sense, fine subdivision codes can be used to study localized transfer phenomena and thereby upgrade the models used in the subchannel codes.

In a typical reactor fuel channel many different shapes and sizes of subchannels interact in a complex manner. To simplify the study of fundamental heat and momentum transfer mechanisms between the channels, and to reduce the number of computational nodes, the geometry is often simplified to isolate the particular phenomena of interest. In the limit, the problem can be reduced to two interconnected subchannels. In this way a particular segment of the geometry can be isolated and studied in detail. Also, the simplified geometry can be made to fit a convenient grid such as a rectangular Cartesian coordinate system.

Referring again to Figure I.2, one notices that there is a significant variation in subchannel sizes. This variation in size can greatly affect the flow distribution. The purpose of this study is to understand the way in which the flow distributes itself between two adjacent subchannels of unequal size. A representative geometry consisting of two adjacent rectangular subchannels will be studied from an experimental and analytic viewpoint with the aim of validating the analytic model with the experimental results. The size of one of the subchannels can be varied to study the effect of different size ratios.

The study begins in Section II with a literature survey. Relevant work detailing velocity measurements in various irregular shaped geometries are cited. Earlier work on transfer mechanisms between subchannels and the effect of relative subchannel size is outlined.

Section III will describe the experimental apparatus and instrumentation used. After this description, the results of the measurements are presented. These measurements consist of velocity and pressure profiles at various axial locations in the test section.

Section IV describes the three dimensional finite difference code used for the analysis. The governing equations modelled by the code are presented and their numerical approximation is detailed. The code employs the two equation k-ε model of turbulence. After describing the solution procedure involved, finite difference grids are presented for the geometry of interest. The code's predictions of the flow fields within this geometry are presented.

Then in Section V the experimental and analytic results are compared directly to evaluate the performance of the mathematical model.

Section VI describes the conclusions reached in the study. First, conclusions are made regarding the transport mechanisms and flow distribution in two adjacent unequal subchannels, and second, conclusions are made about the effectiveness of the mathematical model used in making accurate predictions for such flow configurations.

II. LITERATURE SURVEY

The investigation of flow distributions in subchannel geometries is progressing on several fronts. One method is to obtain experimental data and use it to develop correlations based on simplified analytic models of the phenomena. The intention is to develop relationships that are applicable over a wide range of geometries and conditions. Another approach is the more purely analytic one in which a minimum amount of empiricism is introduced. This involves numerically solving the equations of fluid motion for the geometry of interest. The hope is that by confining the empiricism to more fundamental phenomena, the range of applicability of the method can be greatly increased.

The first series of papers to be discussed were concerned with the flow distribution in ducts of general, non-circular cross section, usually square or rectangular. Although they are not specified as subchannel studies, their content is of direct interest to this work because the two unequal subchannel geometry is really an irregular shaped duct.

A fundamental study of flow in a two dimensional channel was done by Laufer [1951]. With air as the working fluid, he used hot wire anemometry to measure the average and fluctuating components of velocity. This work provides an important data base for validation of many analytic models because it reports measurements of turbulent quantities as well as the mean flow field. The main observation made was the dimensionless mean fluctuating quantities were found to decrease with increasing Reynolds number. Although the study was restricted to a two dimensional geometry, this observation was important and was corroborated by later investigators working with more complex geometries.

Concerned with the applicability of the Deissler-Taylor method of predicting fully developed velocity distribution and pressure drop in irregular geometries, Hartnett, Koh and McComas [1962] initiated a study of friction factors through rectangular ducts. By studying rectangular ducts of various aspect ratios, they found good agreement [illegible] aspect ratios greater than 5:1, but discovered that the method underpre[illegible]cted friction factor at lower aspect ratios (maximum error of 12% for square ducts). They observed that the secondary flow pattern carrying high axial momentum fluid toward the wall along the duct diagonals was more pronounced at the lower aspect ratios. Therefore, the underprediction of friction factor was attributed to these secondary velocities.

Leutheusser [1963] performed an experimental study of fully developed turbulent flow in smooth walled conduits of general cross section. Using rectangular cross sections of aspect ratio 3:1 to 1:1 he investigated the hypothesis of a unique resistance function in terms of the equivalent hydraulic diameter. To this end, he measured axial velocity, static pressure and wall shear stress distributions and found a difference between the measured and predicted friction factors using the von Karman-Prandtl resistance law for smooth pipes and an equivalent hydraulic diameter. He concluded that the law of the wall appeared valid for rectangular channels although it was applicable over a smaller distance from the wall than for circular pipe flow. However, the velocity defect law did not appear to be universal, implying that Reynolds number similarity did not extend reliably to rectangular geometries. His measured friction coefficients for rectangular conduits appeared to be lower than for circular pipes. He also observed that the velocity and shear stress distributions were more uniform at higher Reynolds numbers.

Gessner and Jones [1965] did an extensive experimental study of fully developed turbulent air flow in square and rectangular ducts. Again, one of the primary observations in this study was that the non-dimensionalized strength of the secondary flows decreases with increasing Reynolds number. By doing measurements of the directional characteristics of the local wall shear stress they found that the greatest skewness of wall shear stress vectors occurred near the corners where the secondary flows are a maximum. They also measured the orientation of the Reynolds stress principal planes in a plane normal to the axial flow direction. By experimentally evaluating the momentum balance along a secondary flow streamline they showed that secondary flow is the result of small differences in the magnitude of opposing forces exerted by the Reynolds stresses and static pressure gradients in planes normal to the axial flow direction.

Launder and Ying [1973] did a numerical prediction of fully developed turbulent flow in square ducts. They related the Reynolds stresses to the axial gradients of mean velocity to generate secondary motion. Rapley [1982] computed the fully developed turbulent flow in non-circular passages and simulated the secondary flow with diffusion transport to eliminate solution of the cross plane momentum and continuity equations. He reported his method as satisfactory for calculating mean flows.

Up to this point, the studies described have dealt only with fully developed flow with no mention of the developing or entrance region in non-circular ducts. Byrne, Hatton and Marriott [1969] did an experimental study of developing flow in a parallel wall passage. They used a pitot tube traverse to measure the axial velocity at various lateral and axial positions. Their major observation was that boundary layer parameters, such as momentum thickness, do not approach their fully developed values asymptotically. They concluded that predictions based on the law of the wall for such quantities as displacement thickness, momentum thickness and friction factor agree well with their measurements in the entrance region.

Ahmed and Brundrett [1971] did a similar study in square ducts. Their major observation was that the wall shear stress distribution develops very quickly (6 hydraulic diameters) whereas the core fluid required development lengths an order of magnitude larger and appeared to be more controlled by Reynolds number. This was consistent with the results of several previous studies that could see no Reynolds number similarity even for fully developed conditions.

Neti and Eichhorn [1979] undertook a computational solution of developing flow in a square duct. They used an algebraic model for the Reynolds stresses and reported a successful prediction of the flow field including the effects of secondary velocities.

Several specific studies of the mass transfer between two communicating subchannels have also been undertaken. The work of Slutsker, Bolonov and Tarasova [1983] investigated three different geometries; two equal square subchannels communicating by a narrow slot, two equal round subchannels communicating by a narrow slot, and a seven rod bundle. They defined a coefficient of turbulent cross transfer (α), as the ratio of effective cross flow to the arithmetic mean of the flowrates between the subchannels and determined this quantity to be larger for subchannels of unequal size as compared with those of equal size. They went on to develop correlations for α as a function of geometric parameters and Reynolds number for both equal and unequal subchannels and both single and two phase flows.

Lyall [1973] studied single phase flow in two unequal subchannels with a provision to reduce the size of the communicating gap between the two subchannels. He measured the single phase flow distribution of atmospheric air with a pitot tube and a hot wire anemometer. The pitot tube was used to measure the magnitude of the velocity while the hot wire measured its direction. His major observation was a region of low primary velocity in the gap between the two subchannels which he attributed to a measured secondary velocity away from the wall in that region.

Tracey [1976] made extensive measurements of the velocity distribution and turbulence parameters for a fully developed turbulent flow in a complex duct with particular attention to the production and effect of secondary motions.

The variations in the cross stream components of the fluctuating velocity in the corner regions were pinpointed as the probable cause of the secondary motions.

Tsuge et. al. [1979] measured void fraction distributions along the centerline of a two subchannel geometry with the same dimensions as were used in this study. The section was oriented vertically with an air/water mixture as the working fluid. They reported only void fraction measurements along the centerline.

Tapucu [1977] measured the diversion cross flow in two equal subchannels communicating by a narrow slot. He reported axial pressure gradients, average axial velocities and cross flow velocities for the subchannels. He formulated a theoretical model of the phenomena from the axial momentum equations for both subchannels. Using his experimental data, coefficients for the transport of momentum between the channels were determined and were found to be functions of the axial flow velocity in the subchannels and geometric parameters. He also observed a sinusoidal pressure difference oscillation between the two subchannels. Their wavelength seemed to be a function of the communicating gap clearance. The data from this work will be used as a code validation case in this study. Papers by Rogers and Tarasuk [1968], Van der Ros and Bogaardt [1970], and Verheugen et. al. [1967] have all concentrated on developing similar mixing correlations based on experimental data and theoretical models.

The COMMIX-1A three dimensional finite difference code was applied to the

Tapucu subchannels by Fohs et. al. [1981]. They simulated turbulent flow by applying an elevated viscosity uniformly over the flow field. Although it provided attractive qualitative results, it was unable to reproduce accurate pressure and mass transfer data.

Other relevant work can be found in the field of hydraulics and in particular the study of open channel flows with an adjacent floodplane inundated. This forms a geometry similar to that used in this study but with a free surface instead of a plane of symmetry. Demuren [1983] reports computational results for such a case using a three dimensional finite difference code that used the k-ε model. The contribution of secondary velocities were considered neglible in the initial flow interaction region where it was felt that pressure effects dominated. The main conclusion reached was the importance of having a model capable of prescribing an elliptic pressure field. This was deduced by comparing the superior results obtained with the poorer results from a previous study using a boundary layer method.

Prinos, et. al. [1985] performed an analytic and experimental study of the Reynolds stresses in the mixing region between the main channel and the flood plane. They concluded that longitudinal and vertical turbulence intensities were significantly higher in this region than in the central region of the main channel. Also, these turbulence intensities were found to increase with increasing relative boundary roughness between the main channel and the floodplane. They were also found to increase with a decrease in the relative depth parameter.

Knight and Lai [1985] took measurements in a compound channel and reported velocity, turbulent kinetic energy and wall shear stress data. Consistent with with the work of Lyall [1973] the isovels bulged inwards at convex interior corn corners and this effect was attributed to secondary flows.

Most of the literature concerned with making detailed measurements of velocity did so in rather simple rectangular or square duct arrangements. The more complicated geometry subchannel studies generally restricted their measurements to bulk average velocities with the aim of developing correlations for cross flow.

The present study was undertaken to provide detailed velocity profile measurements in two subchannel geometries which do not seem to be readily available in the literature. This detail is necessary for the task of verifying multidimensional fluid flow codes for use with such geometries.

III. EXPERIMENTAL INVESTIGATION

The study begins with an experimental investigation of the flow distribution in two adjacent subchannels of unequal size. For clarity, the experimental stage is divided into three categories. In Section III.1 the hydraulic loop facility, flow conditioning considerations and test section geometry are described. Section III.2 describes the instrumentation used to make the velocity and pressure measurements. The calibration of some of the important instruments is also presented. In Section III.3 the results of the measurements are given. The data are presented in the form of contour plots of velocity and plots of the axial pressure variation. The actual numerical data are contained in various Appendices.

III.1 Apparatus

III.1.1 Loop

The tests were performed in the MR-2 hydraulics loop at the Chalk River Nuclear Laboratories. This facility is an adiabatic water loop capable of delivering flows up to 16.0 kg/sec to the test section. The system contained a large (40.0 m^3) reservoir which helped greatly in maintaining constant water temperature over long running times. A schematic of the loop is shown in Figure III.1.

The centrifugal pump (capacity, 14 kg/s at 1.MPa) was powered by a 14.9 KW electric motor. The flowrate supplied to the test section could be controlled in two ways. An automatic control system used the signal from the flow transmitter (FT-1) across an orifice plate in the delivery pipe and linearized it with a square root extractor. The extractor output was fed into a process signal amplifier and to a flow controller which automatically actuated the pneumatic valve (V-1) through a current to air transducer. The controller featured proportional, integral, and derivative control. The second method was to overide the automatic control and fix the valve position manually. Under most conditions this maintained the flowrate within +/- 1% over very long operating periods with a minimal amount of manual readjustment from time to time. Generally, it was found that the automatic controller worked well at low flowrates, but at higher flowrates more stable conditions could be maintained by using manual control.

On the outlet, a diverter valve was used to route water either into the weigh tank or directly return it to the reservoir. The diverter valve movement automatically triggered an interval timer to measure the collection time of the weighed sample. Since tank capacity was about 2700 kg, accurate measurements of mass flowrate could be made and reliable calibrations of flow measuring elements within the system could be obtained.

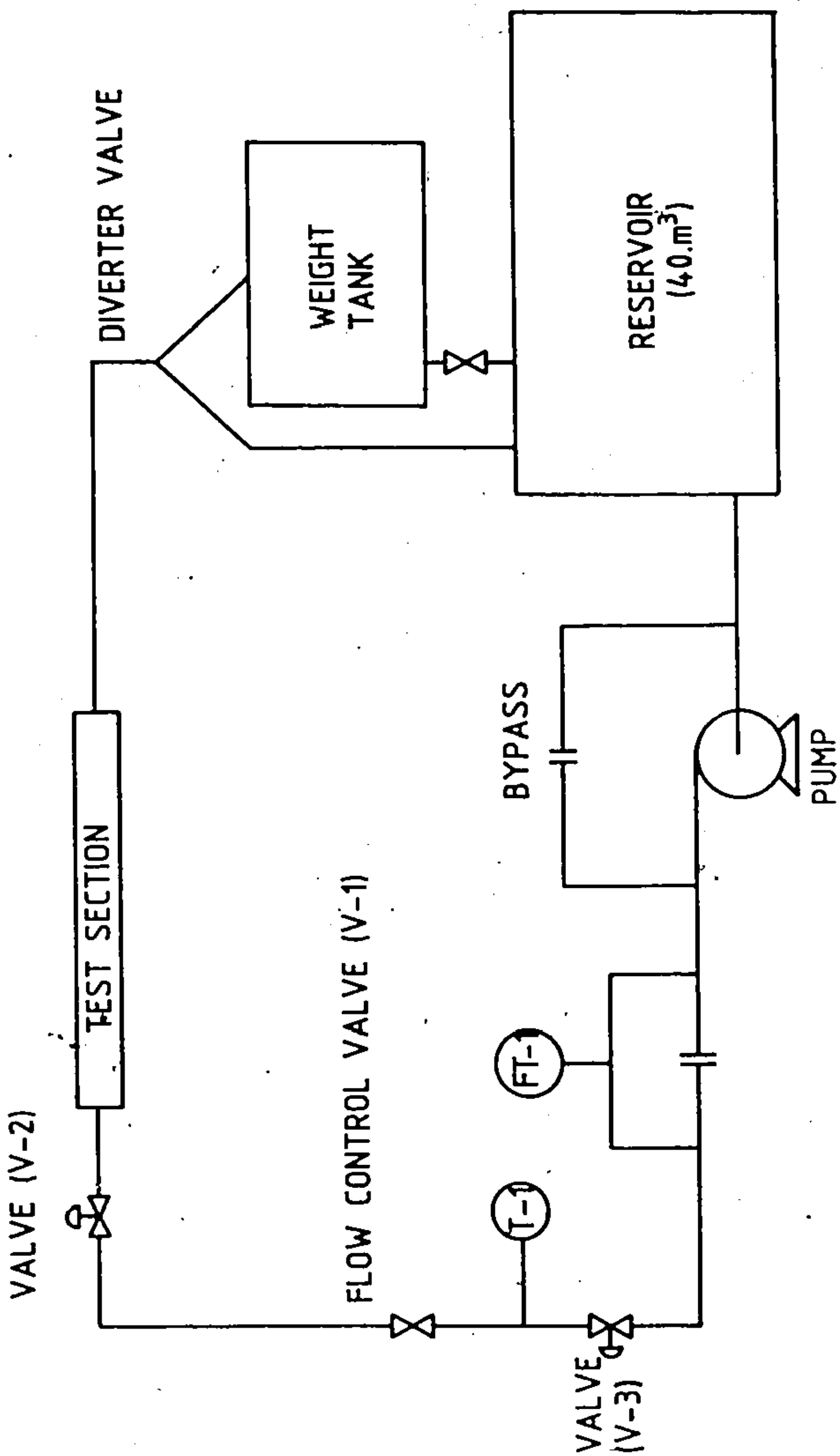

Figure III.1 MR-2 Loop Schematic

III.1.2 Flow Conditioning

Water was delivered by the pump through a 6.35 cm line to the test station. Several features were required to ensure acceptable velocity profiles at the inlet to the test section. The devices used to achieve such profiles will now be discussed. The goal of the following apparatus was to provide symmetrical but not necessarily fully developed profiles.

Since a centrifugal pump was used, measures had to be taken to ensure that the swirl induced by the pump's impeller was removed. To counter this swirl, a bundle consisting of nineteen 1.27 cm tubes was placed inside the 6.35 cm delivery pipe. Their position can be seen in the schematic in Figure III.2. The L/D ratio of these straightening vanes was 80. The 6.35 cm delivery pipe then connected to a 35 cm long lucite section that provided a transition from 6.35 cm round to 14 cm by 14 cm square. After the transition, a bundle of 1.98 cm diameter tubes formed an additional set of straightening vanes with an L/D of 12. Immediately after these vanes, the channel converged in one dimension only to form a rectangular section 14 cm by 7 cm. This dimension was then maintained for 102 cm until the inlet of the test section itself. The 102 cm represented a development length with an L/D of 11.

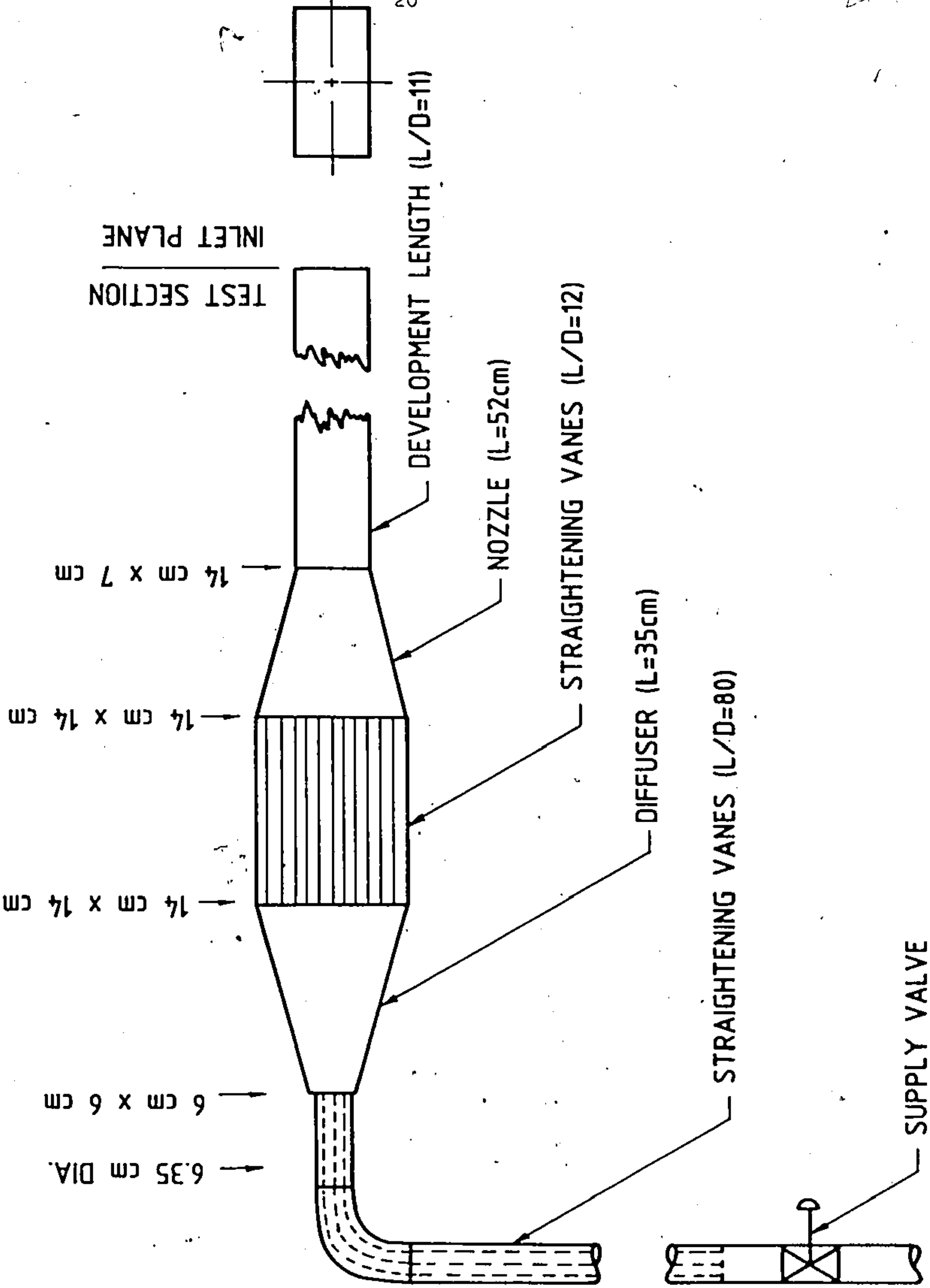

Figure III.2 Flow Development Section

Figure III.3 Photograph of Apparatus

The object was not to have fully developed channel flow at the inlet to the test section, since this would have required at least 20 diameters (dependent on Reynolds number (Hartnett [1962])). The main concern was that the profiles were symmetrical about the planes of symmetry of the section. A great deal of effort was required to ensure that this condition was met but it was achieved by the apparatus just described. The contour plots to be presented in Section III.3.3 confirm this. The actual apparatus is shown in the photograph of Figure III.3.

III.1.3 Test Section

A schematic of the test section is shown in Figure III.4. The overall cross sectional dimensions are the same as the inlet development section leading up to it. However, the test section could be fitted with various sized blocks which formed a cross section representing two adjacent subchannels of unequal size. Although one subchannel was of fixed size (7 cm X 7 cm), the thickness of the blockages could be altered to vary the size of the second subchannel. The various sizes used and the subchannel area ratios they represented are tabulated in Figure III.4.

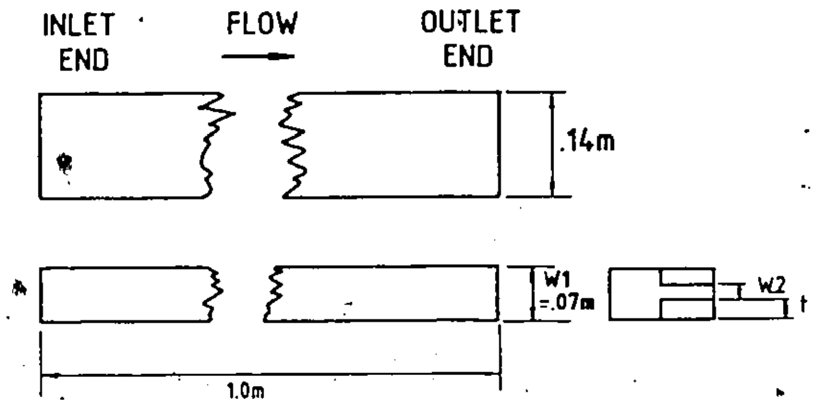

Area Ratio Summary	
t(m)	W2/W1
0.0000	1.0
0.0112	0.68
0.0175	0.50
0.0238	0.32

Figure III.4 Test Section

The transition from the 14 cm X 7 cm inlet development length to the two subchannel geometry was accomplished by tapering the leading edge of the two flow blockages. This is shown in Figure III.5. The constriction created by the tapered sections was completed before the inlet of the test section. The inlet of the test section was defined as the plane at which the inlet velocity profile measurements were made. Beyond the inlet, the test section extended for 1 meter. Velocity profile measurements were taken at various locations along this length to study the way in which the flow redistributed itself. The various measurement locations will be described in Section III.3 when the results are presented.

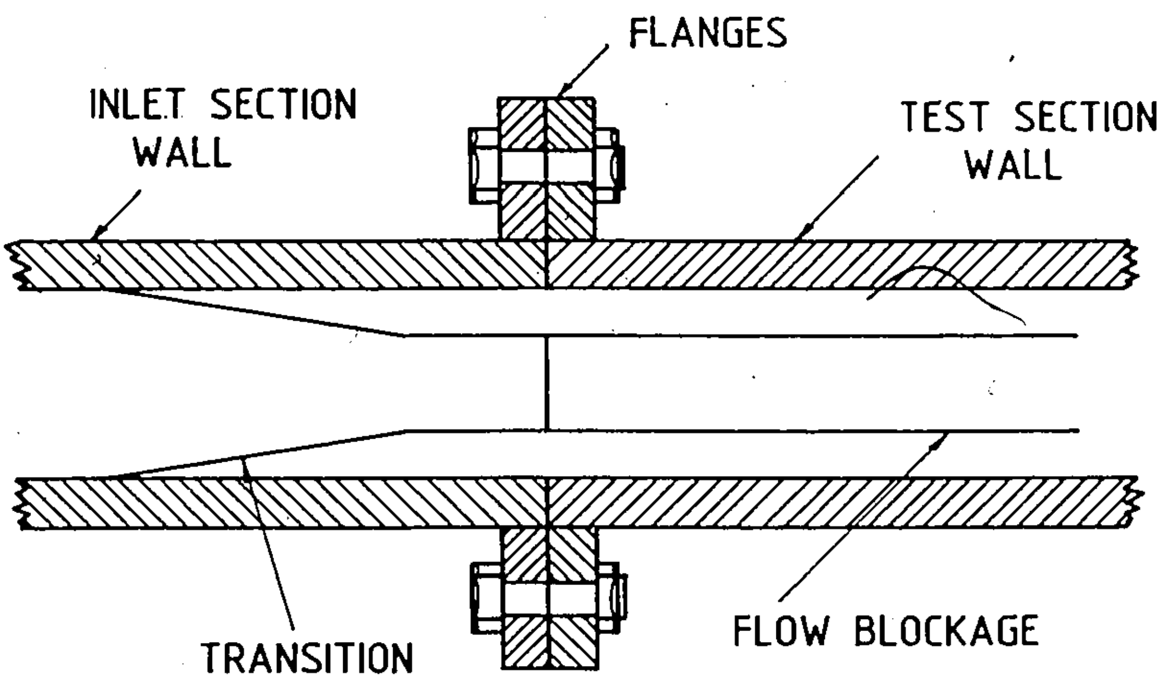

Figure III.5 Transition to Two Subchannel Geometry

III.2 Instrumentation

The measurements taken in this study consisted of velocity and pressure profiles of a single phase liquid. Since all velocity profiles were taken with pitot tube instruments, the primary sensing element for all measurements was a differential pressure (DP) cell. A single DP cell was used for all pressure and velocity measurements within the test section and its characteristics and calibration will now be presented.

III.2.1 Primary Sensing Element

The primary sensing element for all data taken was a Foxboro Model 613HM DP cell nominally calibrated for a range of 0-50 cm H_2O differential pressure. An inverted air over water U-tube manometer was attached across the DP cell to give a continuous visual check of its output during all the runs. The same manometer was used to check the calibration of the instrument from time to time. This was done by varying the height of a column of water connected to the high side of the DP cell and recording both the DP cell and manometer readings. The graduations on the manometer were in 1 mm intervals. Since the height of both columns of water had to be read, the manometer was accurate to within +/- 2 mm H_2O. Figure III.6 shows the calibration curve obtained by this method and confirms the linearity and output of the DP cell used.

A short discussion will now be given of the electronics used to measure pressure with this cell. The cell itself employs a diaphragm, moment arm and differential transformer detector to produce a 10-50 ma output over the calibrated range. A Model 610AT-OH excitation unit detected this current and provided an output of 1 to 5 volts corresponding to a nominal pressure range of 0-50 cm H_2O. All pressure and velocity measurements taken naturally fluctuated a certain amount and therefore the signal had to be averaged. To accomplish this a VIDAR Model 521B integrating digital voltmeter was used. The integration period was accurately started and stopped by a Hewlett-Packard Model 5330B Preset Counter. The output from the voltmeter could then be reduced through a simple formula to the average pressure during the integration period. The averaging time used was 30 seconds for the velocity measurements. This was chosen by examining the scatter in a set of readings taken at a particular averaging time. The averaging time was increased until the scatter became independent of averaging time. Thirty seconds was even more than this value to account for variations in turbulence intensity at other locations.

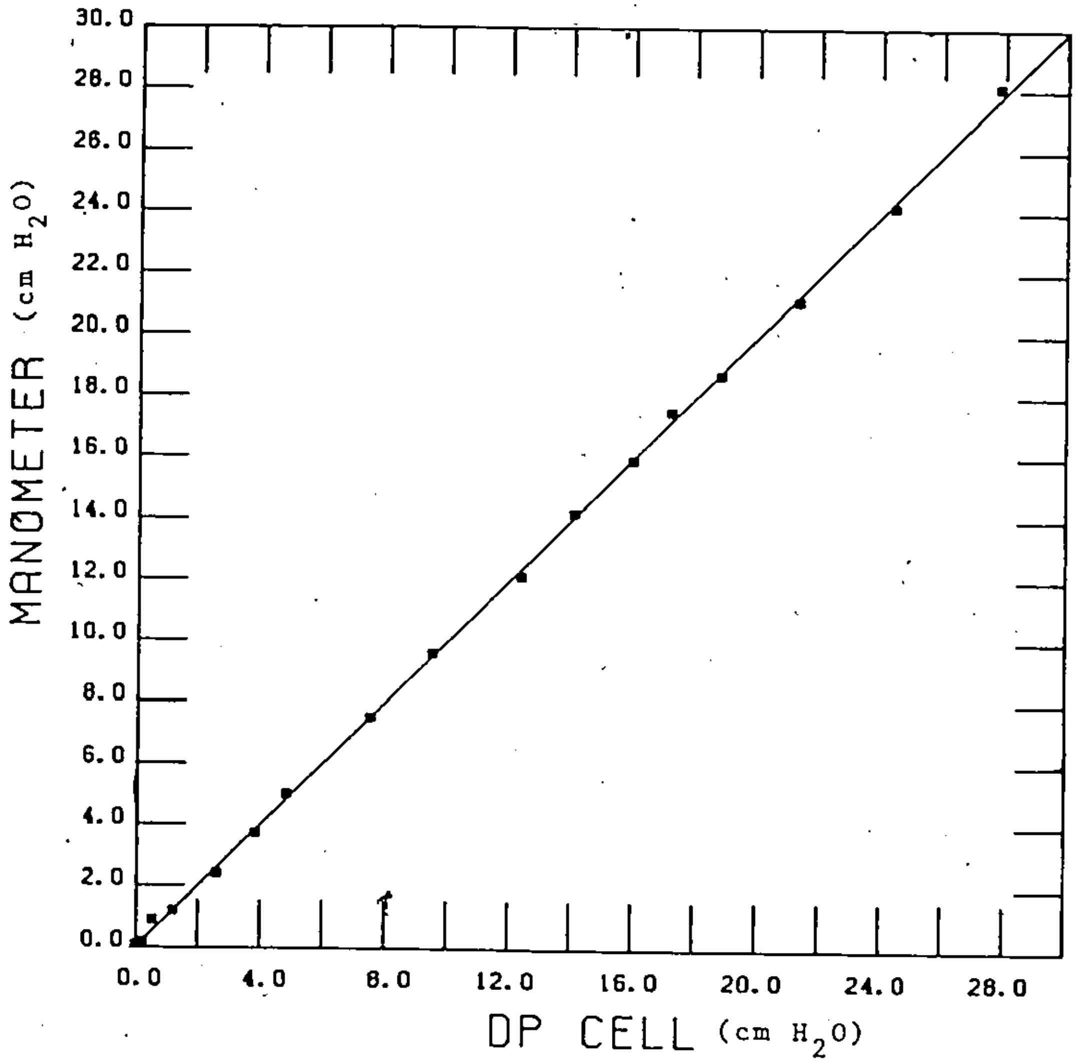

Figure III.6. DP Cell Calibration Curve

III.2.2 Stagnation Tube

To measure the velocity distribution in the subchannels a small (1.6 mm OD , 0.826 mm ID) tube was formed into a simple stagnation tube which is shown in Figure III.7. All velocity data reported were taken with this instrument.

Accurate positioning of the probe within the test section was very important. At any axial station the traversing mechanism required two degrees of freedom to enable the probe to completely map the velocity fields. The mechanism used to achieve this is shown in the photograph in Figure III.8. The probe was mounted on a brass base which slid in a groove machined into the lucite test section. Movement of this sliding base was measured to within 0.001 inches by the dial guage shown. Movement in the other direction was achieved by the screw type traversing mechanism in which the probe was mounted and was accurate to 0.005 inches.

In order to calculate velocity from the stagnation pressure it was necessary to know the local static pressure. In the process of taking data with this instrument the nearest convenient static wall tap on the test section was used as a reference pressure. Since this pressure was not always the same as the local static pressure a correction had to be introduced during the data analysis. The actual static pressure was inferred from the detailed pressure profiles and used to correct the velocity measurements. The measurement of these local detailed pressure profiles will—now be discussed.

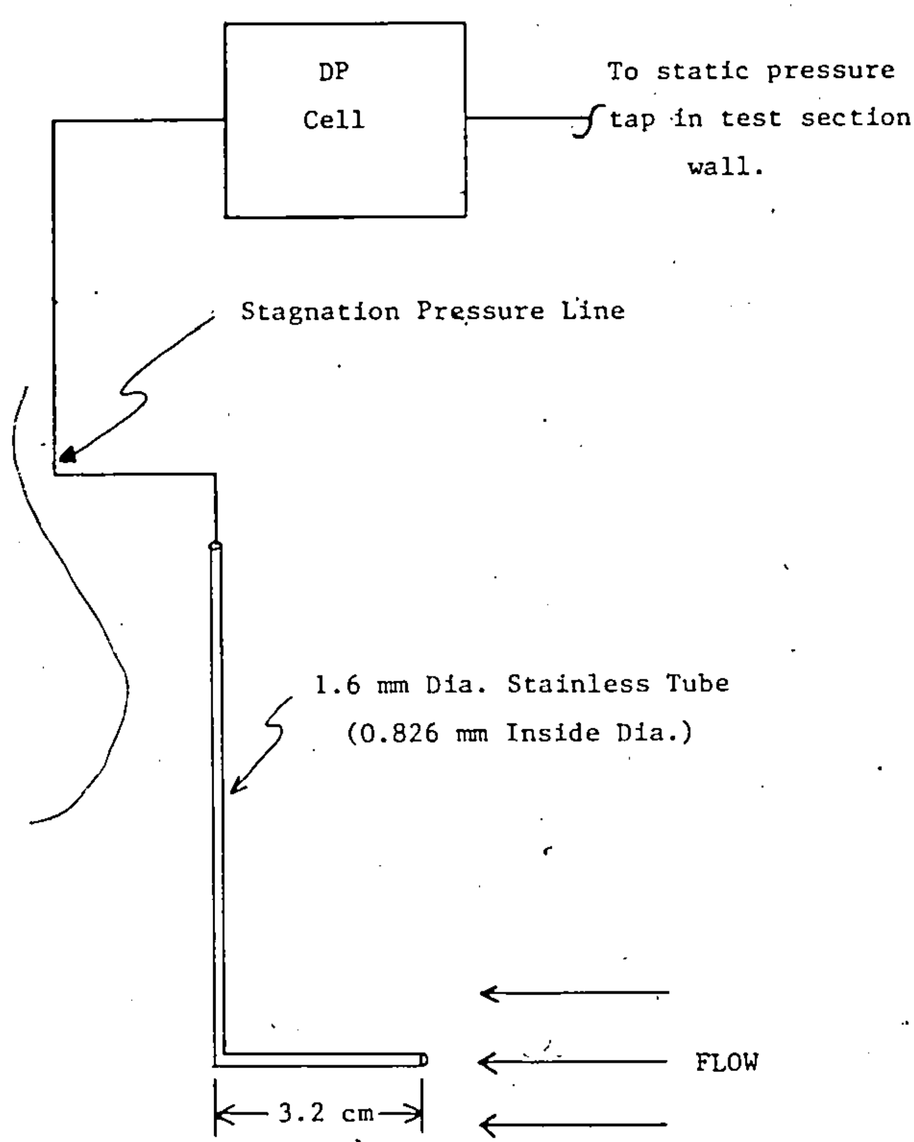

Figure III.7 Stagnation Tube Schematic

ATOMIC ENERGY [illegible] ANADA LTD. RESEARCH CO

8409-1667V-1

III.2.3 Pressure

No instruments beyond what have already been described were required to make the pressure profile measurements. The Foxboro DP cell was directly applied to the static wall taps in the test section. The wall taps were 1.6 mm diameter holes carefully machined perpendicular to the surface with no burrs or lips that could cause erroneous readings. The many taps were connected to the single DP cell by a toggle valve system. Figure III.9 shows the location of the pressure taps on the test section. Note that two rows of pressure taps required holes to be machined through the flow blockages which created the small subchannel. Vacuum grease was used to seal the flow blockages against the test section wall.

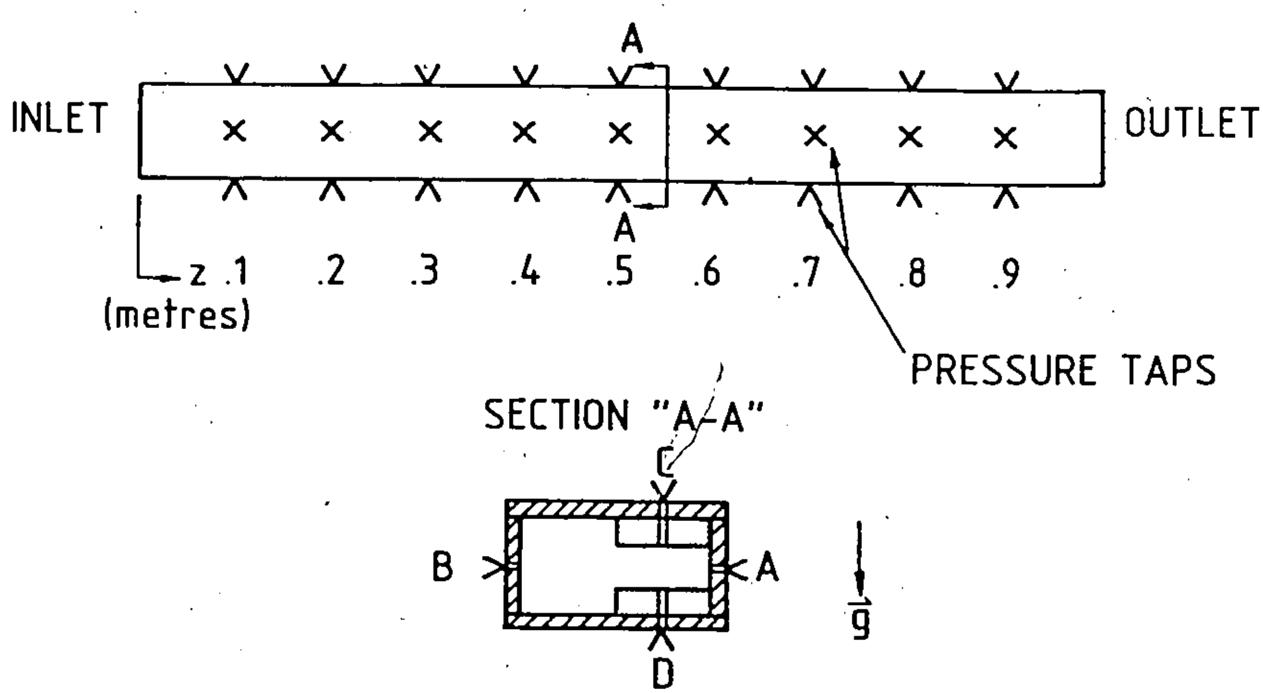

Figure III.9 Pressure Tap Locations

III.2.4 Other Instrumentation

In addition to the instruments already described, the calibration of the supply orifice plate should be presented. The orifice plate had a d/D of 0.69 in a 6.35 cm line with flange taps connected to a Foxboro Model 613HM DP cell. The output of the DP cell was fed into a square root extractor and then to a digital panel instrument to give a linearized indication of the mass flowrate. The panel instrument read 0-100% with 100% corresponding to a known full scale flowrate. Because of the linearizing circuit, a reasonable indication of the mass flowrate could be quickly obtained by simply scaling this known full scale flowrate with the percentage reading of the digital panel instrument. With the use of the weigh tank an in situ calibration of this instrument was performed. This was a very reliable calibration since it was done with the orifice plate in situ and used all of the process electronics (excitation, square root extractor, digital panel instrument) of the final configuration. Figure III.10 shows the calibration curve obtained. Also given on the figure is a third order polynomial fit to the calibration data. Use of this relationship will give a more accurate result than a simple scaling of the full scale flow (15.5 kg/sec) with the digital panel instrument's readout.

In order to detect and compensate for temperature variations in the water, an iron/constantan thermocouple was installed in the supply pipe. This gave a constant digital output of temperature on a panel instrument which was recorded periodically. Temperature variations were usually very minor (2-3 deg. C/day) and were accounted for in the data reduction routines.

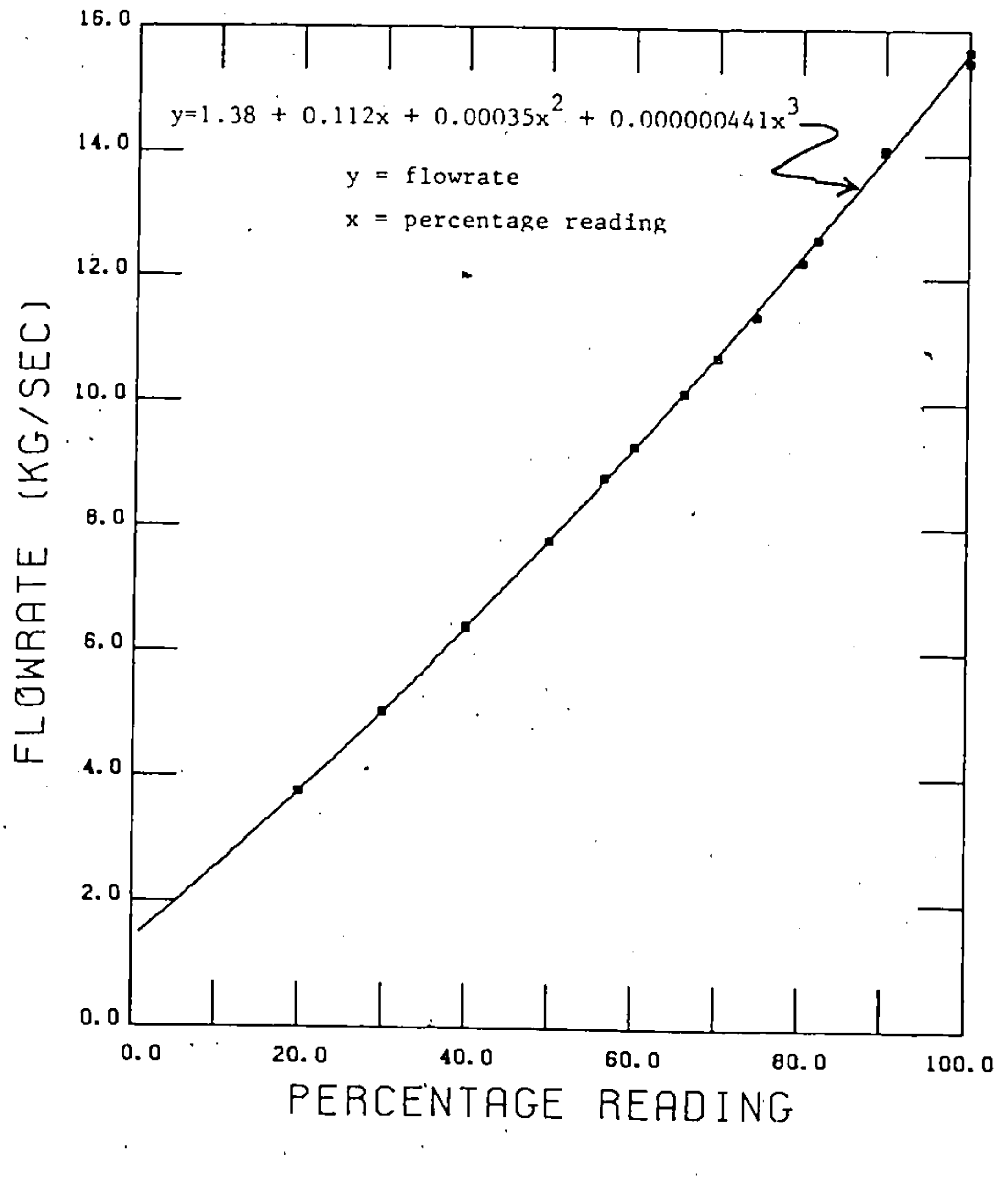

Figure III.10 Supply Orifice Calibration Curve

III.3 Experimental Results

The results of the detailed flow profile measurements will now be presented. This will begin with a description of the run matrix to describe the range of conditions tested. Then the results of the pressure profiles and velocity profiles will be given.

III.3.1 Run Matrix

The run matrix for these tests was created by varying two parameters. First, the geometry of the test section could be varied to give four possible configurations. Of these, three were two unequal subchannels and one was a simple rectangular channel. The various cross sections possible are shown in Figure III.4. The unequal subchannel configurations are of interest since the effect of different subchannel area ratios can be studied. The rectangular channel case was useful in checking the symmetry of flow profiles during commissioning and provided an additional test case for code validation. All four configurations will be compared with code results.

Each of these geometries was run at two Reynolds numbers to study the effect of Reynolds number on the flow distribution. These Reynolds numbers were nominally set at 180 000 and 108 000 and are based on the hydraulic diameter of the channel and the bulk velocity. The combination of varying Reynolds number and the geometry gives eight different cases for which data was taken.

III.3.2 Pressure Profiles

The pressure tap locations have been previously presented in Figure III.8. The labelling scheme is indicated on the figure with each tap having a letter and number associated with it. The letter indicates which of the four rows (A,B,C, or D) the tap is in, while the number indicates its axial location along the test section. The reference tap for all readings was the 90.0 cm tap in row A.

All of the pressure profile data is presented in tabular form in Appendix A. Since presenting all of this data here in graphical form would be redundant, only a couple of representative plots will be given. For any given run the profiles measured along row A,B,C, or D were very close to the same, so, for clarity, only row A will be plotted. The two plots presented are for a subchannel area ratio of 0.32 at two different Reynolds numbers and are shown in Figures III.11 and III.12. Their shape is very typical of the rest of the data.

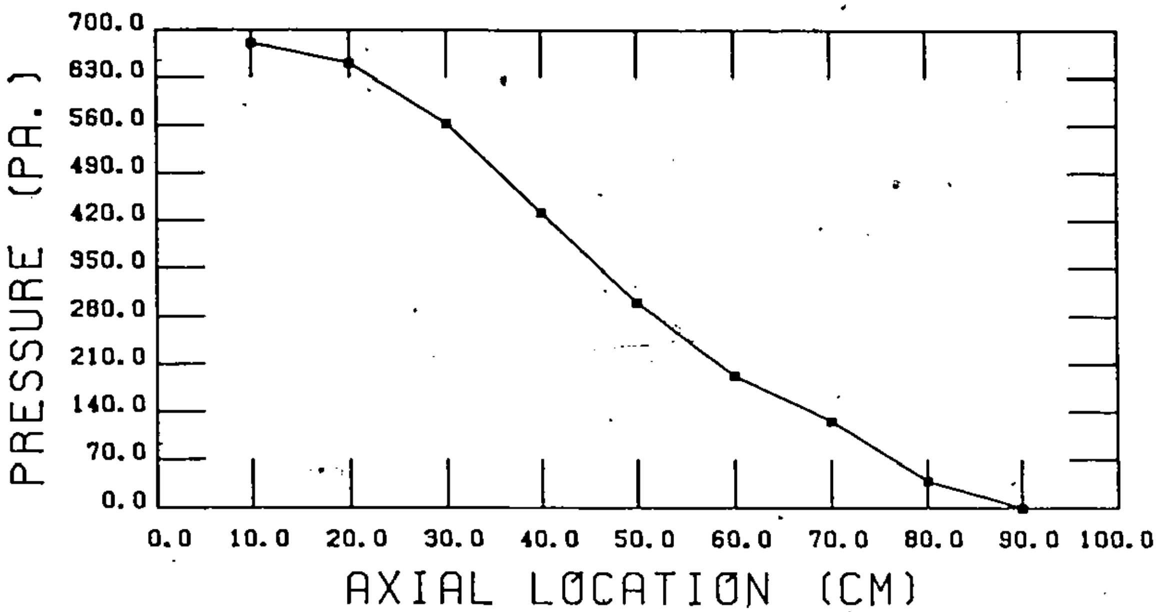

Figure III.11 Static Pressure Profile (reference location, 90.0 cm)
W2/W1=0.32 ; R=180 000

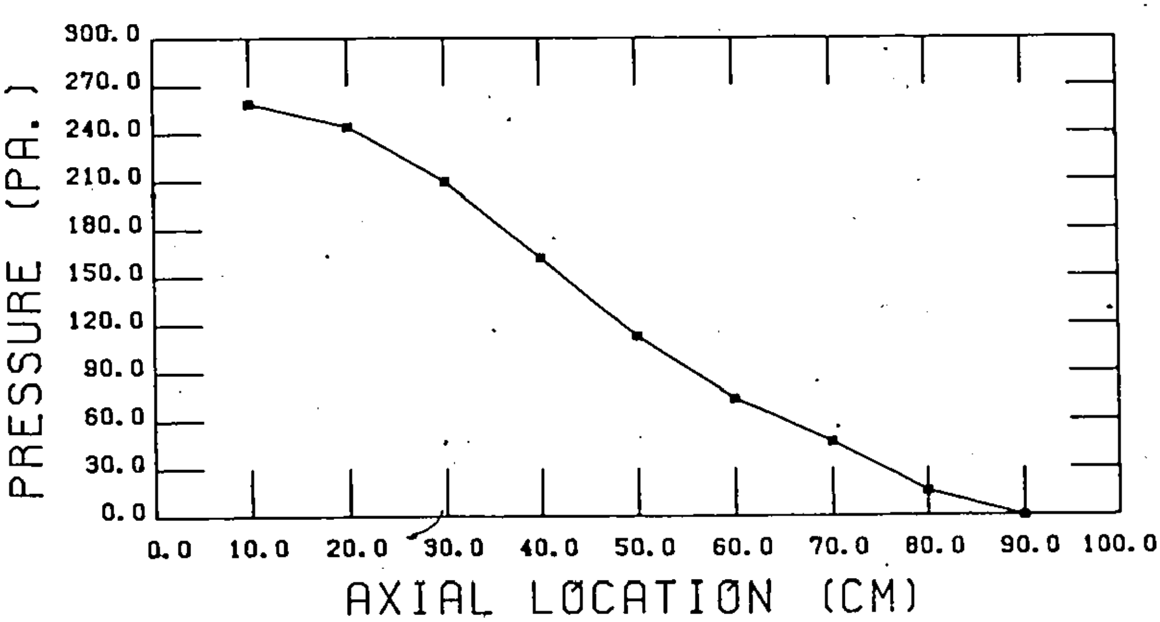

Figure III.12 Static Pressure Profile (reference location, 90.0 cm)
W2/W1=0.32 ; R=108 000

III.3.3 Velocity Profiles

All the velocity data presented here was measured with the simple stagnation tube as described in Section III.2.2. The locations of all the measurements are shown for W2/W1=0.50 in Figure III.13. For the other area ratios, points were added or deleted as required but their proximity to the wall was constant. Figure III.13 gives only a qualitative idea of the density ~~of the~~ grid, the precise locations of the measurement points are tabulated with the data in Appendix B.

The velocity data is presented in tabular form in Appendix B. Figures III.14 through III.17 show the data graphed in contour plot form for a Reynolds number of 180 000. Figures III.18 through III.21 show data for a Reynolds number of 108 000. Each figure contains three contour plots, one at each of the three axial locations at which measurements were made. The contours represent lines of constant velocity normalized by the average axial velocity. The contour interval is 0.05 and the 1.0 line is indicated on the figure.

Note that since the stagnation tube used was relatively insensitive to yaw angle (see Appendix C), the velocity data reported here is actually the total velocity.

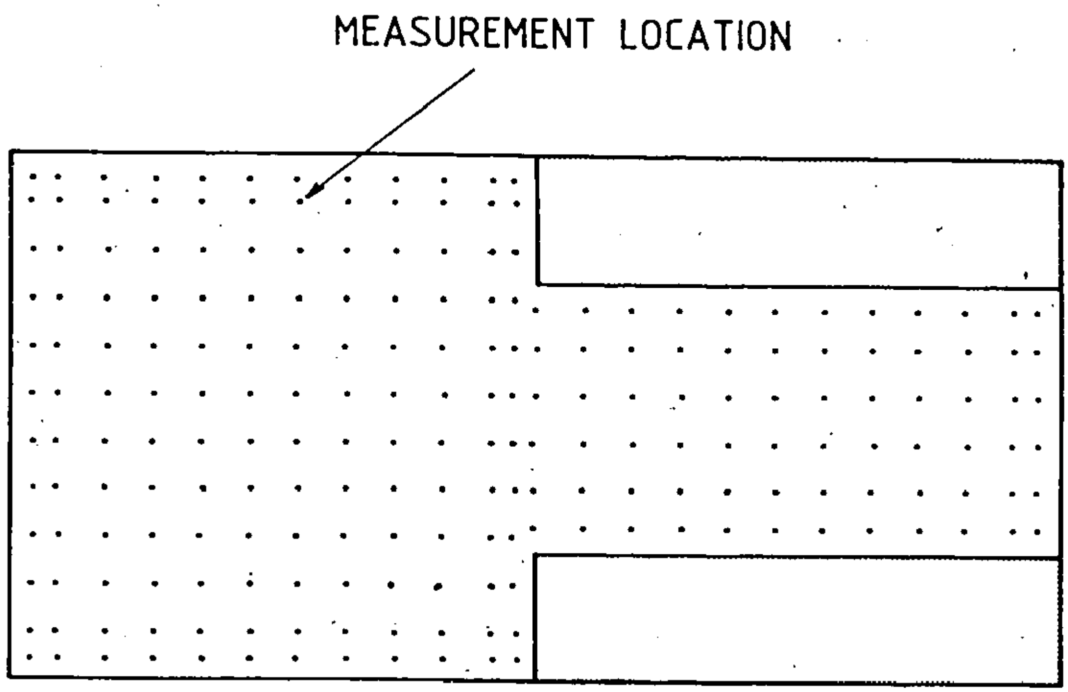

Figure III.13 Experimental Grid for Velocity

W_{ave} = 1.60 m/s ; Contour Interval = 0.05

z/Z = 0.0

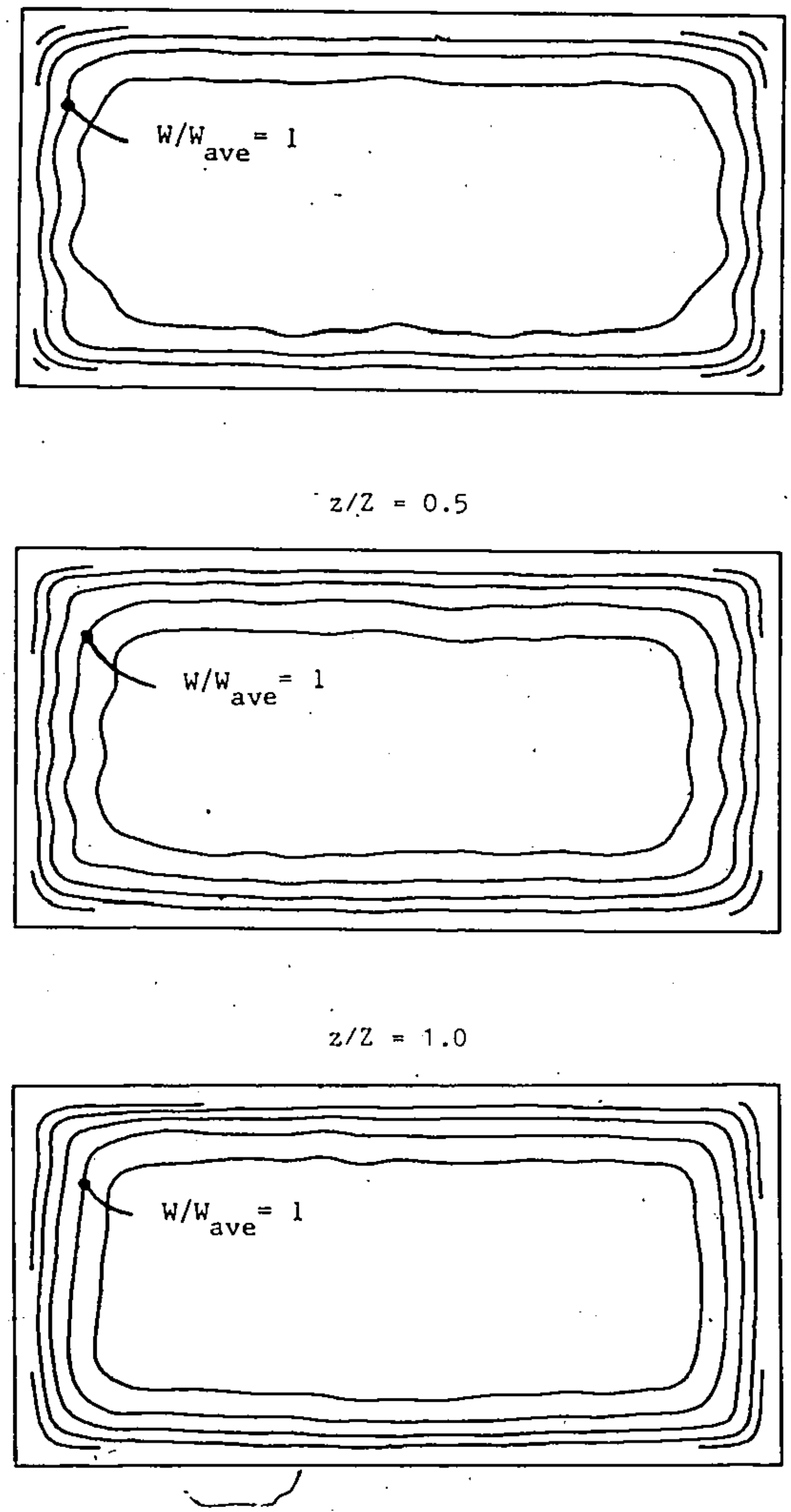

Figure III.14 Velocity Contours (W2/W1=1.0 ; R=180 000)

W_{ave} = 1.91 m/s ; Contour Interval = 0.05

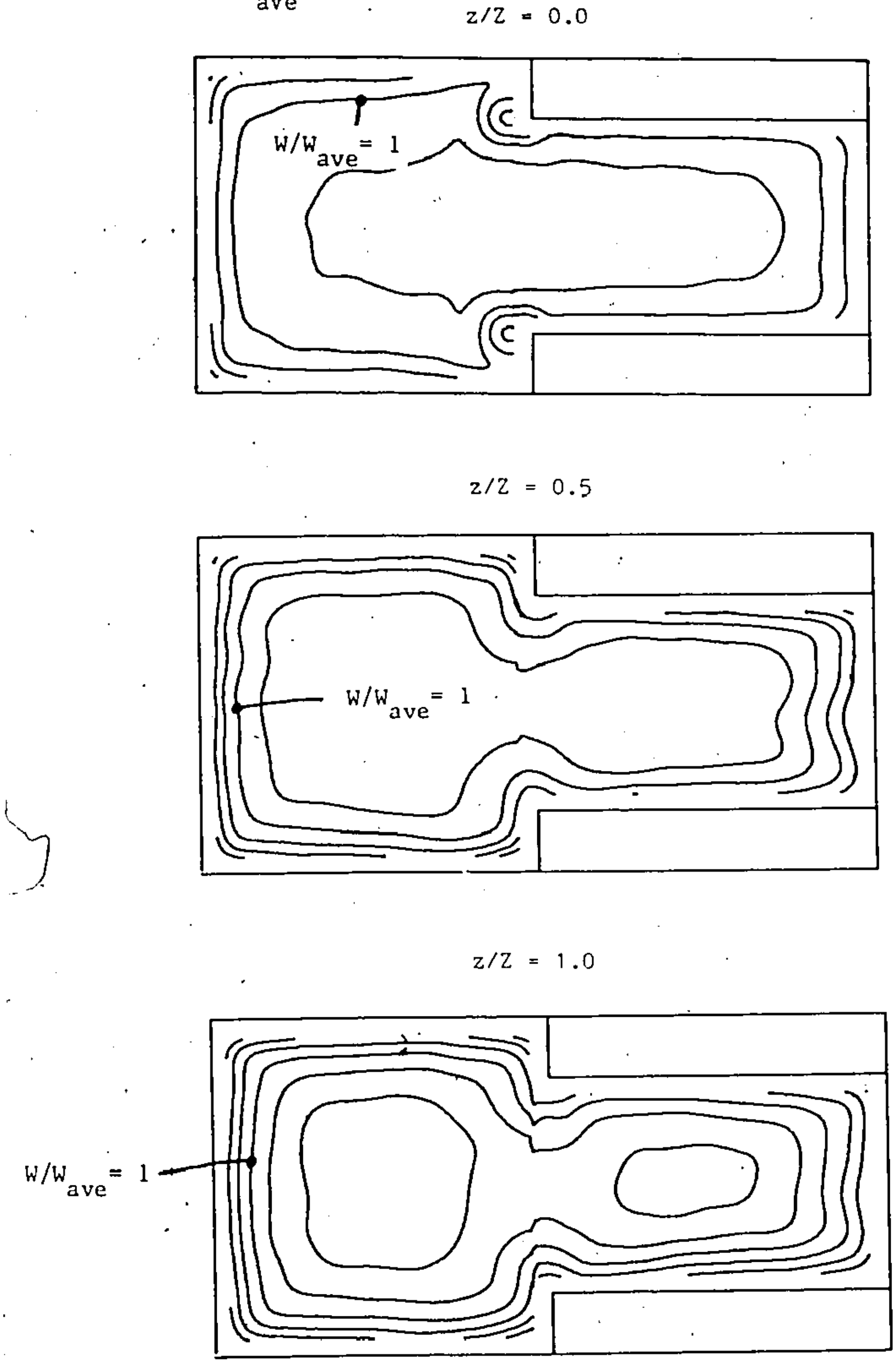

Figure III.15 Velocity Contours (W2/W1=0.68 ; R=180 000)

W_{ave} = 2.13 m/s ; Contour Interval = 0.05

z/Z = 0.0

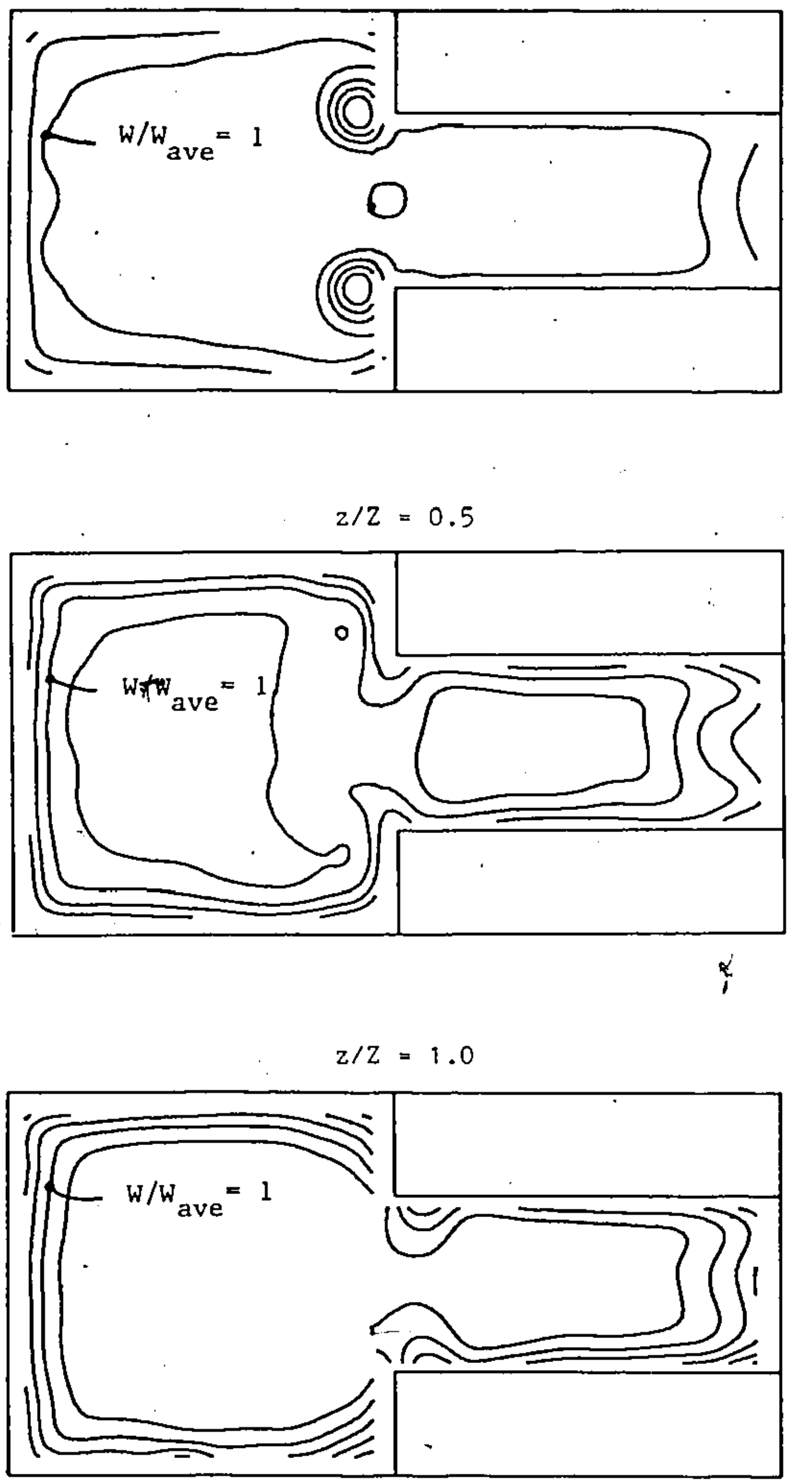

Figure III.16 Velocity Contours (W2/W1=0.50 ; R=180 000)

W_{ave} = 2.42 m/s ; Contour Interval = 0.05

z/Z = 0.0

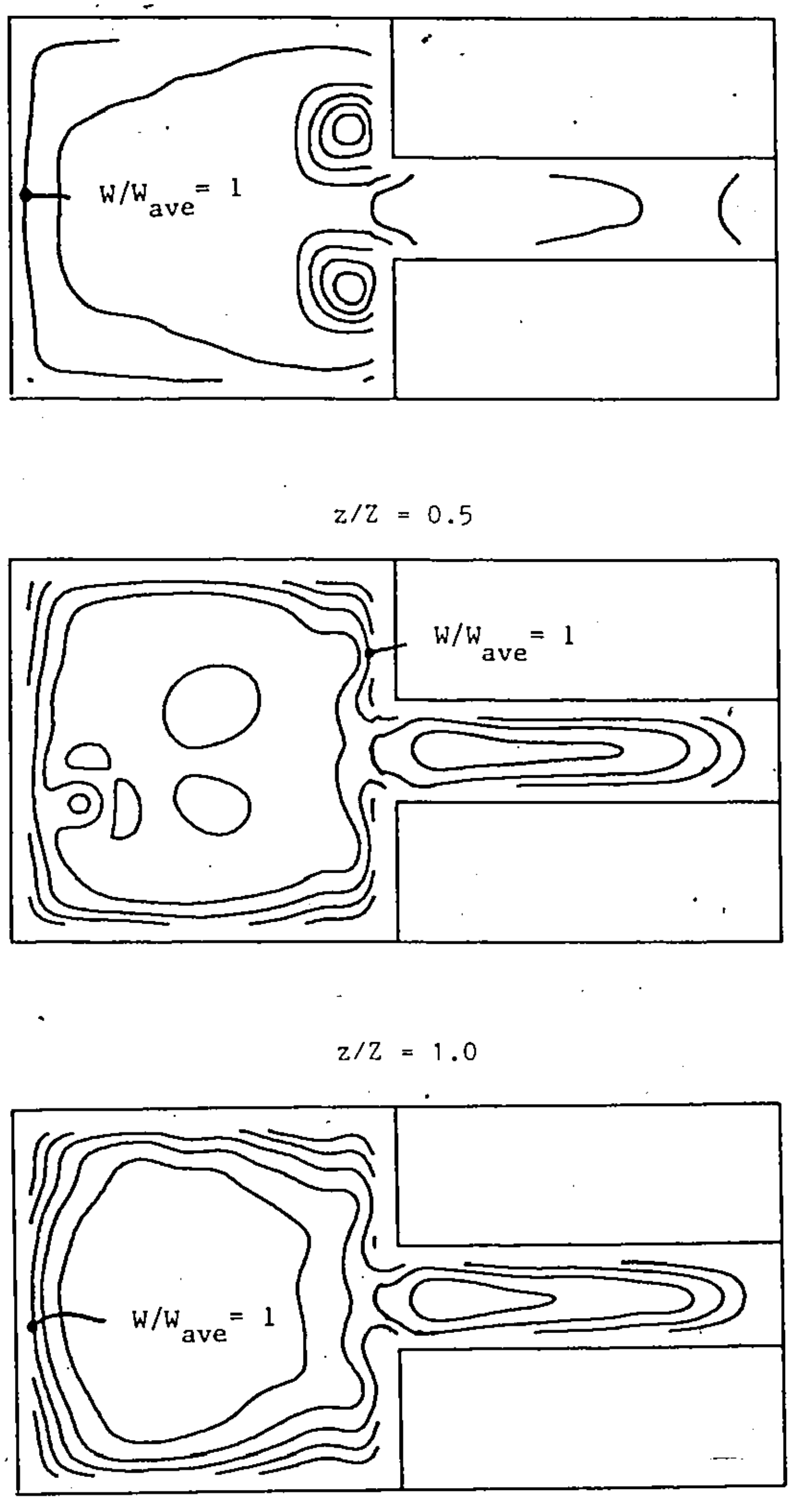

Figure III.17 Velocity Contours (W2/W1=0.32 ; R=180 000)

W_{ave} = 0.95 m/s ; Contour Interval = 0.05

z/Z = 0.0

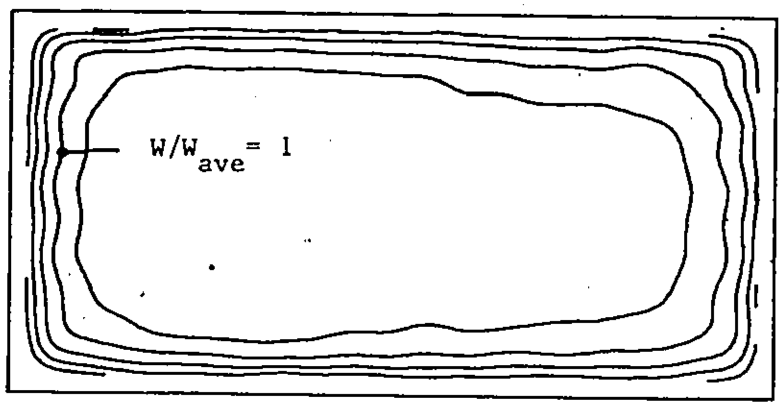

z/Z = 0.5

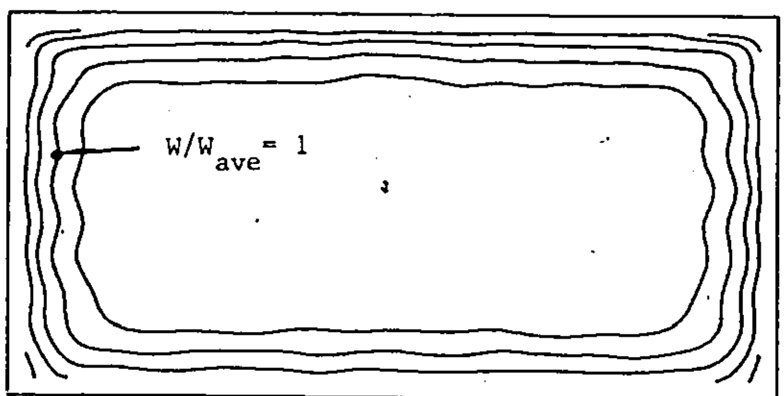

z/Z = 1.0

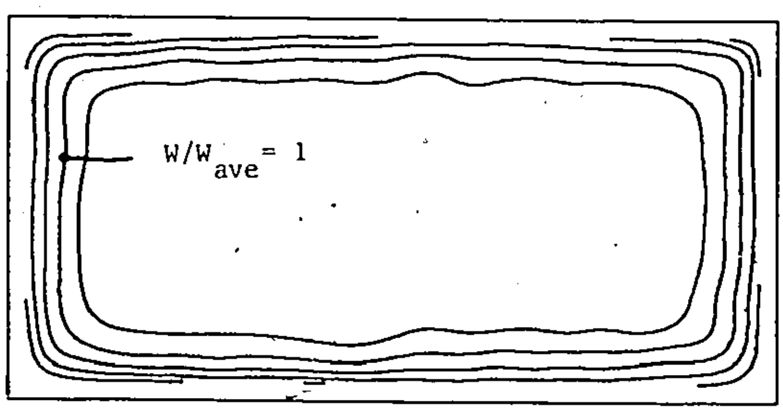

Figure III.18 Velocity Contours (W2/W1=1.0 ; R=108 000)

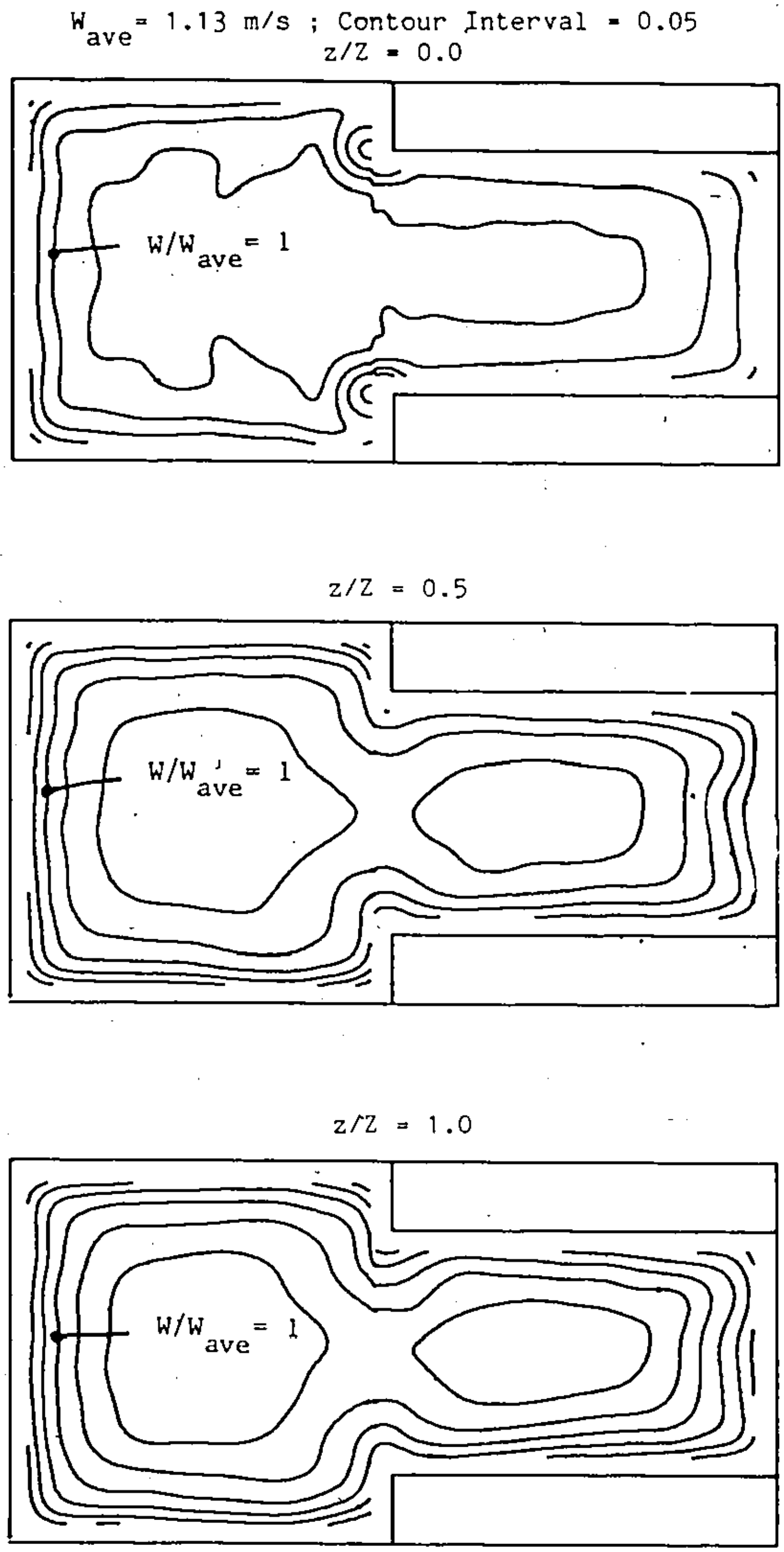

Figure III.19 Velocity Contours (W2/W1=0.68 ; R=108 000)

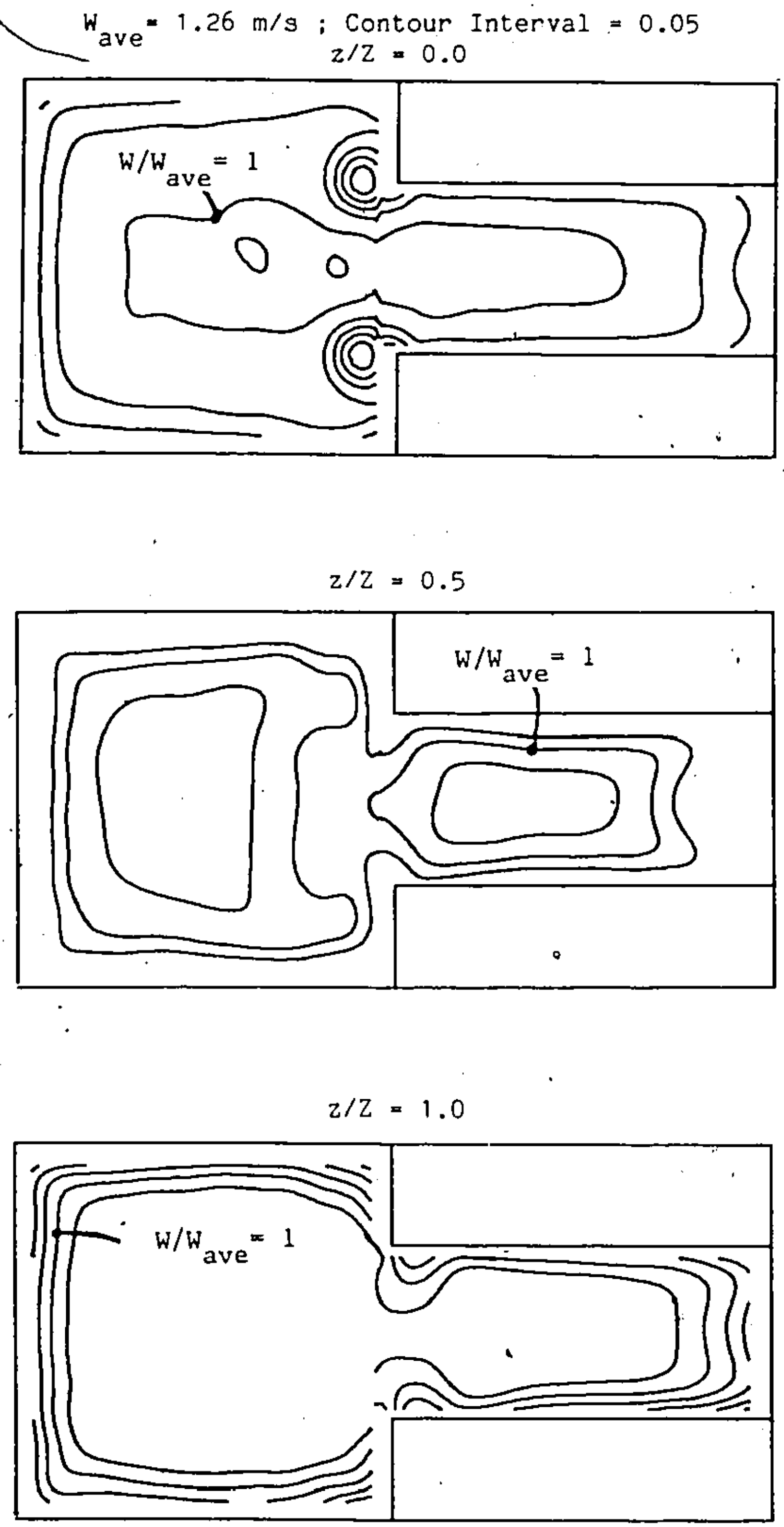

Figure III.20 Velocity Contours (W2/W1=0.50 ; R=108 000)

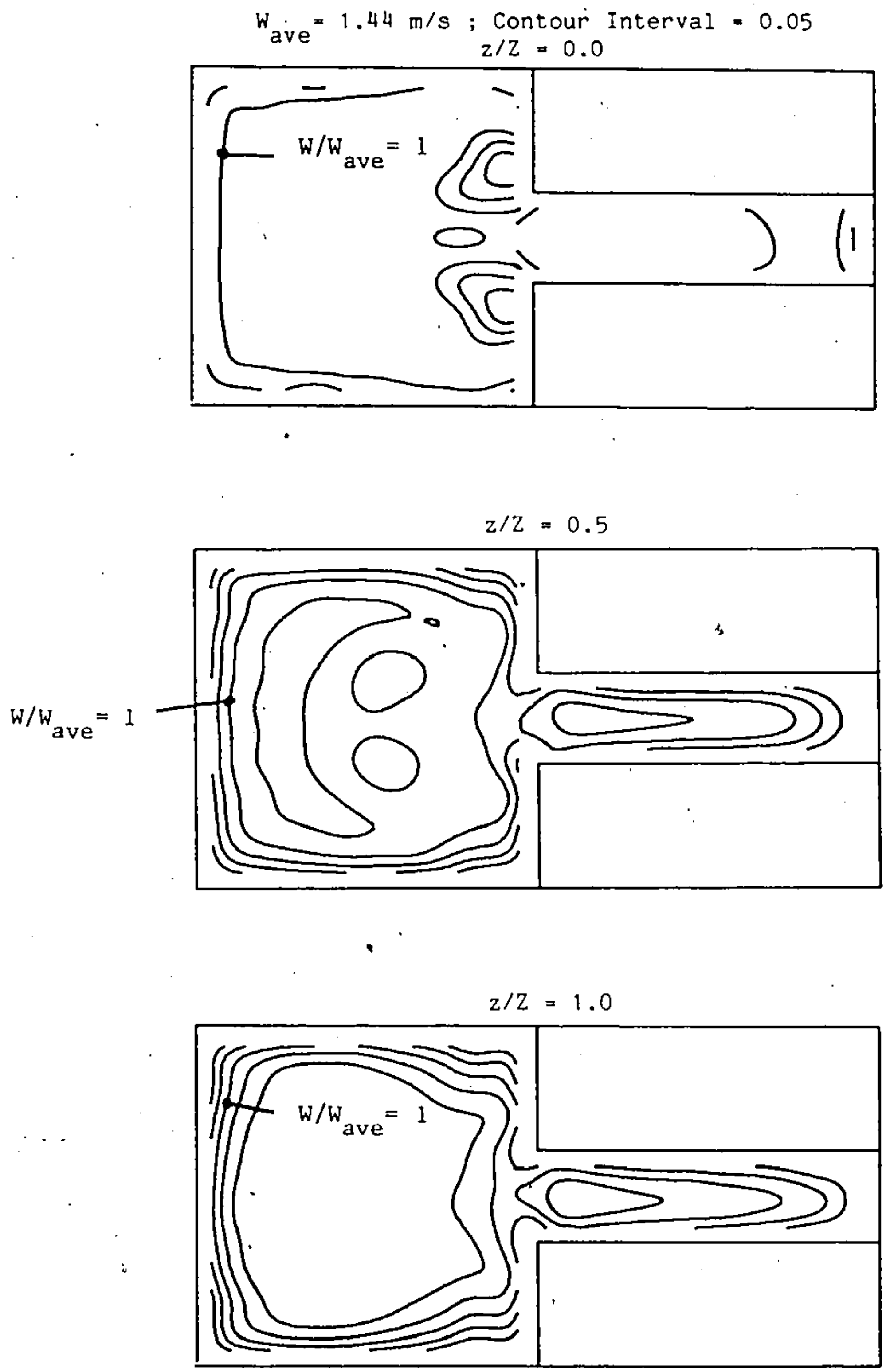

Figure III.21 Velocity Contours (W2/W1=0.32 ; R=108 000)

Initial confidence in the data can be based on the fact that the velocity contour plots show generally good symmetry. For the rectangular channel cases (W2/W1=1.0), there are two planes of symmetry. As can be seen in the figures, good symmetry was attained in these cases. For the other three test section configurations, the addition of flow blockages allowed only one plane of symmetry to exist. Again, in most cases, good symmetry exists across the plane. It was vital that symmetrical profiles were obtained before data taking in earnest since code predictions were calculated on a grid which used the various planes of symmetry to reduce the number of nodes. If the experimental results were grossly asymmetrical, comparisons with the perfectly symmetrical code results would be fruitless.

A second check on the experimental results was obtained by calculating the total mass flow based on integrating the point velocity measurements and comparing it with the inlet mass flow as measured by the orifice plate in the supply line. This check also indicated accurate results since the mass flows were consistently within 5% of each other.

IV. ANALYTIC INVESTIGATION

To complement the experimental investigation, an analytic solution was also attempted. Although such solutions offer many desirable advantages (speed, accuracy, flexibility), they are often difficult to obtain. The process begins by formulating a mathematical model which consists of a closed set of governing differential equations. In some very simple cases an exact solution to these equations can be found. However, such solutions are rare, and are not available for any complex internal flows of practical interest. The alternative to an exact solution is a numerical approximation to the solution. This section describes a finite difference numerical solution procedure used for the analysis. Section IV.1 presents the equation set that embodies the mathematical model to be used. In Section IV.2 the numerical solution procedure used to solve the equation set will be described. Section IV.3 will describe the actual code and some aspects of its implementation. Section IV.4 will present the results obtained.

IV.1 Equation Set

The governing equations of fluid flow are mathematical statements of the conservation of some quantity over an infinitesimal control volume. Before working with these equations, it is necessary to define the coordinate system that will be used. In this analysis, a three dimensional Cartesian coordinate system provides the reference frame. With the reference frame established the unknowns should now be identified. Since the problem deals with a single phase continuum, the unknowns are field variables and, in general, can be expressed as functions of the three spatial coordinates and time. In addition, the flow is assumed to be incompressible and isothermal so that the only unknowns are the pressure field and velocity fields. Using tensor notation, as will be used through most of this work, the fields can be expressed as follows;

$$P = P(x,y,z,t) \qquad \text{... IV.1}$$

$$U_i = U_i(x,y,z,t) \qquad \text{... IV.2}$$

Since there are three components of velocity, this represents four scalar unknowns. Note that the subscript, i, denotes U as a vector (first order tensor) where i can assume a value of 1, 2, or 3 representing the three coordinate directions.

The expressions given by Eqns. IV.1 and IV.2 define the unknown field variables in their most general sense, as a function of all four independent variables. It is because of this generality that the flow field can be described by only four field variables. As will be seen, additional field variables such as turbulent kinetic energy and dissipation rate will enter the problem in order to reduce this generality of the primary field variables (P and U_i) and make their specification simpler.

The highly complex nature of turbulent flow makes this simplification necessary. Since a numerical scheme will eventually be applied to the solution of the velocity and pressure fields, a discretized numerical grid, and time step will have to be chosen. The grid would have to be very fine in order to have the spatial resolution to accurately define the very small scale eddies in a turbulent flow. Viscous dissipation of turbulent kinetic energy into thermal energy is a very important phenomenon in a turbulent flow since it represents the sink for turbulent kinetic energy and this process occurs at very small eddy sizes, typically in the order of 1 mm (Launder, Spalding [1974]). In order to resolve such small length scales and still cover a domain of any practical interest, the number of grid points (nodes) would be far in excess of the storage capacity of modern computers. Even more restrictive is the tremendous time it would take to solve the equations for such large numbers of nodes. In addition, time scales of turbulent fluctuations are so small that attempting to develop a transient code capable of resolving turbulent fluctuations is hopeless at present. As a result of this complexity, the time averaged effects of the turbulent fluctuations, not the microscopic details, must be considered. Although the method for doing this will be described later, it is sufficient to say that it will allow the time dependence to be dropped and larger, more practical grid spacing to be employed.

The common method of modelling the effect of the turbulent fluctuations is to re-define the field variables already given as a sum of a mean component and a fluctuating component. This procedure was initiated by O. Reynolds and is known as Reynolds decomposition (Hinze [1959]).

$$P = \bar{P} + p \qquad \ldots \text{IV.3}$$

$$U_i = \bar{U}_i + u_i \qquad \text{... IV.4}$$

The equations that will be presented shortly are valid for the instantaneous values of P and U_i. The effect of the mean and fluctuating components can be determined by substituting IV.3 and IV.4 into the governing equations and simplifying. As will be seen, this procedure produces additional unknowns involving the fluctuating components and thereby introduces a closure problem in the equation set.

IV.1.1 Mass Conservation

The simplest conservation equation is the continuity equation which states that the net mass efflux from an elemental control volume must equal the net production of mass within the control volume. For an incompressible, isothermal, single phase flow this essentially demands that the net mass efflux must be zero at all times. The continuity equation is presented here in tensor form for an incompressible steady flow.

$$\partial U_i/\partial x_i = 0 \qquad \text{... IV.5}$$

Substituting Eqn. IV.4 into IV.5,

$$\partial(\bar{U}+u_i)/\partial x_i = 0 \qquad \text{... IV.6}$$

Expand and average to obtain,

$$\overline{\partial U_i/\partial x_i} + \overline{\partial u_i/\partial x_i} = 0 \qquad \text{... IV.7}$$

Using Reynolds conditions this can be simplified since;

$$\overline{\partial u_i/\partial x_i} = 0$$

$$\partial \bar{U}_i/\partial x_i = 0 \qquad \text{... IV.8}$$

Equation IV.8 is the continuity equation for the mean velocity. If Eqn. IV.8 is subtracted from IV.6, a continuity equation for the fluctuation, as shown below, is obtained.

$$\partial u_i'/\partial x_i = 0 \qquad \text{... IV.9}$$

Since the original continuity equation was linear (Eqn. IV.5), Reynolds decompostion did not result in any additional unknowns in Eqn. IV.8 and the continuity equation for the instantaneous, mean, and fluctuating velocities are of the same form.

Note that Eqn. IV.5 expresses the laminar form of the continuity equation. Since no fluctuating components contribute to the laminar velocity field, Reynolds decomposition need not be applied.

IV.1.2 Navier-Stokes Equations

The Navier-Stokes equations express the conservation of momentum for an elemental control volume of the flow field. They can appear in many forms depending on the assumptions and subsequent simplifications that have been applied to them. The following form is for an incompressible Newtonian fluid and is taken from Currie [1974]. The variables are defined in the nomenclature.

$$\rho(\partial U_i/\partial t + U_j \partial U_i/\partial x_j) = -\partial P/\partial x_i - \partial(2/3\mu\partial U_j/\partial x_j)/\partial x_i$$
$$+ \partial(\mu(\partial U_i/\partial x_j + \partial U_j/\partial x_i))/\partial x_j + \rho f_i \qquad \text{... IV.10}$$

Since this is a steady state analysis the time derivatives can be dropped. Since the formulation is for an incompressible fluid, continuity can be applied to eliminate the second term on the right hand side. After these simplifications there remains;

$$\rho U_j \partial U_i/\partial x_j = -\partial P/\partial x_i + \partial(\mu(\partial U_i/\partial x_j + \partial U_j/\partial x_i))/\partial x_j$$
$$+ \rho f_i \qquad \text{... IV.11}$$

This equation is written using the instantaneous velocity, U_i. If U_i is a laminar velocity field this form of the equation can be solved by numerical methods. However, the small time scales of a turbulent flow require that an expression for the average velocity, $\bar{U}_i$, be found. Reynolds decomposition of turbulent fluctuating velocities and pressures must be introduced to obtain conservation equation for the mean velocity. Therefore, substituting

Eqns. IV.3 and IV.4 into Eqn. IV.11 gives,

$$\rho(\bar{U}_j+u_j)\ \partial(\bar{U}_i+u_i)/\partial x_j = -\partial(\bar{P}+p)/\partial x_i + \partial(\mu(\partial(\bar{U}_i+u_i)/\partial x_j + \partial(\bar{U}_j+u_j)/\partial x_i))/\partial x_j + \rho f_i \quad \ldots \text{ IV.12}$$

Eqn. IV.12 can now be expanded and each term averaged. Noting at this point that the time average of a first order fluctuating term is zero since its mean is zero, but products of two fluctuating terms are non-zero , the following expression is obtained:

$$\rho\bar{U}_j\partial\bar{U}_i/\partial x_j + \overline{\rho u_j\partial u_i/\partial x_j} = -\partial\bar{P}/\partial x_i + \partial(\mu(\partial\bar{U}_i/\partial x_j+\partial\bar{U}_j/\partial x_i))/\partial x_j + \rho f_i \quad \ldots \text{ IV.13}$$

Consider the second term on the left hand side and expand as follows:

$$\rho u_j\partial u_i/\partial x_j = \rho(\partial u_ju_i/\partial x_j - u_i\partial u_j/\partial x_j) \quad \ldots \text{ IV.14}$$

but by Eqn. IV.9;

$$\rho u_j\partial u_i/\partial x_j = \rho\partial(u_iu_j)/\partial x_j \quad \ldots \text{ IV.15}$$

so IV.13 becomes,

$$\rho\bar{U}_j\partial\bar{U}_i/\partial x_j = -\partial\bar{P}/\partial x_i + \partial(\mu(\partial\bar{U}_i/\partial x_j+\partial\bar{U}_j/\partial x_i))/\partial x_j - \rho\partial\overline{u_iu_j}/\partial x_j + \rho f_i \quad \ldots \text{ IV.16}$$

Since the Navier-Stokes equations are really a statement of Newton's Second Law for an element of fluid, the various terms in Eqn. IV.16 can be defined in terms of a force/momentum balance. The left hand side is the rate of change of momentum for the fluid in the elemental control volume. Since the transient terms have been eliminated only the spatial rate of change remains. The right hand side contains all the forces acting on the fluid element to produce this change of momentum. The first term is the pressure force and represents the resultant force acting on the surfaces of the control volume due to pressure. The next two terms represent the viscous forces acting on the surface of the element from the surrounding fluid. The last term is simply the body force from the weight of the fluid in the elemental control volume.

There remains one term to consider in Eqn. IV.16. The second last term on the right hand side represents a force on the element due to the turbulent fluctuations in the flow and is known as Reynolds stress. The fluctuations in ~~velocity~~ transfer momentum (i.e. exert a force) across the boundaries of the control volume. It is this extra term that introduces additional unknowns and creates the closure problem which plagues any attempt to analyze turbulent flows. The Reynolds stress tensor, $\overline{\rho u_i u_j}$, is symmetric and therefore contains six unknown components. Conservation equations can be written for the various components but in doing so, higher order products of fluctuating velocities are introduced and the problem persists. This closure problem will now be addressed.

IV.1.3 Closure

In order to close the present set of equations, additional relationships which will model the effect of the Reynolds stresses must be obtained. Such relationships are called turbulence models and are essentially constitutive equations which model the effect of turbulence in terms of calculable quantities.

The first step in closing the equation set is to recognize a concept first formulated by Boussinesq (Hinze [1959]). He considered the effect of the Reynolds turbulent stress tensor as analagous to an additional laminar shear stress. Since the laminar shear stress is expressed as a product of a laminar viscosity and the mean velocity gradient (as in Eqn. IV.17), he proposed that the turbulent shear stress could also be modelled as a product of the same mean velocity gradient and a turbulent viscosity, μ_t, as in Eqn. IV.18.

$$\tau_{ij} = \mu(\partial\bar{U}_i/\partial x_j + \partial\bar{U}_j/\partial x_i) \qquad \ldots \text{ IV.17}$$

$$\tau_{ij} = \mu_t(\partial\bar{U}_i/\partial x_j + \partial\bar{U}_j/\partial x_i) = -\overline{\rho u_i u_j} \qquad \ldots \text{ IV.18}$$

Note that this assumption allows convenient reformulation of Eqn. IV.16 into the following form:

$$\rho\bar{U}_j\partial\bar{U}_i/\partial x_j = -\partial\bar{P}/\partial x_i + \partial(\mu\partial\bar{U}_i/\partial x_j + \mu\partial\bar{U}_j/\partial x_i + \mu_t\partial\bar{U}_i/\partial x_j + \mu_t\partial\bar{U}_j/\partial x_i)\partial x_j + \rho f_i \qquad \ldots \text{ IV.19}$$

Now the problem is reduced to finding a relationship for a single scalar, the turbulent viscosity, instead of the six components of the Reynolds stress tensor. It is important to note that while the laminar viscosity, μ, is a fluid property, the turbulent viscosity is not, but instead is dependeant upon the structure of turbulence at the point of interest. Thus, μ_t is a field variable. The model used to specify μ_t defines it in terms of calculable quantities which are themselves field variables.

The model used here was the two equation, k-ε model proposed by Launder and Spalding [1974]. Two additional differential transport equations are introduced, one for the turbulent kinetic energy, k, and the other for the dissipation rate of turbulent kinetic energy, ε. After solution of these two new field variables, the turbulent viscosity can be found from the following relationship:

$$\mu_t = C_\mu \rho k^2/\varepsilon \qquad \text{... IV.20}$$

The differential equations that express the conservation of k and ε will now be presented. These equations can be developed from the momentum equation using the definitions of k and ε and appropriate manipulations. Consider first the turbulent kinetic energy equation from Launder and Spalding [1974].

$$\tilde{U}_i \partial k/\partial x_i = A + B - \varepsilon \qquad \text{... IV.21}$$

$$\text{where; } A = \frac{1}{\rho}\partial((\mu_t/\sigma_k)(\partial k/\partial x_i))/\partial x_i$$

$$B = \mu_t(\partial\bar{U}_i/\partial x_j + \partial\bar{U}_j/\partial x_i)\partial\bar{U}_j/\partial x_i$$

The left hand side contains the convective rate of change of turbulent kinetic energy. Recall that this is the total change since the temporal rate of change is zero in a steady state analysis. The right hand side of the equation contains the production and dissipation terms which result in the rate of change of k. A represents diffusion of turbulent kinetic energy into the elemental control volume. The terms shown by B are the production of turbulent kinetic energy by interaction of Reynolds stresses with the mean velocity gradients. ε is the dissipation, which is merely a sink for the kinetic energy of turbulence.

Note that the diffusion term contains a new diffusion coefficient, μ_t/σ_k, to model the diffusion rate of k. In general though, all the terms of the actual k balance equation have been modelled in terms of known quantities (i.e. the velocity field). Now, the dissipation equation can be presented.

$$\bar{U}_i \partial\varepsilon/\partial x_i = \frac{1}{\rho}\partial((\mu_t/\sigma_\varepsilon)(\partial\varepsilon/\partial x_i))/\partial x_i + \frac{\varepsilon}{k}(C_1\mu_t/\rho(\partial\bar{U}_i/\partial x_j - \partial\bar{U}_j/\partial x_i)\partial\bar{U}_j/\partial x_i - C_2\varepsilon^2/k) \qquad \text{... IV.22}$$

Again, the various terms have much the same significance as the k equation with the new diffusion coefficient now being, μ_t/σ_ε.

The important thing to note about these equations is that several empirical constants have been introduced whose values have been estimated through comparison of model predictions with available experimental data. This has been done by several investigators and the values generally agreed upon, and used in this study, are presented in Table IV.1.

C_μ	0.09
C_1	1.55
C_2	2.00
σ_k	1.0
σ_ε	1.3

Table IV.1 Empirical Constants (Launder, Spalding [1974])

The equation set describing the turbulent flow is now closed. Four equations (1 continuity, 3 momentum) were presented for the four original unknowns. In so doing, an additional unknown, the Reynolds stress tensor, was introduced. At this point, one must resort to empiricism and describe the Reynolds stress tensor in terms of an effective viscosity. The turbulent viscosity was in turn prescribed by solution of two turbulent field variables, k and ε. Eqn. IV.20 closes the set by describing μ_t in terms of k and ε.

IV.1.4. Boundary Conditions

Before any set of differential equations can be solved, it must be constrained by an appropriate set of boundary conditions. The following sections will present the modifications to the various transport equations to account for the presence of solid surfaces.

IV.1.4.1 Continuity Equation

The boundary conditions for the continuity equation are simply imposed by setting all mass fluxes across the solid boundary of any control volume to zero. This is done in all equations since the flux across control volume boundaries convects all dependent variables into and out of the control volume.

An exception to this practice obviously occurs where there is flow across the problem boundaries. This requires a modification to the mass flux allowed through the control volume faces on the peripheries of the solution domain. The technique used will now be discussed. The velocity profile at the inlet is a boundary condition which must be specified by the user. Once the inlet velocity profile is specified the appropriate fluxes are imposed upon all control volumes at the inlet. At the outlet the velocity profile is allowed to develop on its own and no predetermined distribution is imposed. The efflux from outlet boundary control volumes is calculated based on the velocity at the center of the control volume.

IV.1.4.2 Momentum Equations

There are two boundary conditions that must be imposed on the velocity field: the traditional zero penetration and zero slip conditions. The zero penetration condition is clearly enforced by suppressing the mass flux through all solid boundaries.

The zero slip condition is more complicated and must be applied in terms of a skin friction, τ, experienced by the fluid near the wall. The shear stress at the wall is deduced from the generalized log law as given by Spalding [1982].

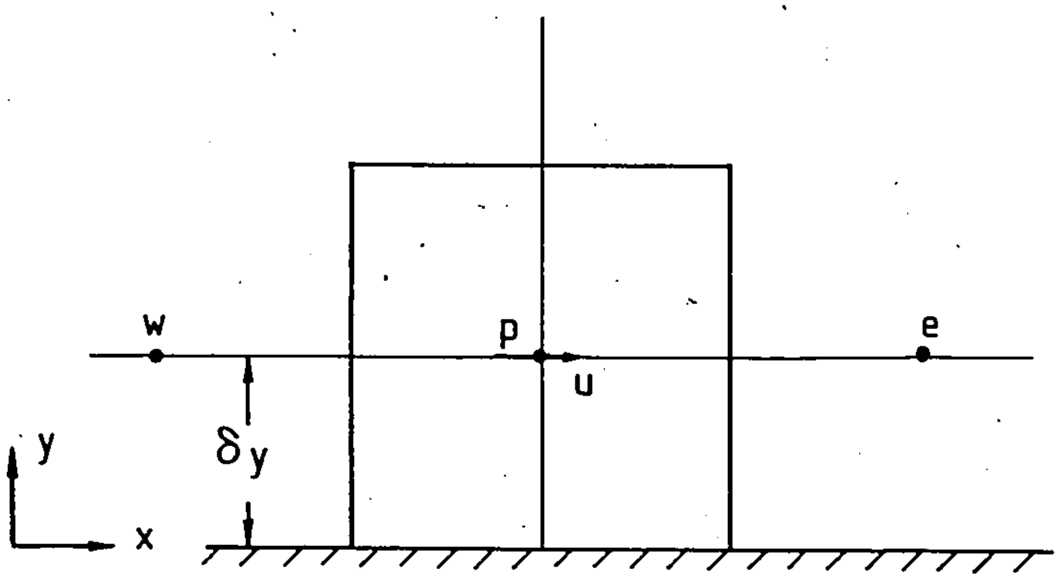

Figure IV.1 Momentum Boundary Conditions

$$\tau = \rho U_p C_\mu^{.25} \frac{\kappa k^{.5}}{\ln(E\rho C_\mu^{.25} k^{.5}/\mu^{.5})} \qquad \ldots \text{IV.23}$$

The shear stress in this equation can easily be converted to a force which acts as an additional source in the momentum equation for the appropriate control volume. E is a surface roughness parameter and is taken as 9.79 (Restivo [1979]). κ is von Karman's constant and is set at 0.350. Several investigators (Byrne [1970]) have determined its value and their results lie in the 0.343 to 0.418 range. A value of 0.350 gave good agreement with the overall axial pressure gradient and was within this range. Eqn. IV.23 is only valid for turbulent boundary layers so a check is done by the code to ensure turbulent conditions. Consider the following dimensionless parameter:

$$y^+ = C_\mu^{.25} k^{.5} \delta y \, \rho/\mu \qquad \ldots \text{IV.24}$$

For $y^+ > 11.63$, Eqn. IV.23 is valid (Chieng, Launder [1980]). When $y^+ < 11.63$ the shear stress is based on a simple linear calculation of the velocity gradient from the near-wall node point to the boundary resulting in the following shear stress expression:

$$\tau = \mu U_p/\delta y \qquad \ldots \text{IV.25}$$

In addition to introducing this extra source term, the convection of momentum across the solid boundary is suppressed by setting the mass flux across the solid boundary equal to zero.

IV.1.4.3 k and ε Equations

The value of the turbulent kinetic energy, k, at a near wall node point is calculated from the regular balance equation for the control volume with the assumption of zero diffusion to the wall. The value of the energy dissipation rate is fixed at that node point by the following:

$$\varepsilon_p = (C_\mu^{.75}/\kappa)*(k^{1.5}/\delta y) \qquad \text{... IV.26}$$

which is based on the hypothesis that the length scale of turbulence varies linearly with distance from the wall. Further explanation of these assumptions can be found in Launder and Spalding [1974].

IV.2 Numerical Solution

Now that the equation set describing the mathematical model has been established, a method of solving the equations must be developed. Since direct solution of such complex equations is not possible, a numerical solution must be attempted. A numerical solution to a differential equation consists of a set of numbers from which the distribution of the dependent variable can be reconstructed. The solution domain is divided into a three dimensional array of control volumes. Within each control volume resides a grid or node at which the value of the dependent variables are calculated. The governing differential equations must be integrated over these control volumes to yield algebraic equations containing the dependent variable at the current node and at neighboring nodes. This procedure yields a set of algebraic equations that must be solved simultaneously to give the value of the dependent variable in question at each node. If the original differential equation is non-linear the resulting algebraic equation will have to be linearized before a large set of them can be solved simultaneously. The finite difference procedure used to solve the current set of equations will now be detailed.

IV.2.1 Standard Form of Equations

Since there are essentially six differential equations to be solved (P,U,V,W,k,ε), it would be very convenient if they could be cast in a standard form. This would result in a much shorter code since the same simultaneous equation solving algorithm could be used for all six field variables. Since all six equations express the balance of some conservable quantity, it turns out that casting them in a standard form is not a problem.

Let the dependent variable in this general equation be ϕ. Now, the conservation of ϕ can be expressed by the following differential equation, taken from Patankar [1980].

$$\partial(\rho\phi)/\partial t + \mathrm{div}(\rho\bar{U}_i\phi) \hat{=} \mathrm{div}(\Gamma\ \mathrm{grad}\ \phi) + S \qquad \ldots\ \mathrm{IV.27}$$

Since a steady state solution is used in this study, the first term on the left hand side can be immediately dropped. The remaining terms have a very simple explanation. The second term on the left hand side is the rate of change of ϕ in the elemental control volume due to convection. It equals the net efflux of ϕ as it is carried by the flowing fluid. The first term on the right hand side is the transport of ϕ into the control volume by diffusion. The last term is a source term. Rewriting the equation as below;

$$\mathrm{div}(\rho \bar{U}_i \phi) - \mathrm{div}(\Gamma \mathrm{grad}\phi) = S \qquad \ldots \text{ IV.28}$$

it can be seen that the source of ϕ (R.H.S) is balanced by the flux of ϕ out of the contol volume (L.H.S.) by convection and diffusion. As a final step, IV.28 will be written in tensor form for further use.

$$\partial(\rho \bar{U}_i \phi)/\partial x_i - \partial(\Gamma \partial\phi/\partial x_i)/\partial x_i = S \qquad \ldots \text{ IV.29}$$

IV.2.2 Grid Layout

As a preamble to discussing the manner in which the equations just presented are discretized, and in order to clarify future references to the grid layout, a description of the grid will now be given.

The grid consists of a three dimensional rectangular layout of orthogonal grid lines with a node point at each intersection. There is no need for the grid lines to be equally spaced in any coordinate direction but they must remain parallel. In order to clarify the graphical representation of the grid, it will be presented here in two dimensions only. The third dimension is merely layers of 2-D grids such as the one depicted in Figure IV.2.

Figure IV.2(a) shows a typical grid with only the scalar nodes and control volumes shown. Note that the nodes can be nonuniformly spaced and therefore concentrated in the near wall region where the largest velocity gradients exist.

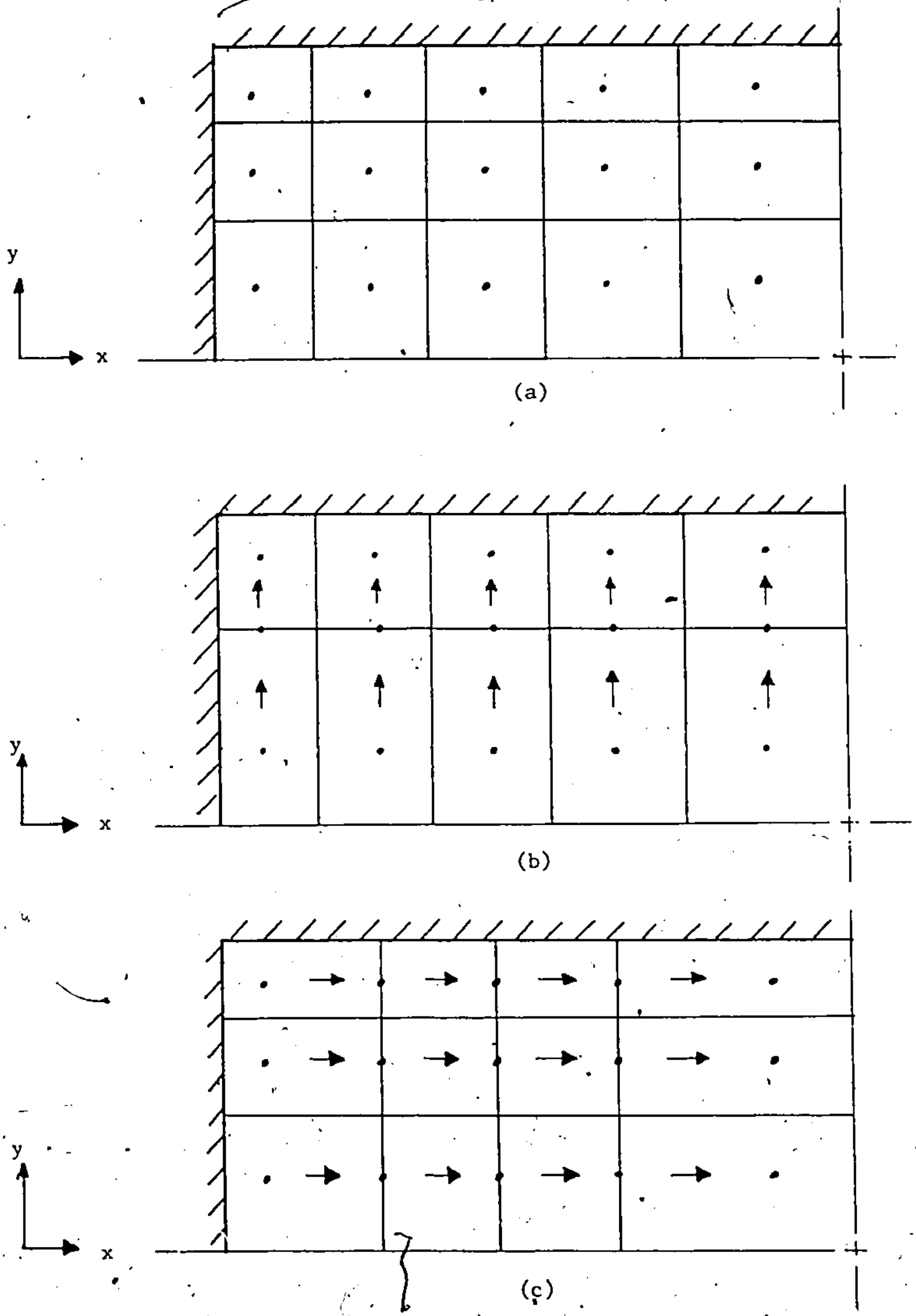

Figure IV.2 Grid Layout

The nodes shown in Figure IV.2(a) were referred to as "scalar" nodes since only the scalar dependent variables, namely P, k, and ε, are evaluated at these locations. The momentum nodes and control volumes are staggered with respect to the scalar grid. This practice was first used by Harlow and Welch [1965] and offers several advantages. The control volumes for each momentum component are staggered from the main scalar grid in the direction of the momentum component (i.e. u- control volumes staggered in x-direction, etc.). The staggering for the v and u components is shown in Figure IV.2(b) and IV.2(c). The w component is similarily arranged.

The first advantage to become apparent is that now the velocity is being calculated on the face of the scalar control volumes. This makes the convection flux terms, (C's), in the scalar transport equations directly available and eliminates the need for an interpolation. Similarly, the pressure is now known on the face of the momentum control volumes so that when evaluating the source terms for the momentum equations the nodal pressures can be used directly. These advantages eliminate some very serious problems which arise if all dependent variables had been evaluated on the same grid. The reader is referred to Patankar [1980] for a complete discussion.

IV.2.3 Discretization

IV.2.3.1 General

The general differential equation can now be discretized on the finite difference grid by integrating it over a typical control volume. Consider the finite difference control volume for a Cartesian coordinate system as shown in Figure IV.3. In addition to the coordinate rosette, the control volume faces are labelled north, south, east, west, up and down. Frequent reference to these names will be made when talking about the various faces and the letters n, s, e, w, u, and d will often be used as subscripts to indicate where various terms are to be evaluated. For the following discussion of differencing schemes it is useful to assume that all control volume faces are exactly half way between node points. Such a uniform grid is not a requirement, but it makes the discussion much simpler since there is no need to introduce complex weighting functions based on grid spacing.

At this point a note about the subscript convention to be followed is also in order. Lower case subscripts refer to values at the neighbor node points while upper case subscripts refer to values at the control volume faces. As will be seen later this is an important distinction.

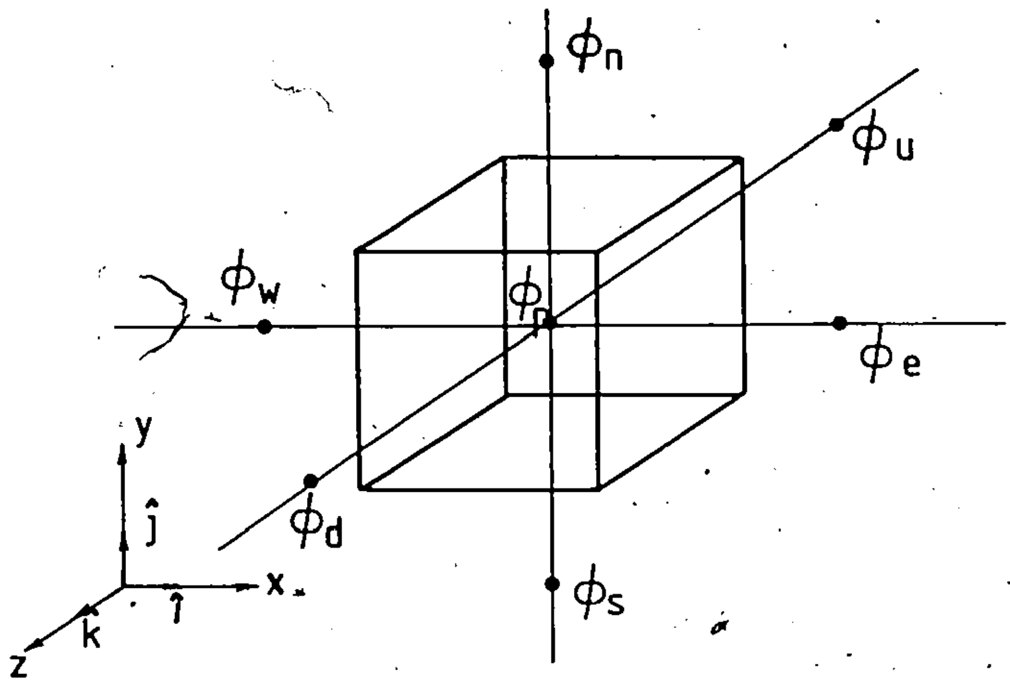

Figure IV.3 Control Volume Nomenclature

Begin by integrating Eqn. IV.29 over the control volume as below.

$$\iiint \partial(\rho \bar{U}_i \phi - \Gamma \partial\phi/\partial x_i)/\partial x_i \, dV = \iiint S \, dV \qquad \text{... IV.30}$$

The left hand side can be simplified from a volume integral to a surface integral by the use of Gauss's theorem as stated in Wylie [1971] as,

$$\iiint (\nabla\cdot F_i)dV = \iint (F_i\cdot\hat{n})dS \quad \ldots \text{IV.31}$$

So, consider the left hand side of Eqn. IV.30 as

$$= \iint (\rho U_i\phi - \Gamma\partial\phi/\partial x_i)\cdot\hat{n}\, dS \quad \ldots \text{IV.32}$$

Expanding the dot produot gives,

$$\begin{aligned} = &\iint (\rho U\phi-\Gamma\partial\phi/\partial x)_E dydz - \iint (\rho U\phi-\Gamma\partial\phi/\partial x)_W dydz \\ &+\iint (\rho V\phi-\Gamma\partial\phi/\partial y)_N dxdz - \iint (\rho V\phi-\Gamma\partial\phi/\partial y)_S dxdz \\ &+\iint (\rho W\phi-\Gamma\partial\phi/\partial z)_D dxdy - \iint (\rho W\phi-\Gamma\partial\phi/\partial z)_U dxdy \end{aligned} \quad \ldots \text{IV.33}$$

Carry out the integration remembering the subscript convention and obtain,

$$\begin{aligned} &(\rho U_E\phi_E-\Gamma(\phi_e-\phi_p)/\delta x)A_E - (\rho U_W\phi_W-\Gamma(\phi_p-\phi_w)/\delta x)A_W \\ &+(\rho V_N\phi_N-\Gamma(\phi_n-\phi_p)/\delta y)A_N - (\rho V_S\phi_S-\Gamma(\phi_p-\phi_s)/\delta y)A_S \\ &+(\rho W_D\phi_D-\Gamma(\phi_d-\phi_p)/\delta z)A_D - (\rho W_U\phi_U-\Gamma(\phi_p-\phi_u)/\delta z)A_U \\ &\qquad = \iiint S\, dV \end{aligned} \quad \ldots \text{IV.34}$$

where A indicates the various control volume face areas.

Note that to express the gradient $\partial\phi/\partial x_i$, required for the diffusion term, a simple linear piecewise profile of ϕ between the point, p, and its appropriate neighbor was assumed. It is another matter to evaluate ϕ at the interface (needed for the convection term) and, as yet, these remain with upper case subscripts (indicating they are evaluated at C.V. faces). To simplify the expression, define the convection and diffusion flux terms as follows:

$$D = \Gamma/\delta x \qquad \text{... IV.35}$$

and

$$C = \rho U \qquad \text{... IV.36}$$

With this notation, Eqn. IV.34 becomes,

$$\begin{aligned}
&(C_E\phi_E - D_E(\phi_e - \phi_p))A_E - (C_W\phi_W - D_W(\phi_p - \phi_w))A_W \\
&+(C_N\phi_N - D_N(\phi_n - \phi_p))A_N - (C_S\phi_S - D_S(\phi_p - \phi_s))A_S \\
&+(C_D\phi_D - D_D(\phi_d - \phi_p))A_D - (C_U\phi_U - D_U(\phi_p - \phi_u))A_U \\
&= \iiint S dV
\end{aligned} \qquad \text{... 4 .37}$$

Recall that the result of the discretization procedure is to be a set of linear algebraic equations for each of the unknowns in the problem. At this point, each unknown is represented by the general variable, ϕ. Assuming the solution domain is divided into n control volumes, a system of n linear equations in the n unknown nodal values of ϕ is required for a closed solution. This set of equations is obtained by writing an equation like IV.37 for each control volume.

In order to evaluate the dependent variables at the control volume faces, some assumption about the variation of the dependent variables between node points is required. Regardless of what this assumption is, the expression for ϕ at a control volume face will contain as unknowns both ϕ at the control volume under consideration and ϕ within the neighbor control volume to which the face is common. The manner in which these interface values are specified is often called the differencing scheme. When this differencing scheme is substituted into Eqn. IV.37 and the equation is appropriately rearranged, ϕ_p can be expressed as a linear combination of ϕ at its six neighboring nodes and the source term, as in Eqn. IV.38. A differencing scheme, then, provides the link between Eqns. IV.37 and IV.38 and is the expression of a_n, a_s etc. in terms of the convection and diffusion fluxes (C's and D's).

$$a_p\phi_p = a_e\phi_e + a_w\phi_w + a_n\phi_n + a_s\phi_s + a_u\phi_u + a_d\phi_d + \iiint SdV \quad \text{... IV.38}$$

A system of equations such as Eqn. IV.38 written for each nodal point can be solved simultaneously to find all of the ϕ's.

Recall that there are two types of flux terms in Eqn. IV.37; convective and diffusive. The relative strength of the convection and diffusion is a very important parameter in selecting a differencing scheme. The Peclet number, Pe, is a dimensionless group which expresses the ratio of convection to diffusion and is defined in Eqn. IV.39.

$$Pe = \rho U\delta x/\Gamma \quad \text{... IV.39}$$

IV.2.3.2 Central Differencing

The most obvious choice for a differencing scheme would be a linear interpolation at the control volume face from the two adjacent node points. This is termed the central differencing scheme and is the natural outcome of a Taylor series expansion. The following expressions state the neighbor coefficient in terms of the various diffusion and convection fluxes:

$$
\begin{aligned}
a_e &= D_E - C_E/2 \\
a_w &= D_W + C_W/2 \\
a_n &= D_N - C_N/2 \\
a_s &= D_S + C_S/2 \\
a_d &= D_D - C_D/2 \\
a_u &= D_U + C_U/2 \\
a_p &= a_e + a_w + a_n + a_s + a_u + a_d + \\
&\qquad (C_E - C_W + C_N - C_S + C_D - C_U) \qquad \ldots \text{IV.40}
\end{aligned}
$$

These expressions can be easily verified by substituting expressions such as $\phi_N = 1/2(\phi_n + \phi_p)$ into Eqn. IV.37 and rearranging the result to fit Eqn. IV.38.

Although this scheme seems intuitively attractive, its practical implementation results in some serious problems for many situations. In order to illuminate the major problem with this method, again consider Eqn. IV.38 and apply some physical reasoning to the meaning of the neighbor coefficients. These neighbor coefficients are basically weighted factors which express ϕ as some appropriate linear combination of all its neighbors.

Since the process expressed by the original general differential equation (Eqn. IV.27) is one of convection and diffusion, it follows that all of these coefficients must be positive. In effect, this is saying that an increase in ϕ at some neighboring point can only cause ϕ_p to increase, with all other factors remaining unchanged. Therefore, the neighbor coefficients must always be positive. To cite a physical example, consider a solid body and let the dependent variable be temperature. An increase in temperature at one point in the body can only cause neighboring points to increase in temperature and can not cause them to become cooler.

Returning to the central difference formulas given by Eqn. IV.40, it can be seen that the coefficients can easily become negative. In addition to the violation of logic just mentioned above, negative coefficients tend to make the equation set numerically unstable. These are unacceptable hazards and render the scheme useless except in cases where the conditions are such that positive coefficients are assured.

IV.2.3.3 Upwind Differencing

In order to formulate a more appropriate scheme, the source of the problem in the central difference scheme should be pinpointed. Note that the diffusion term (D_e, D_w, etc.) is always positive (see Eqns. IV.35 and IV.36), whereas the sign of the convection term (C_e, C_w, etc.) depends on the sign of the velocity. Therefore, it is the convection term which has the potential to make the coefficients expressed in Eqns. IV.40 become negative. If the convection is of the appropriate sign and at least twice as big as the diffusion term, a negative coefficient will result. This is serious indeed because convection is very dominant in fluid flow problems.

A remedy for this problem is the upwind differencing scheme. The diffusion term is left unaffected but it is recognized that a simple linear interpolation at the interface is not realistic for the convected property. This scheme sets the interface value of the convected property, ϕ, equal to ϕ at the "upwind" grid point. This is intuitively attractive since one would expect that, especially for strongly convective flows (i.e. high Pe), the interface value would be much closer to the upstream neighbor and would not be influenced very much by the downstream value.

In application, the consequences of this formulation give expressions for the neighbor coefficients as follows:

$$
\begin{aligned}
a_e &= D_E + [-C_E,0] \\
a_w &= D_W + [C_W,0] \\
a_n &= D_N + [-C_N,0] \\
a_s &= D_S + [C_S,0] \\
a_d &= D_D + [-C_D,0] \\
a_u &= D_U + [C_U,0] \\
a_p &= a_e + a_w + a_n + a_s + a_u + a_d + \\
&\qquad (C_E - C_W + C_N - C_S + C_D - C_U) \qquad \ldots \text{ IV.41}
\end{aligned}
$$

Note that the square bracket operator $[C_W,0]$ indicates the maximum of C_W and 0. It is clear that this scheme cannot result in any negative coefficients as plagued the central difference scheme. Recall, however, that the formulation of the diffusion term remained unchanged and is therefore still calculated based on a linear piecewise profile of ϕ . This leads to overestimation of diffusion by this scheme for large values of Peclet number.

IV.2.3.4 Hybrid Differencing

To overcome the difficulties of the previous two formulations and provide a method for a large range of Peclet numbers, a scheme was developed (Spalding [1972]) which is essentially a combination of the two schemes already described. Each of these schemes is only effective for a certain range of Peclet numbers. The central difference scheme is valid in the low Peclet number range while the upwind scheme becomes more effective for high Peclet numbers. The hybrid scheme is formulated such that for $-2 < Pe < 2$ it reduces to the central difference scheme, while for $Pe < -2$ or $Pe > 2$ it is equivalent to the upwind scheme with the diffusion term set to zero. This removes the difficulty mentioned earlier with the upwind scheme and does not adversely affect the results since it is only applied for high Pe situations. The formulation of the hybrid scheme is given by following relationships:

$$a_e = [-C_E, D_E - C_E/2, 0]$$
$$a_w = [C_W, D_W + C_W/2, 0]$$
$$a_n = [-C_N, D_N - C_N/2, 0]$$
$$a_s = [C_S, D_S + C_S/2, 0]$$
$$a_d = [-C_D, D_D - C_D/2, 0]$$
$$a_u = [C_U, D_U + C_U/2, 0]$$

$$a_p = a_e + a_w + a_n + a_s + a_u + a_d + (C_E - C_W + C_N - C_S + C_D - C_U) \qquad \text{... IV.42}$$

Because of its applicability to a large range of Pe numbers and its relative computational efficiency, this is the scheme used in this study.

IV.2.3.5 Source Terms

Now that a scheme for specifying the neighbor coefficients has been chosen, the source term in Eqn. IV.37 should be considered. Very often, the source term is a function of the dependent variable, ϕ. However, the algebraic equation set must be linear so only a linear dependence of S on ϕ can be accommodated. If the true relationship is non-linear, it must be linearized. The linearized form of the source term is given by,

$$S = S_p\phi + S_u \qquad \text{... IV.43}$$

where S_u is the constant term and S_p the linear term. With the source term linearized, the general algebraic difference equation becomes:

$$a_p\phi_p = \sum a_n\phi_n + S_u \qquad \text{... IV.44}$$

where n denotes each neighbor.

$$a_p = \sum a_n - S_p \qquad \text{... IV.45}$$

The source terms for the various transport equations essentially consist of all terms which cannot fit into the convection and diffusion terms of the standardized equation (Eqn. IV.29). The next section will deal with the problem of casting the various conservation equations into the standard form and will further illustrate the source term formulation.

IV.2.3.6 Fitting the Standard Form

The x-momentum equation will be used to illustrate the procedure of casting the various transport equations into the standard form. After this is done, the standardized form of five of the equations will be presented in tabular form. The sixth equation, continuity, is a special case and will be considered in Section IV.2.4.

Consider Eqn. IV.19 written for the x component of momentum as below;

$$\rho\bar{U}_i \partial U/\partial x_i = -\partial\bar{P}/\partial x + \partial(\mu\partial U/\partial x_i + \mu\partial\bar{U}_i/\partial x + \mu_t\partial U/\partial x_i + \mu_t\partial\bar{U}_i/\partial x)/\partial x_i + \rho f_x \quad \ldots \text{IV.46}$$

rearrange as shown;

$$\partial(\rho\bar{U}_i U)/\partial x_i - \partial((\mu+\mu_t)\partial U/\partial x_i)/\partial x_i = -\partial\bar{P}/\partial x + \rho f_x + \partial((\mu+\mu_t)\partial\bar{U}_i/\partial x)/\partial x_i \quad \ldots \text{IV.47}$$

Comparing this to Eqn. IV.29 it can be seen that;

$$\phi = U$$

$$\Gamma = \mu + \mu_t = \mu_{eff}$$

$$S = -\partial\bar{P}/\partial x + \rho f_x + \partial(\mu_{eff}\partial\bar{U}_i/\partial x)/\partial x_i$$

Now, to complete the discretization, the volume integral for the source term (See Eqn. IV.37) must be performed.

$$\iiint SdV = \iiint [-\partial\bar{P}/\partial x + f_x + \partial(\mu_{eff}\partial U/\partial x)/\partial x + \partial(\mu_{eff}\partial V/\partial x)/\partial y$$
$$+ \partial(\mu_{eff}\partial W/\partial x)/\partial z]\, dxdydz$$

$$= (P_W - P_E)A_E + \rho g_x \cdot Vol + \iint(\mu_{eff}\partial U/\partial x)_E dydz - \iint(\mu_{eff}\partial U/\partial x)_W dydz$$
$$+ \iint(\mu_{eff}\partial V/\partial x)_N dxdz - \iint(\mu_{eff}\partial V/\partial x)_S dxdz + \iint(\mu_{eff}\partial W/\partial x)_D dxdy$$
$$- \iint(\mu_{eff}\partial W\partial\ x)_U dxdy$$

$$= (P_W - P_E)A_E + \rho g_x \cdot Vol + (\mu_{eff}\partial U/\partial x)_E A_E - (\mu_{eff}\partial U/\partial x)_W A_W$$
$$+ (\mu_{eff}\partial V/\partial x)_N A_N - (\mu_{eff}\partial V/\partial x)_S A_S$$
$$+ (\mu_{eff}\partial W/\partial x)_D A_D - (\mu_{eff}\partial W/\partial x)_U A_U \qquad \text{... IV.48}$$

In this equation, P_E and P_W are the pressures on the east and west faces of the control volume respectively. Recall that an interpolation scheme had to be used to express ϕ at a control volume face in terms of ϕ_p and neighboring ϕ's. However, as was seen in Section IV.2.2, the use of a staggered grid makes the pressure on the momentum control volume faces directly available.

Table IV.2 tabulates all parameters required to cast five of the conservation equations into standard form.

ϕ	Γ	S_p	S_u
U	μ_{eff}	0	$(P_W-P_E)A_E+\rho g_x\cdot Vol$ $+\ (\mu_{eff}\partial U/\partial x)_E A_E-(\mu_{eff}\partial U/\partial x)_W A_W$ $+\ (\mu_{eff}\partial V/\partial x)_N A_N-(\mu_{eff}\partial V/\partial x)_S A_S$ $+\ (\mu_{eff}\partial W/\partial x)_D A_B-(\mu_{eff}\partial W/\partial x)_U A_U$
V	μ_{eff}	0	$(P_S-P_N)A_N+\rho g_y\cdot Vol$ $+\ (\mu_{eff}\partial U/\partial y)_E A_E-(\mu_{eff}\partial U/\partial y)_W A_W$ $+\ (\mu_{eff}\partial V/\partial y)_N A_N-(\mu_{eff}\partial V/\partial y)_S A_S$ $+\ (\mu_{eff}\partial W/\partial y)_D A_D-(\mu_{eff}\partial W/\partial y)_U A_U$
W	μ_{eff}	0	$(P_U-P_D)A_U+\rho g_z\cdot Vol$ $+\ (\mu_{eff}\partial U/\partial z)_E A_E-(\mu_{eff}\partial U/\partial z)_W A_W$ $+\ (\mu_{eff}\partial V/\partial z)_N A_N-(\mu_{eff}\partial V/\partial z)_S A_S$ $+\ (\mu_{eff}\partial W/\partial z)_D A_D-(\mu_{eff}\partial W/\partial z)_U A_U$
k	μ_t/σ_k	$-C_\mu \rho^2 k\cdot Vol/\mu_{eff}$	$\mu_{eff}\cdot Vol(2((\partial U/\partial x)^2+(\partial V/\partial y)^2$ $+\ (\partial W/\partial z)^2)+(\partial U/\partial y+\partial V/\partial x)^2$ $+\ (\partial V/\partial z+\partial W/\partial y)^2+(\partial U/\partial z+\partial W/\partial x)^2$
ε	μ_t/σ_ε	$-C_2\rho\varepsilon\cdot Vol/k$	$\rho C_1 C_\mu\ k\cdot Vol(2((\partial U/\partial x)^2+(\partial V/\partial y)^2$ $+\ (\partial W/\partial z)^2)+(\partial U/\partial y+\partial V/\partial x)^2$ $+\ (\partial V/\partial z+\partial W/\partial y)^2+(\partial U/\partial z+\partial W/\partial x)^2$

Table IV.2 Summary of Conservation Equations

IV.2.4 Pressure Correction

For the three momentum equations, one of the major components of the source term just described is the pressure force. However, the pressure field is unknown and therefore the source terms for solving the three momentum equations can not be accurately evaluated at first. Instead it is necessary to solve the velocity field (via the three momentum equations) using an assumed pressure field. If this pressure field were correct, the resulting velocity field would satisfy continuity. Before the result converges, however, the velocity field will violate continuity. To correct for continuity, and drive both the velocity and pressure fields towards convergence, a pressure correction scheme as described by Patankar [1980] was used. Since no explicit equation exists for pressure, the continuity equation is reformulated so that the independent variable becomes a pressure correction term. This pressure correction is the pressure that must be added to the current pressure to arrive at the correct pressure field. From this pressure correction, velocity corrections can be applied to the velocity field which adjust it to satisfy continuity. The derivation of the pressure correction equation will now be outlined.

Consider the following:

$$P = P^{o} + P' \qquad \text{... IV.49}$$

where P is the actual pressure, P^{o} is the pressure during the current iteration and P' is the required pressure correction. Similarly, velocity corrections can be formulated as follows:

$$U = U^{o}+U' \qquad \text{... IV.50}$$

$$V = V^{o}+V' \qquad \text{... IV.51}$$

$$W = W^{o}+W' \qquad \text{... IV.52}$$

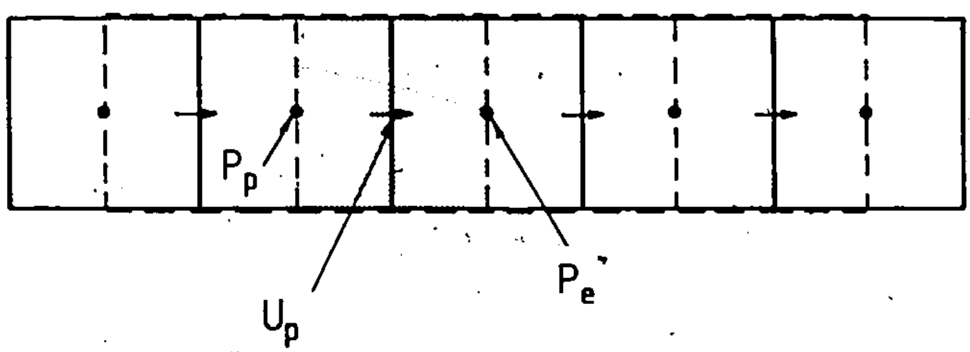

Figure IV.4 Pressure Correction Scheme

Referring to Figure IV.4, consider the x-momentum equation as written for the shaded x-momentum control volume,

$$(\sum a_n - S_p)U_p = \sum a_n U_n + A(P_p - P_E) + b \qquad \ldots \text{ IV.53}$$

where A = control volume face area.

P_p = pressure on west face of shaded C.V.

P_E = pressure on east face of shaded C.V.

b = other source terms.

Note that $A(P_p-P_E)$ is simply the static pressure part of the source term and has the units of force as would be expected.

Now substitute Eqn. IV.49 into IV.53

$$(\sum a_n - S_p)U_p = \sum a_n U_n + A(P_p^o - P_p' - P_E^o + P_E') + b \qquad \ldots \text{ IV.54}$$

Also, substitute the old conditions, P^o and U_p^o, into IV.53 to get,

$$(\sum a_n - S_p)U_p^o = \sum a_n U_n^o + A(P_p^o - P_E^o) + b \qquad \ldots \text{ IV.55}$$

Now, subtracting IV.55 from IV.54 yields,

$$(U_p - U_p^o)(\sum a_n - S_p) = \sum (U_n - U_n^o) + A(P_p' - P_E') \qquad \ldots \text{ IV.56}$$

In order to cast the present equation into the standard form, recognize that at convergence,

$$U_n = U_n^o$$

so that,

$$(U_p - U_p^o)(\sum a_n - S_p) = A(P_p' - P_E') \qquad \text{... IV.57}$$

and

$$U_p = U_p^o + DU(P_p' - P_E') \qquad \text{... IV.58}$$

$$DU = A/(\sum a_n - S_p) \qquad \text{... IV.59}$$

This is a velocity correction formula and is used to correct the current velocity, U_p^o, to a velocity field which will satisfy continuity, U_p. Before it can be applied, the pressure corrections, P_p' and P_E' must be found. An equation, in the standard form, with P' as the dependent variable is formed by considering the continuity equation as follows:

$$(\rho UA)_W - (\rho UA)_E + (\rho VA)_S - (\rho VA)_N + (\rho WA)_U - (\rho WA)_D = 0 \qquad \text{... IV.60}$$

Now an equation of the form of IV.58 can be written for each of U_w, U_e, V_n, V_s, W_u, and W_d and substituted into IV.60 to get,

$$P_p'(\sum a_n - S_p) = \sum a_n P_n' + S_u \qquad \text{... IV.61}$$

where,

$$a = \rho A.DU$$

This equation fits the standard form of the discretized finite difference equation and has the pressure correction term, P', as the unknown. It essentially replaces the continuity equation in the equation set. The method with which it is applied will be detailed in the next section where the solution scheme is described.

IV.2.5 Solution Scheme

The sequence in which the various equations are solved and pressure corrections applied follows the SIMPLE (Semi-Implicit Method for Pressure Linked Equations) algorithm as described by Patankar and Spalding [1972]. The important item to note is that this procedure does not involve a simultaneous solution of all unknowns at once. Instead, it solves each field variable separately in a sequence which is designed to promote convergence. Note that during the solution of one of the field variables, many of the other unknown field variables exist in the linear coefficients of the discretized equations. In fact, in the case of the momentum equations, which are truly nonlinear, the old value of the dependent variable itself must appear in the coefficient in order to linearize the equations. This is already taken care of in the derivation of the generalized difference equation since when the dependent variable, ϕ, is one of the momentum components (say x-momentum), ϕ is equal to U, the specific momentum (momentum per unit mass). U already appears in the convection component of the coefficients so the equations are non-linear.

Additional non-linearity is introduced by the effective viscosity hypothesis. The local viscosity becomes dependent on the velocity field and therefore introduces further coupling between the dependent variable and its linear coefficients in the algebraic difference equations.

Because of the non-linearity, an iterative solution procedure is required. The coefficients must be calculated based on current knowledge of the velocity and viscosity fields. The linearized equations are then solved to give updated velocity fields. At convergence there will be little or no change in the newly calculated velocities as compared to those from the previous iteration.

The following step by step solution procedure embodies the SIMPLE algorithm:

1. Guess pressure field.
2. Solve momentum equation for U, V, and W.
3. Solve pressure correction equation for P' field.
4. Correct pressure field (Eqn. IV.49).
5. Correct velocity field (Eqn. IV.58).
6. Solve for k and ε fields.
7. Recalculate μ_t based on k and ε.
8. Return to step 2 unless convergence has been attained.

IV.2.6 Convergence Criterion

The convergence of each of the six dependent variables is monitored by calculating a residual source at each iteration and iterating until these residuals are driven to an acceptably low value. Expressing the residual source for a single control volume in terms of the general discretization equation, the following is obtained:

$$R_\phi = a_p\phi_p - \sum a_n\phi_n - S_u \qquad \text{... IV.62}$$

As this equation indicates, the residual is merely the imbalance in the left and right sides of the difference equation. The residual is summed over all control volumes to arrive at the residual for each dependent variable. As the solution procedes, these residuals are monitored. If they become erratic or begin to grow, the solution is aborted by allowing a maximum number of iterations. An acceptable residual is specified and when all residuals are below it, a successful solution is declared.

IV.2.7 Linear Equation Solver

The solution procedure just described requires the services of a linear equation solving algorithm for successful implementation. Since all equations were cast in a standard form, the same equation solver can be used for all six field variables. During the course of a typical solution, this algorithm will be called many times so it is important that it be as efficient as possible. It is also important to recall that during the solution, all of the linear coefficients being passed to the routine are based on guesses or unconverged solutions (ie. they are only estimates). Therefore, the benefits of using a sophisticated equation solver which will provide an exact solution must be carefully evaluated. The additional time for an algorithm which would find an exact solution to the "wrong" set of equations is not justified. Instead a faster, more convenient, solution procedure is used.

One of the fastest linear equation solving algorithms available is the tri-diagonal matrix algorithm or TDMA (Burden et. al. [1978]) This technique demands a tri-diagonally banded coefficient matrix in order to be implemented. This means that although the equation set can be as large as required, there can only be three unknowns per equation (ie. only three non zero members in each row of the coefficient matrix). It must also be possible to arrange the equations such that these non-zero coefficients lie along the diagonal.

Recall that in a three-dimensional problem, as is being considered here, each node has six neighbors. Therefore, each equation will have seven unknowns. In order to solve them using the TDMA algorithm, four of the terms involving unknowns are evaluated using values from the previous iteration and moved to the right hand side with the other source terms. This simplification adds an extra degree of implicitness to the solution and yields only an approximate solution. However, as discussed, the consequences of this are not so drastic since the coefficients themselves are only approximations. In addition, the error introduced at convergence will be practically zero since the changes in the dependent variable will be very small. Therefore, this approximate method will not affect the final answer, but will increase the execution speed greatly.

In order to reduce the effects of this approximation, a system of sweeping the solution over the three dimensional solution domain is implemented. The three dimensional matrix of control volumes is considered one plane at a time. As a plane is isolated, terms involving unknowns in the two neighboring planes are evaluated with old values and moved into the constant term. After this, each line in the plane is considered in turn. As a line is removed, two additional neighbors are moved to the constant term. At this stage, the algebraic difference equations for any control volume in the line contain only three unknowns and are ready for the TDMA algorithm. This procedure is often called a line by line solution.

For the current program the following sweeping philosophy is used. For all dependent variables except the pressure correction, the coefficients are assembled one plane at a time for each successive K plane (plane perpendicular to the z-axis) marching in the downstream direction. For each plane, a line by line solution is performed in both the I and J directions. This line by line procedure is repeated a few times to give a more accurate solution for the current plane. The number of sweeps can be adjusted to give an optimally fast and accurate solution.

For the pressure correction equation, all of the coefficients for the whole solution domain are determined before the TDMA algorithm is called.

This distinction is based on the fact that the pressure equation is elliptic while the others are hyperbolic. For the hyperbolic equations, the velocities at any K-plane are largely independent of the downstream plane, so the marching technique is adequate. However, for the pressure equation, this independence does not exist and so a line by line sweep is repeated in all three coordinate directions for a prescribed number of repetitions. It is beneficial to repeat the sweeping procedure more times for the pressure correction equation and obtain a more refined solution since the source terms in the other equation depend so heavily on an accurate pressure field.

IV.3 The FAITH Code

The numerical procedure described in the previous sections was implemented in the FORTRAN computer code FAITH (Flow Analysis In THree dimensions). The original version of this code was the TEACH3D program obtained from Imperial College which is discussed in the Ph.D. thesis of Restivo [1979]. Most of the code's numerics have become apparent through previous discussions, but a short explanation of its organization, features and some of the modifications made since its aquisition as TEACH3D, will be given.

IV.3.1 General Code Organization

The organization of the code is shown by the flow chart in Figure IV.5. The program flow generally follows the SIMPLE algorithm as described in Section IV.2.5.

To begin, the main program initializes the grid and reads the inlet velocity profile. The inlet values of the turbulent kinetic energy and dissipation rate are calculated from the inlet velocity and an assumed turbulent intensity of 3%. Measurements by Byrne et. al. [1970] indicated velocity profiles for developing turbulent flows in parallel walled ducts to be quite insensitive to the inlet turbulent intensity. After calling a subroutine named INIT to calculate the coordinates of the staggered grids and all control volume dimensions, the executive program begins the main iteration loop.

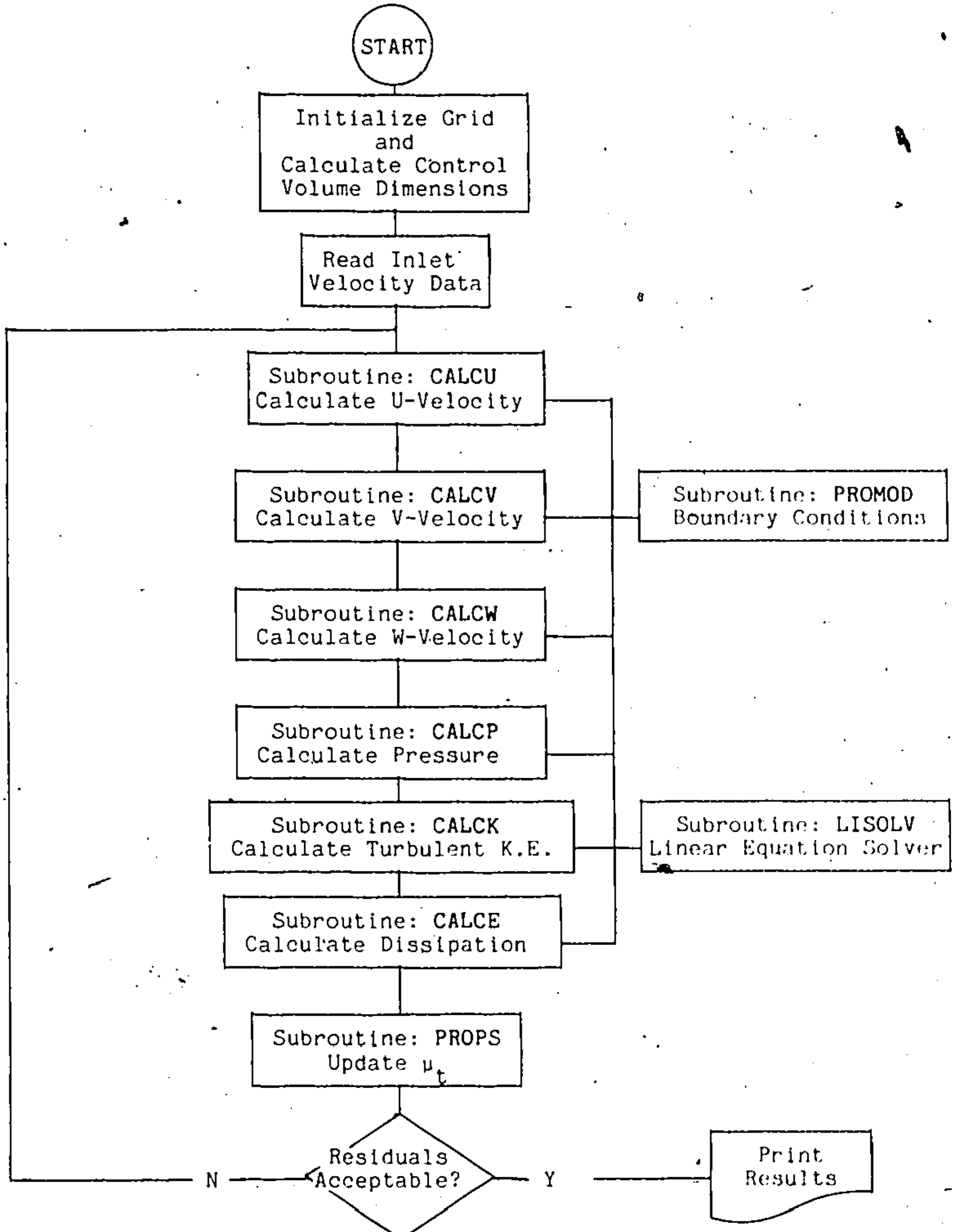

Figure IV.5 FAITH Code Flowchart

Each dependent variable is solved by a seperate subroutine. These subroutines have the same form so only a general discussion will be given here. A flowchart of one such subroutine is shown in Figure IV.6. Their purpose is to assemble the coefficients of the linearized solution matrix.

Referring to Figure IV.6, observe that each K-plane is considered in turn. For each K-plane the control volumes are considered by looping through rows of constant I and for each such row, through the range of J. Once a control volume is isolated in this manner, the six neighbor coefficients are calculated based on the convection and diffusion fluxes at their surfaces and the hybrid differencing scheme, as discussed in Section IV.2.3.4. At this stage, the two components of the source term (S_p and S_u) are calculated as outlined in Section IV.2.3.5. This procedure is repeated for all control volumes in the current K-plane.

Now, in order to account for the effect of the walls, a special subroutine (PROMOD) is called to augment the source terms. This subroutine basically enforces the boundary conditions as described in Section IV.1.4. There is only one PROMOD subroutine but it has a seperate entry point for each dependent variable.

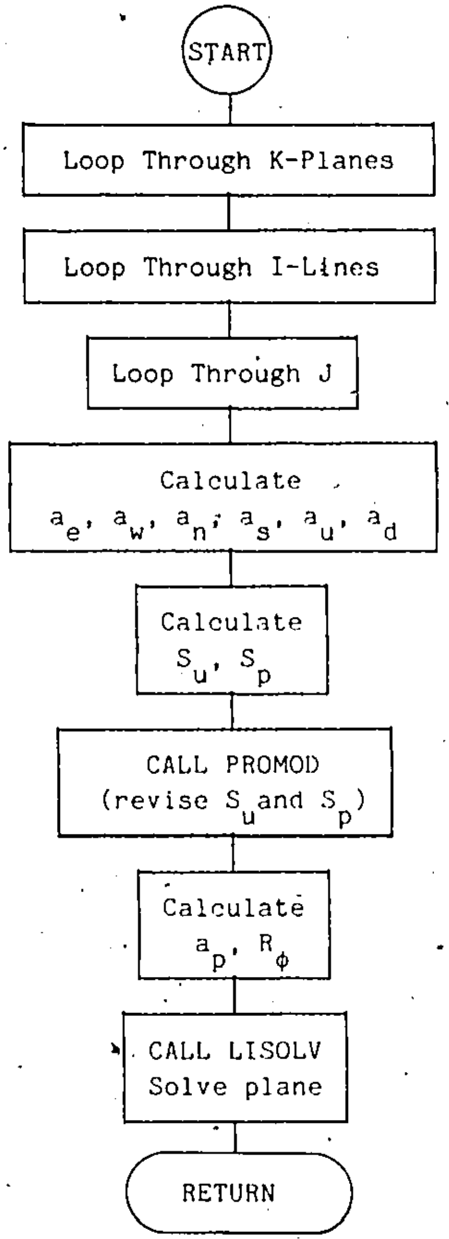

Figure IV.6 Coefficient Assembly Flowchart

Once the neighbor coefficients and source terms have been calculated for the current K-plane, the point coefficients, a_p, and the monitoring residual R_ϕ (see Section IV.2.6) can be calculated. Then the plane is sent to the tri-diagonal matrix linear equation solving routine, LISOLV, to calculate the updated value of the dependent variables for that plane. The whole procedure is then repeated for the next K-plane.

It is important to note that this plane by plane marching takes place in the downstream direction. This makes use of the hyperbolic nature of the U, V, W, k, and ε equations. Since hyperbolic equations make the dependent variable more heavily dependent on upstream neighbors, marching in the downstream direction will enhance convergence by calculating the neighbor coefficients with new values of the dependent variable in the upstream plane.

As mentioned before, the pressure correction equation is an exception to this since it is elliptic. To account for this, the procedure just described is altered. Instead of calling the TDMA algorithm for each plane, the coefficients for all planes are calculated first and LISOLV is called only once for the whole solution domain.

After all six dependent variables are solved, the new viscosity field is calculated by the subroutine PROPS. Then control is returned to the executive program where it checks if all six R_ϕ's are below an acceptable limit. If they are not the program returns to the top of the iteration loop and the dependent variables are recalculated. If a good solution has been reached the program prints out the results.

IV.3.2 Inlet and Outlet Conditions

Several changes had to be made to the code to make it applicable to subchannel problems. In the form that it was first received, the code was used for studying the flow distribution of air in a ventilated room. This meant that the regions where flow entered and exited the geometry were restricted to quite small areas. In subchannel and duct problems inlet and outlet generally cover the entire cross section at the ends of the geometry. Changes had to be made to the PROMOD subroutine to accommodate this.

In the original code there was no provision to specify the profile of the inlet velocity, only a single mean velocity could be specified. This was a very important feature so revisions were made to allow specification of the velocity profile at the inlet. This essentially allows the user to define a different velocity at each node point on the inlet plane.

A similar revision had to be made at the outlet. Originally a single outlet velocity, calculated to conserve mass, was imposed on all control volumes in the outlet plane. For duct problems, however, it is vital that a proper outlet velocity profile be allowed to develop or the flow near the outlet will be erroneously distorted.

IV.3.3 Flow Blockages

One of the major restrictions involved in applying the finite difference procedure is that irregular geometries are extremely difficult to model. In this study, all surfaces are parallel to the grid lines but some control volumes must be outside of the flow area. Because of this, some method had to be devised to suppress flow in these regions.

The fluid velocity in such control volumes is forced to zero by introducing an extremely large source in the three momentum equations. In addition, the new internal surfaces created must be represented by the appropriate modifications to the source terms for the control volumes in those regions. This essentially consists of applying the generalized log law described earlier to the appropriate surfaces in the interior of the solution domain.

IV.3.4 False Diffusion

False diffusion is a well known and persistent problem that plagues numerical solutions like the one presented here and as such warrants serious discussion. The problem arises when there is strong convection at an angle to the grid lines. The fundamental problem is that when calculating the flux across the boundary of a control volume, the flow is assumed to be locally one-dimensional. Consider the very simple schematic of a small region of a 2-D flow field as shown in Figure IV.7 where the flow is at 45 degrees to the grid lines, approaching from the SW neighbor of point p. Under the current scheme ϕ_p is a function of ϕ_n, ϕ_s, ϕ_e, ϕ_w, and a source term. With upwind differencing, the actual flux (from the SW corner) will be represented as two streams, one from w and one from s. All things being equal, ϕ_p will be an average of ϕ_w and ϕ_s and this is not necessarily the true value as convected from ϕ_{sw}. Also, the current point is a neighbor for points further downstream so the effect appears as a smearing of the true profile perpendicular to the flow direction. This is, in fact, a false diffusion and its effect is to augment the real diffusion somewhat.

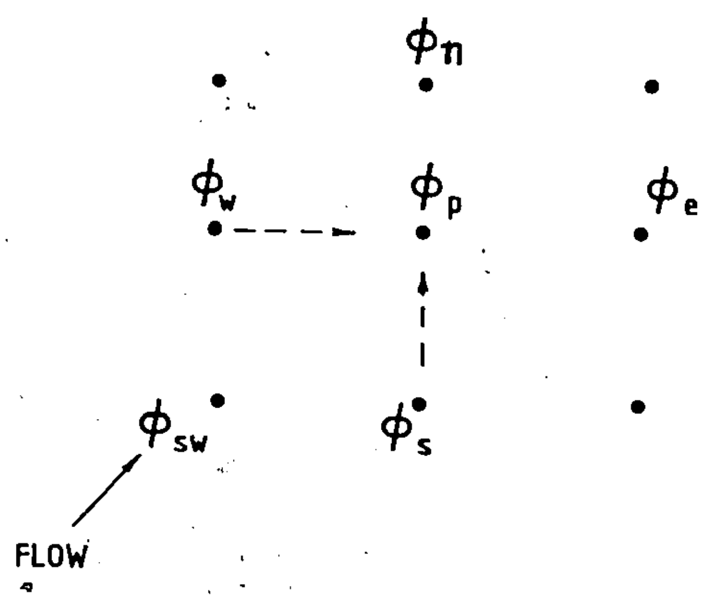

Figure IV.7 Oblique Convection

The problem of false diffusion is not as serious at low Pe numbers since the transport process is dominated by real diffusion. Recall that the Peclet number is the ratio of convection to diffusion. Also recall that the local Peclet number can be reduced by refining the grid mesh spacing. This result makes sense since the finer the grid gets, the closer the numerical solution becomes to the real solution. This is also reflected in the following formula which estimates the strength of the false diffusion coefficient as reported by Raithby [1976(a)].

$$\Gamma_f = \frac{\rho V \, \delta x \, \delta y \, \sin(2\theta)}{4(\delta y \sin^3\theta + \delta x \cos^3\theta)} \qquad \ldots \text{ IV.63}$$

This is for the two dimensional case and θ is the angle that the flow makes with the grid lines.

Care must be taken when applying this method that the false diffusion does not become dominant and mask the effects of the real diffusion. This becomes especially significant in the current study where a k-ε model is being used to calculate an effective viscosity in order to model the effects of turbulence. Since viscosity is merely a diffusion coefficient for momentum, any significant false diffusion will make the added expense of a k-ε model very difficult to justify since the effective viscosity hypothesis will be masked by false diffusion. The problem has been described in detail by Patankar [1980], Raithby [1976(a)] and Raithby [1976(b)].

IV.3.5 Convergence

The solution procedure described earlier contains many iterative procedures such as the TDMA and pressure correction schemes. In addition, it is being applied to the nonlinear Navier-Stokes equations. The result is a highly iterative procedure which could be prone to severe convergence problems. The method of underrelaxation was used to solve any convergence problems which may have arisen.

Briefly, underrelaxation is a method of suppressing large changes in the dependent variable between successive iterations. This helps to prevent divergence and allows the final solution to be approached smoothly and stably. In general, underrelaxation is implemented by setting the value of the dependent variable equal to some combination of its old value (previous iteration) and its newly calculated value (current iteration) with the use of an underrelaxation factor, α, as shown below:

$$\phi_{new} = \phi_{old}(1-\alpha) + \phi_{new}(\alpha) \qquad \text{... IV.64}$$

In FAITH, Equation IV.64 is not applied directly but instead the equations are pre-relaxed. This involves applying the relaxation factor to the coefficients in the linear equation set before they are solved. This method of relaxation provides better convergence characteristics than conventional underrelaxation.

The pressure field is underrelaxed by only applying a portion of the pressure correction to the pressure field at each iteration.

$$P_{new} = P_{old} + \alpha P' \qquad \text{... IV.65}$$

The values of α, the underrelaxation factor, used for the various field variables in this study are given in Table IV.3

u	v	w	k	ε	P	μ
0.5	0.5	0.5	0.7	0.7	0.8	0.7

Table IV.3 Underrelaxation Factors

These values gave satisfactory convergence for all cases in this study. A sample residual history is given in Figure IV.8 and is typical of the convergence characteristics throughout the study. It is for a Reynolds number of 180 000 and a subchannel area ratio of 0.50.

IV.3.6 Plotting Routines

The conventional output from a program such as FAITH, tables of the dependent variables at the node points, becomes very cumbersome for a three dimensional code. Therefore it was essential to develop utilities to provide graphical output of the velocity field. They are much more useful than the standard tables when quickly assessing the qualitative performance of the code.

For the purpose of this work, two routines where added to FAITH. The first provided contour plots of the axial velocity (w-component) while the other gave vector plots of the velocity. The vector plots could be requested on any plane (x, y, or z) in the geometry to examine the predicted flow pattern at various regions. The reader will become familiar with the output from these routines in Section IV.4.

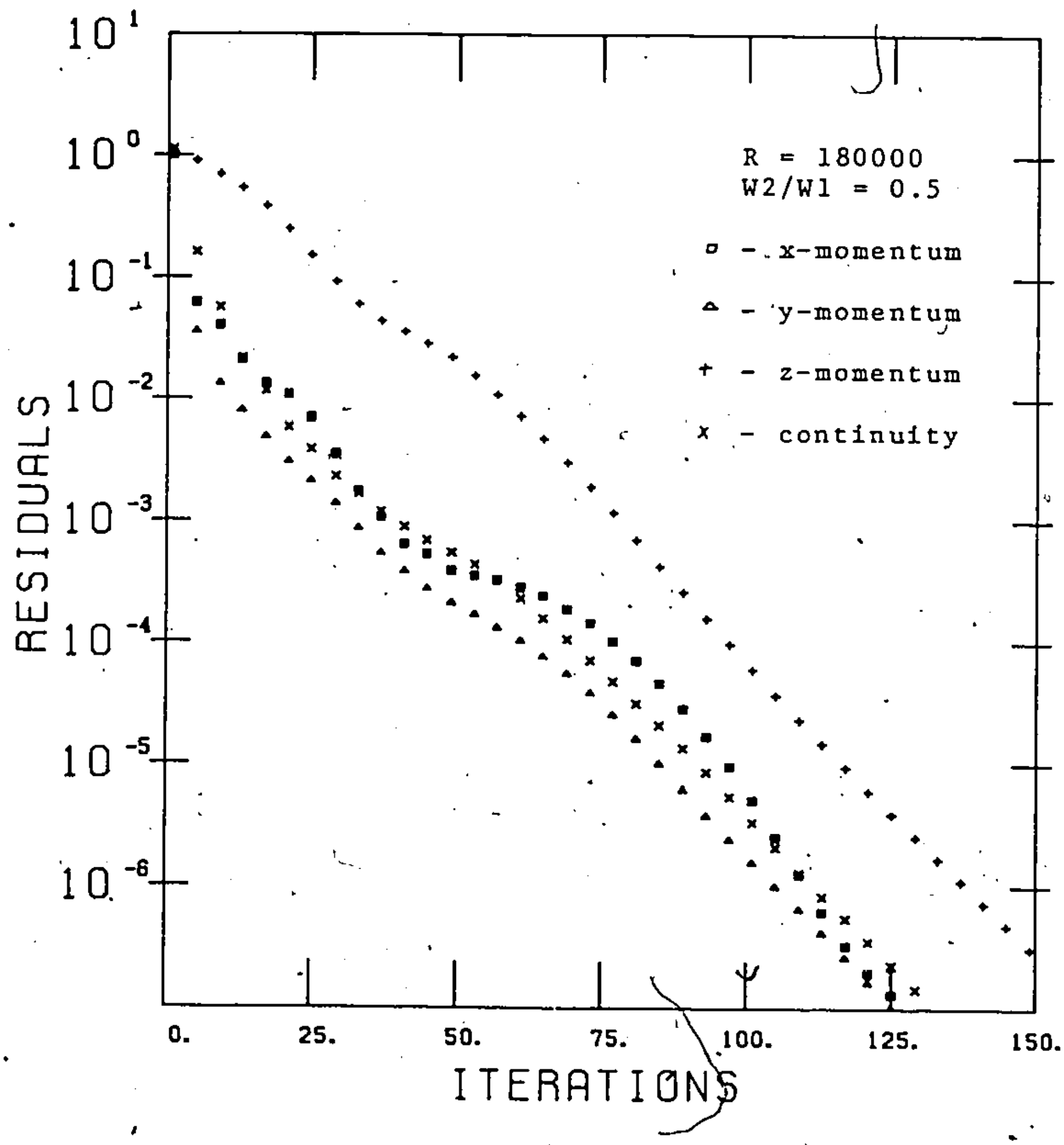

Figure IV.8 Residual Histories

IV.4 Analytic Results

Although a quantitative discussion of code results will be given in Section V, the runs done will be summarized in a qualitative fashion here. There were two distinctly different geometries modelled in this study. The first was the two unequal subchanels which have been thoroughly introduced by the experimental stage described in Section III. To provide an additional test of the code, some experiments done by Tapucu [1977] were also modelled. These two cases will now be presented.

IV.4.1 Unequal Subchannel Results

The solution made use of the single plane of symmetry in the geometry and as such only modelled one half of the cross section (In the case of W2/W1=1.0, two planes of symmetry were used). Figure IV.9 shows an example of the grids used for W2/W1=0.5. Note that they are non-uniform with node points being concentrated in the near wall region where velocity gradients are much higher. In the streamwise direction , z, all cases divided the 1.0 meter length into 20 equal nodes. This grid pattern resulted in a 4200 node solution domain.

The plots in Figures IV.10 through IV.13 present the predicted velocity profiles for the midplane and outlet with the inlet axial velocity matched to experimental conditions for a Reynolds number of 180 000. Since the solution assumes a plane of symmetry, the plots are divided into two along the plane of symmetry. The bottom half shows contours of axial velocity. As with the experimental results presented in Section III, the contours represent velocity normalized with the average. Also, the contour interval is 0.05 and the 1.0 line is as indicated. The top half of each graph shows vector plots of the secondary velocities as a percentage of the average axial velocity. It is clear to see that the blockage creating the small subchannel has, qualitatively at least, been modelled successfully.

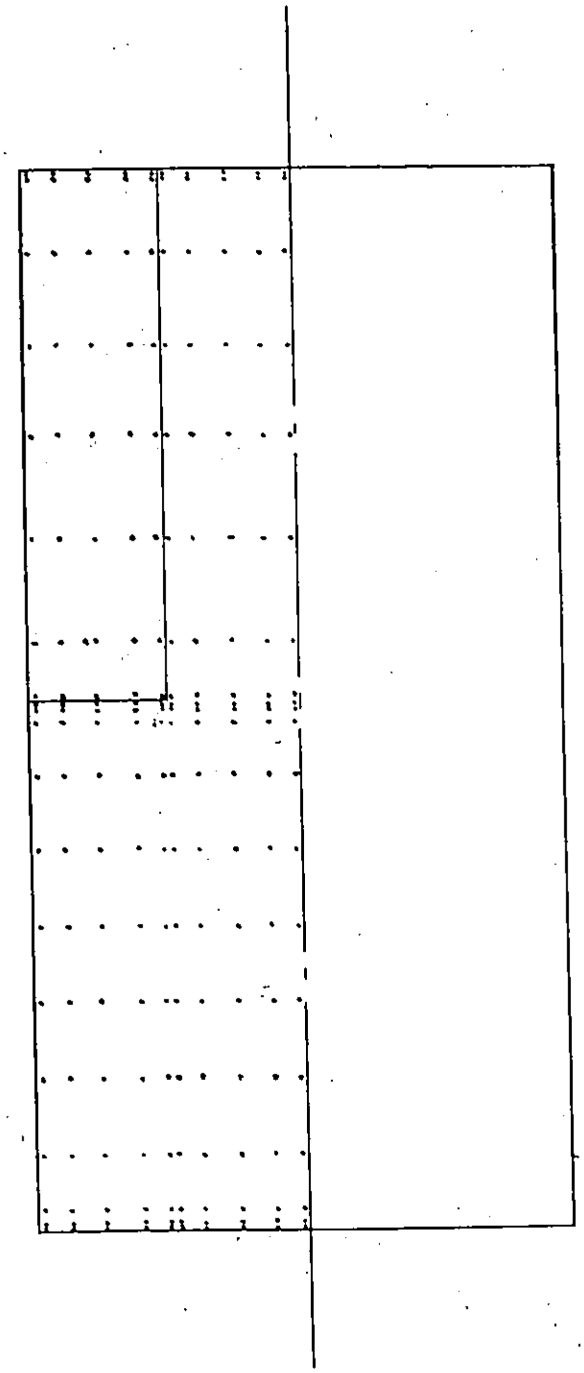

Figure IV.9 Grid for W2/W1=0.5

Vector Scale: 1 cm = 0.17% W_{ave}
Contour Interval: 0.05

z/Z = 0.5

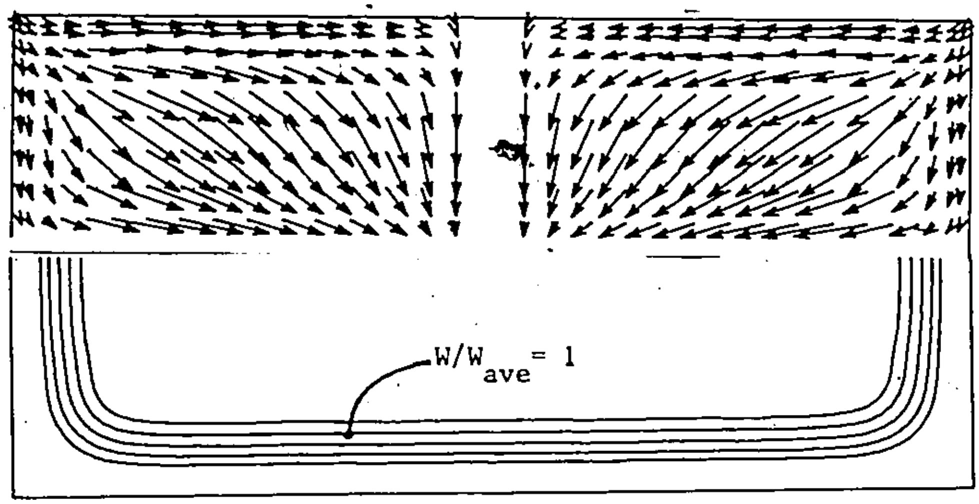

z/Z = 1.0

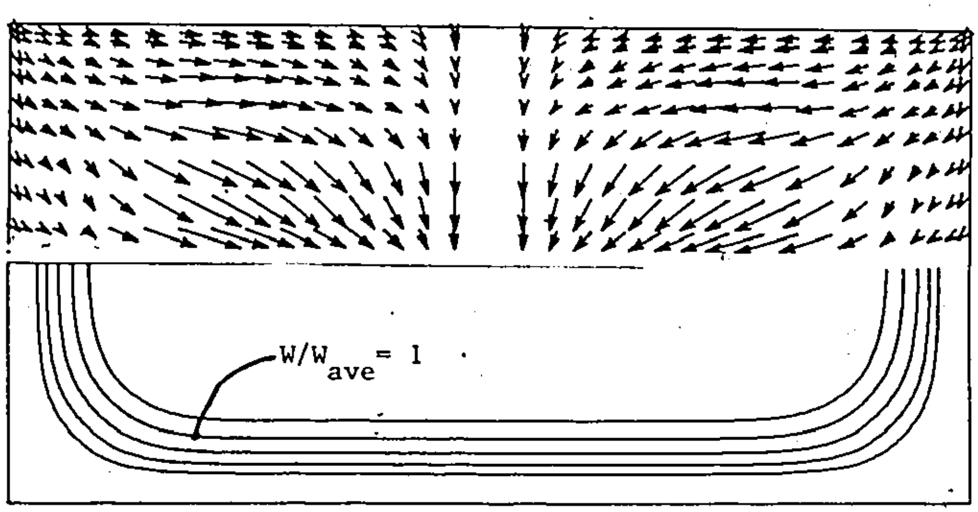

Figure IV.10 Predicted Velocity Fields
($W2/W1=1.0$; $R=180\ 000$; $W_{ave}=1.6$ m/s)

Vector Scale: 1cm = 0.21% W_{ave}
Contour Interval: 0.05

z/Z = 0.5

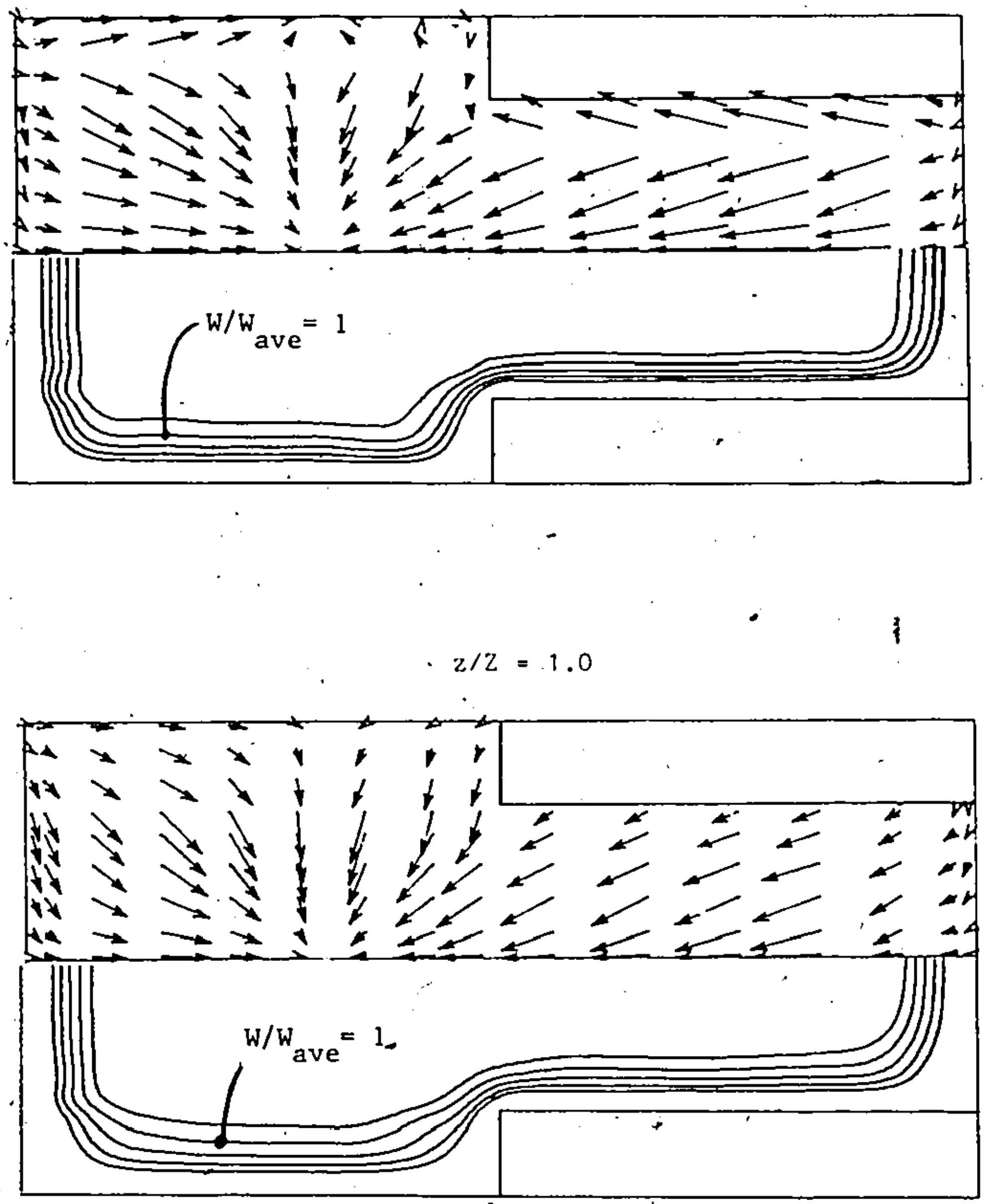

Figure. IV.11 Predicted Velocity Fields
(W2/W1=0.68 ; R=180 000 ; W_{ave}=1.91 m/s)

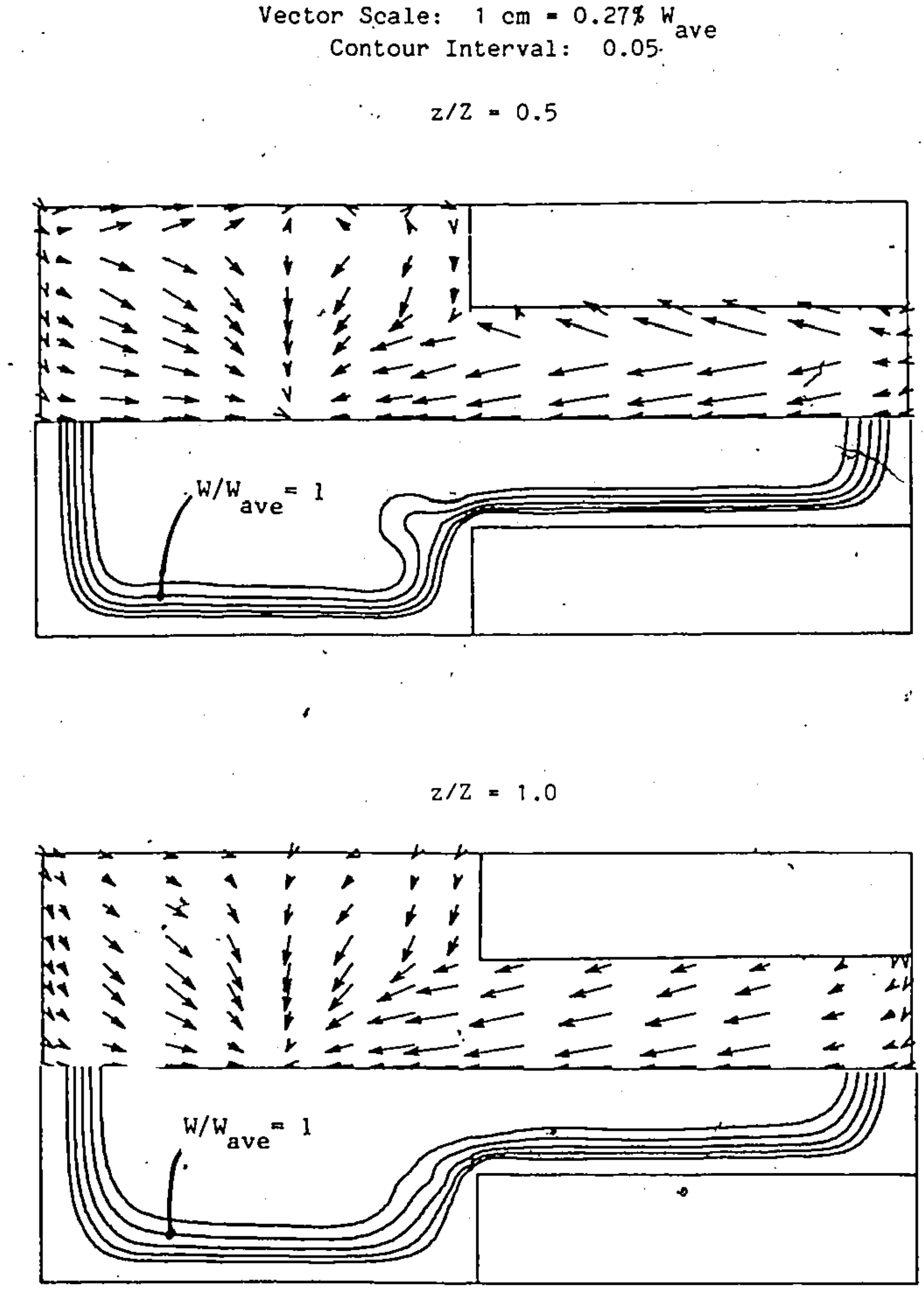

Figure IV.12 Predicted Velocity Fields
(W2/W1=0.50 ; R=180 000 ; W_{ave}=2.13 m/s)

Vector Scale: 1 cm = 0.39% W_{ave}
Contour Interval: 0.05

z/Z = 0.5

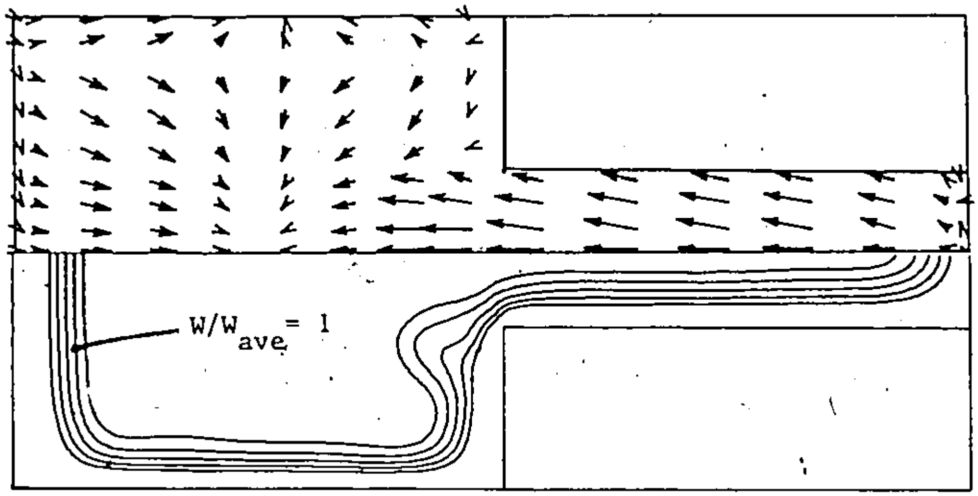

z/Z = 1.0

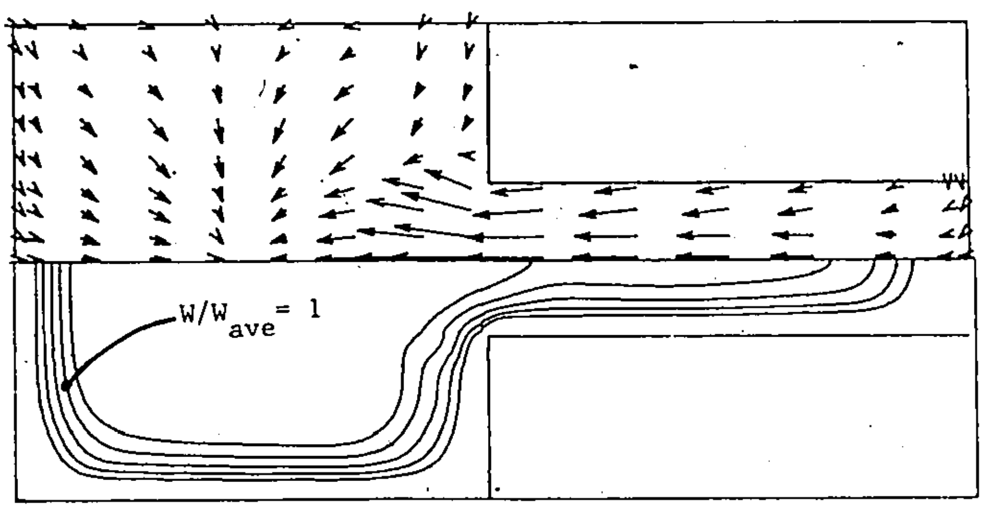

Figure IV.13 Predicted Velocity Fields
(W2/W1=0.32 ; R=180 000 ; W_{ave}=2.42 m/s)

IV.4.2 Tapucu Subchannel Results

The diversion cross flow between two parallel channels communicating by a lateral slot was studied by Tapucu [1977]. The geometry of this experiment is shown in Figure IV.14. The two square subchannels were machined out of acrylic blocks. This allowed the cross flow to be measured by injecting $KMnO_4$ solution into one subchannel and observing the color variation in the other. An optical fiber and phototube arrangement made accurate measurements of this color variation. Wall pressure taps were placed in each subchannel at 19.05 mm intervals. The working fluid was water.

The important difference between this and the two unequal subchannel geometry is the very narrow communicating slot. This geometry was selected as a test case because such a configuration would test the code's ability to model a different type of transport mechanism.

Vector plots of the predicted flow field are given in Figures IV.15 to IV.18 to qualitatively represent the predictions. Figure IV.15 shows the velocities on the plane of symmetry. Note that the axial dimension of the geometry is greatly compressed to fit on the page. Figures IV.16 through IV.18 show the flow pattern at several cross sections along the channels. These are to scale and their axial locations are indicated. Again the flow fields look very realistic. The flow conditions represented in this run are some of the most difficult to model. Note that the inlet conditions specify zero flow in the bottom subchannel. This induces severe cross flow near the beginning of the communicating region. This cross flow is clearly shown in the vector plots. Also clearly visible is the circulation that is induced in the lower subchannel from the jet of fluid entering it from the upper, high flow subchannel.

The data take included axial static pressure variation in both subchannels, average axial velocity in each subchannel, cross flow velocity and integral mass transfer. Figure IV.19 shows the code predictions and the experimental data for the case studied here. A detailed discussion is given in Section V.

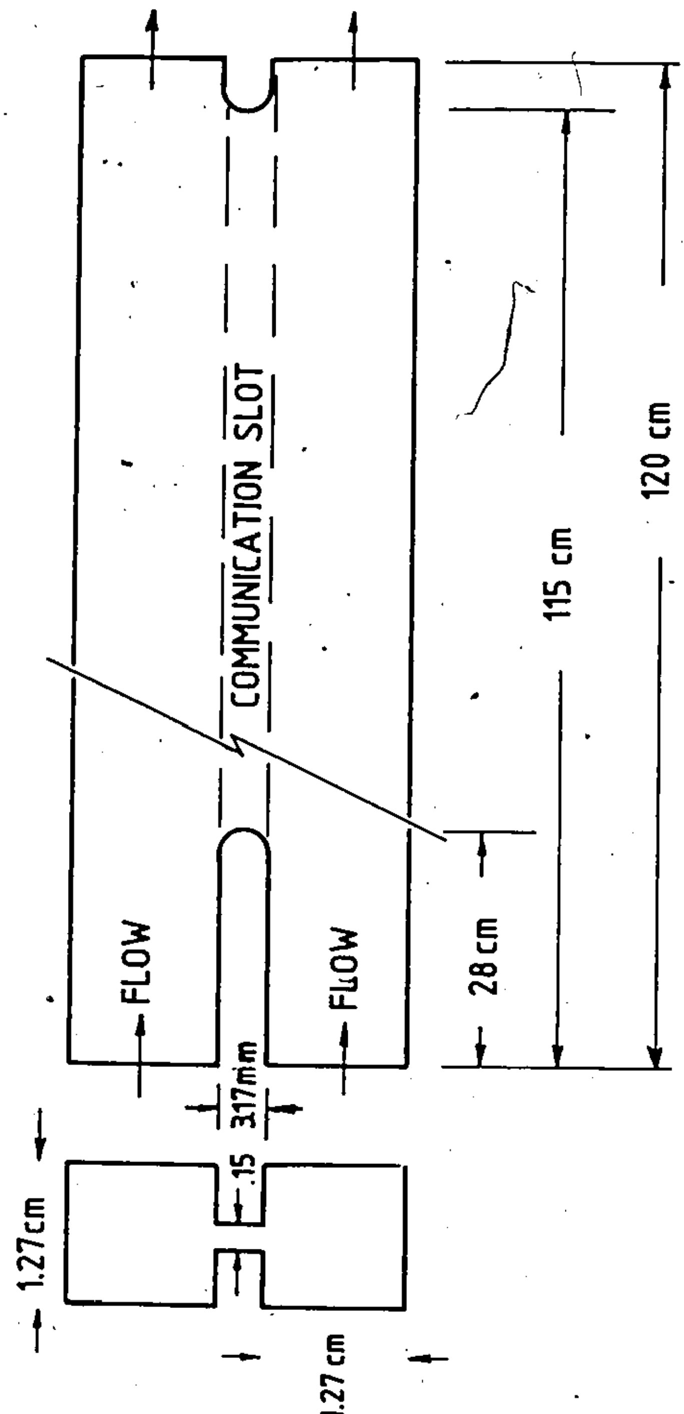

Figure IV.14 Tapucu Subchannel Geometry

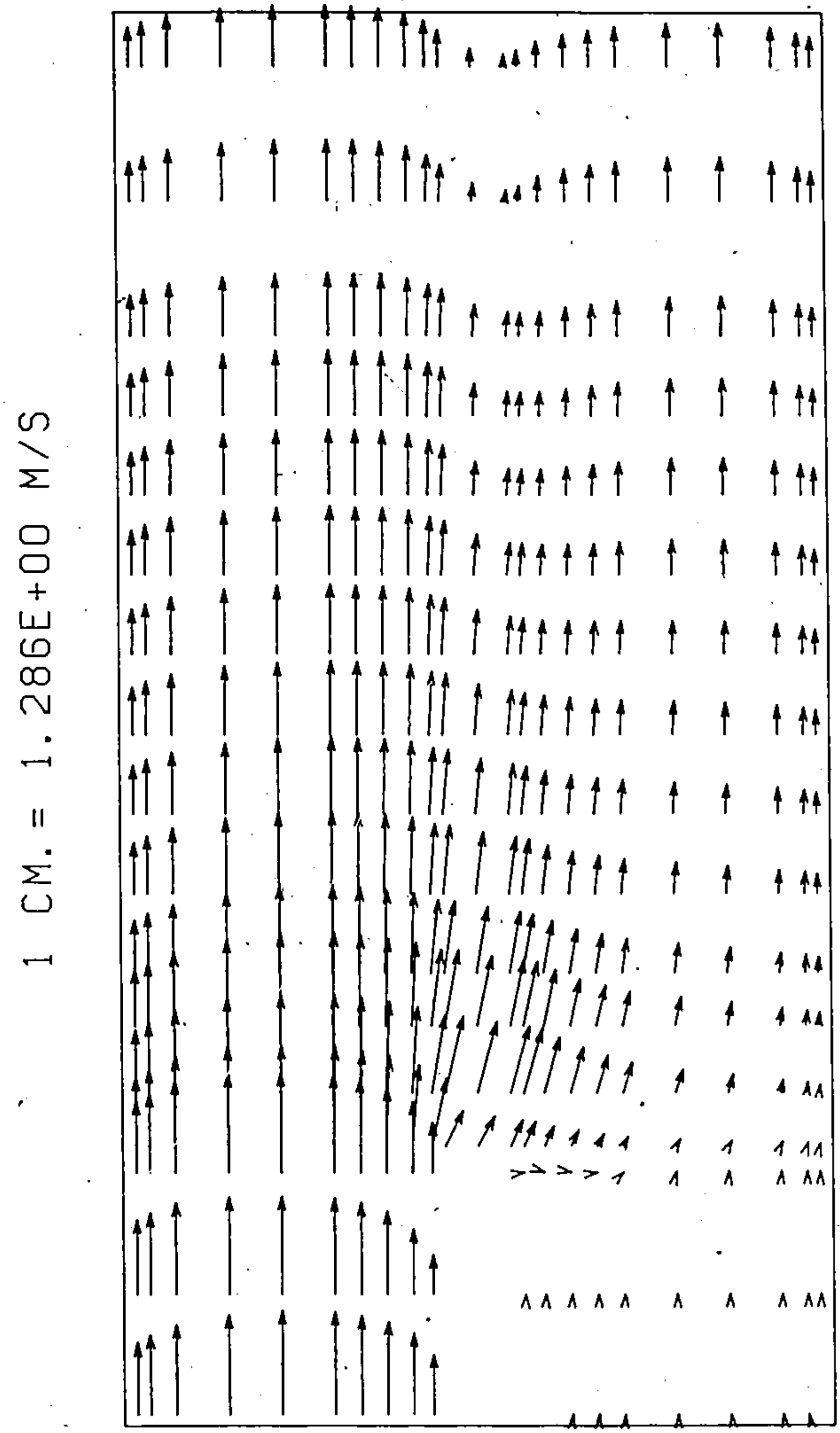

Figure IV.15 Predicted Velocities on Plane of Symmetry of Tapucu Subchannel Geometry

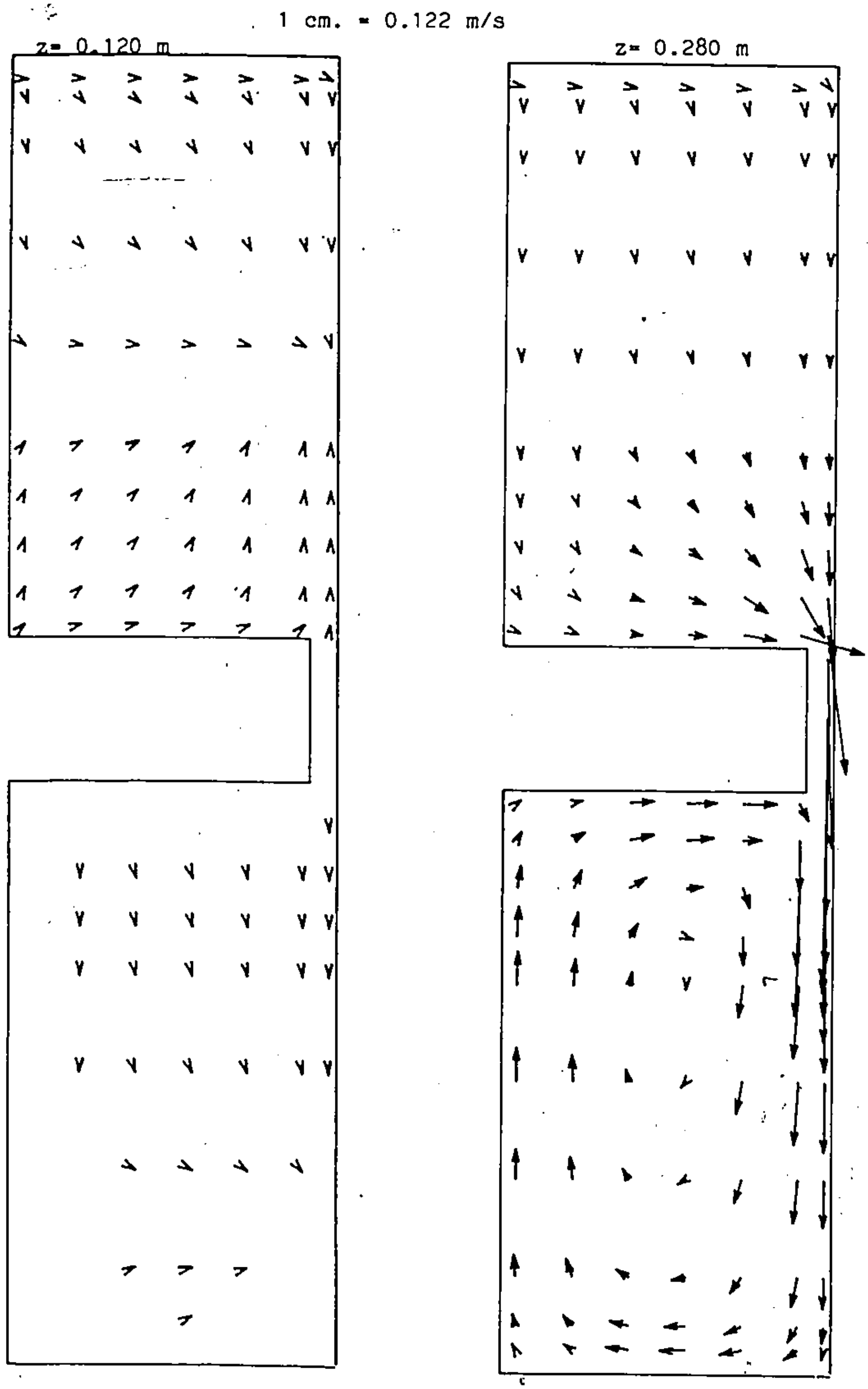

Figure IV.16 Predicted Velocities for Tapucu Subchannels

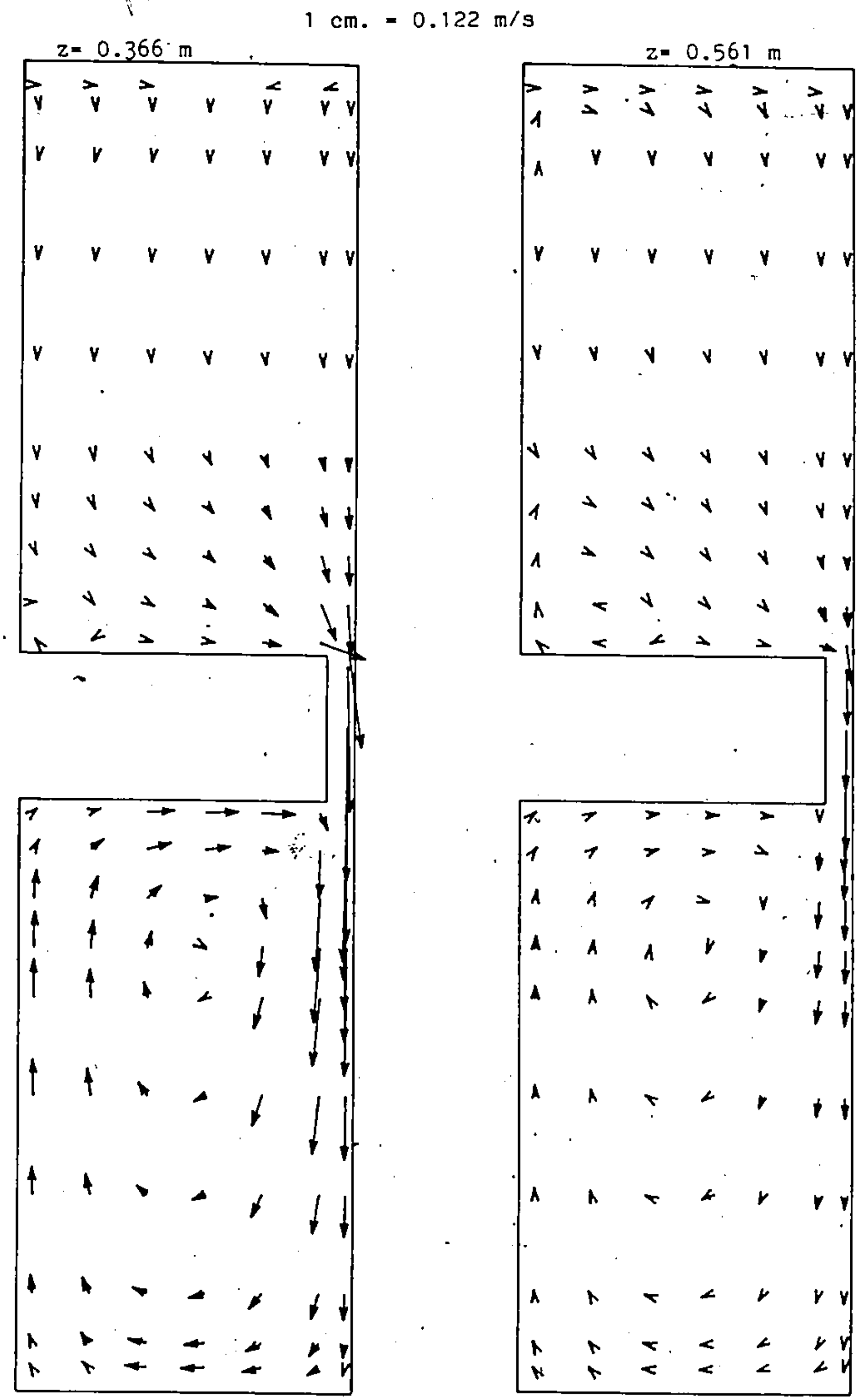

Figure IV.17 Predicted Velocities for Tapucu Subchannels

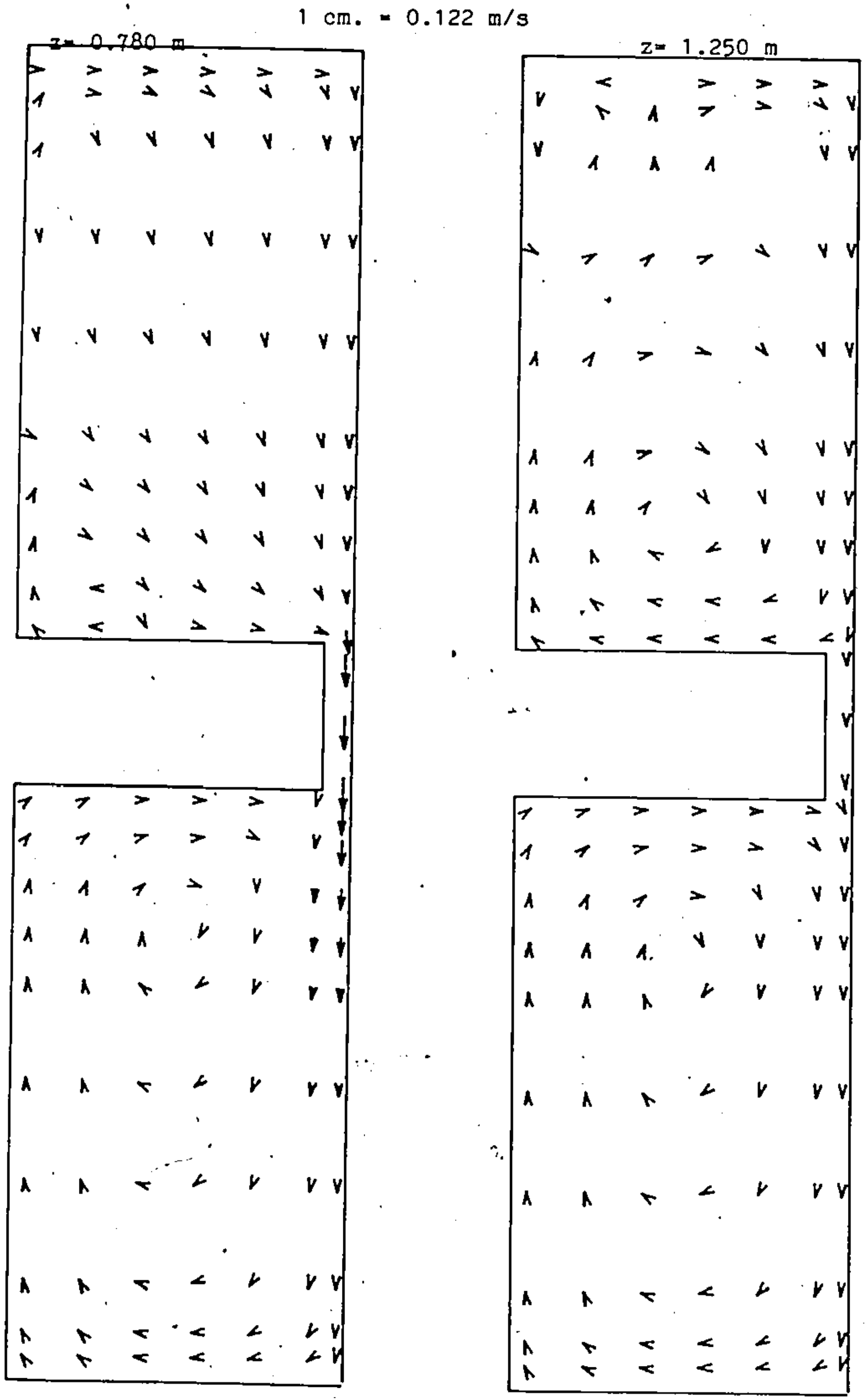

Figure IV.18 Predicted Velocities for Tapucu Subchannels

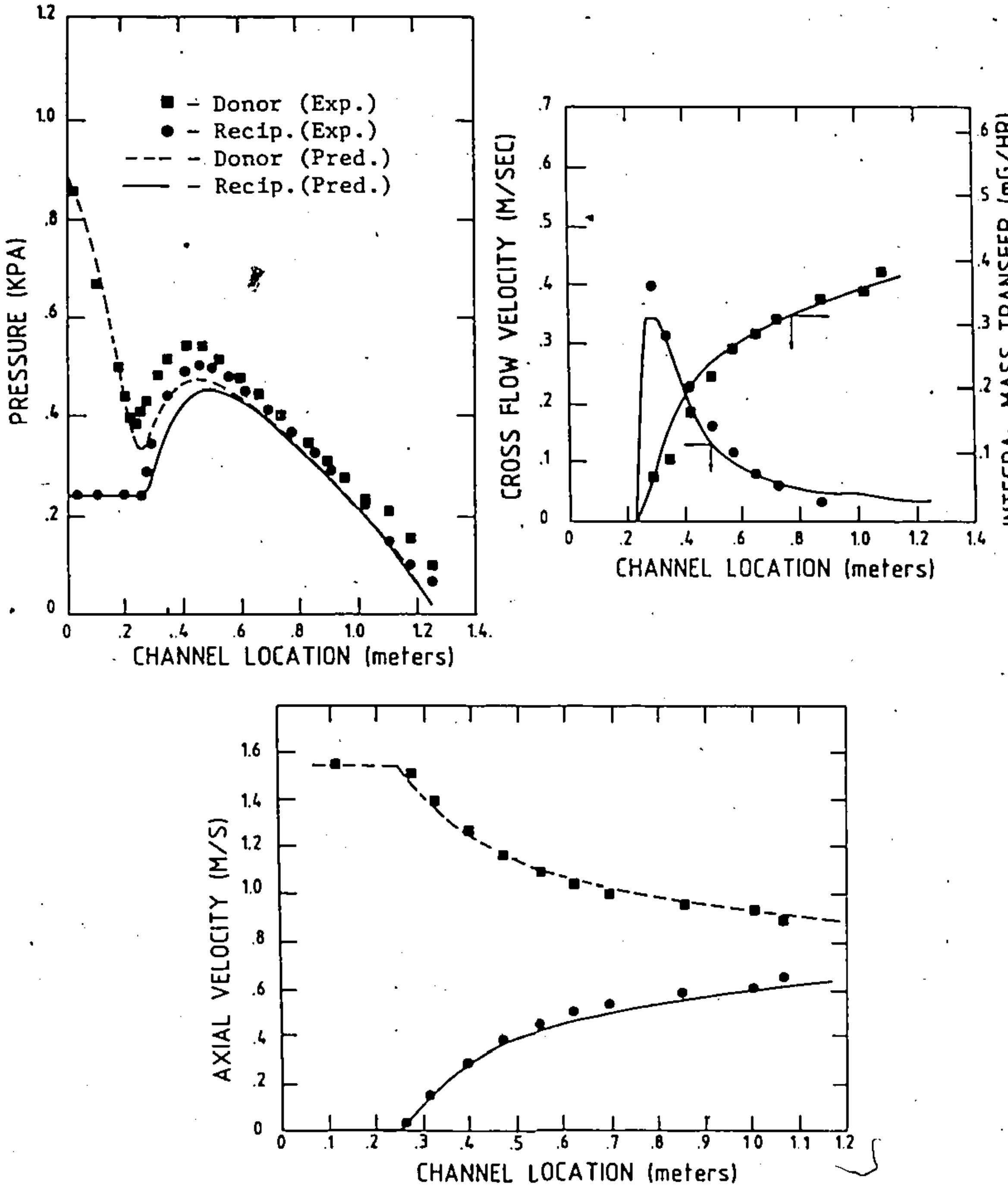

Figure IV.19 Tapucu Subchannel Predictions

V. DISCUSSION OF RESULTS

V.1 Unequal Subchannels

In previous sections both experimental and analytic results have been presented for the unequal subchannel geometry. Section III.3 presented experimental results in contour plot form. Section IV.4.1 contained results of the numerical model for the same geometry and inlet conditions. This section will compare these results and discuss the performance of the model.

It was difficult to compare the results in the form of contour plots. To accommodate comparison in this section, representative results were plotted as cross sections of the contour plots. Their position was indicated by means of the normalized z and x coordinates given at the top of the plots. The axes of the plots were also normalized, with normalized y location on the abscissa and velocity (normalized by the average axial velocity) on the ordinate. The coordinate system is shown in Figure B.1 of Appendix B.

Recall that the inlet conditions to the code were the experimental axial velocities measured at z=0. Therefore the comparisons given here were only based on the other two axial stations at which measurements were made (z/Z=0.5 and z/Z=1.0). A plane of symmetry existed at y/Y=0.5, but the full range of y was given since experimental data was taken on both sides of the plane of symmetry. The model's results were merely reflected about this plane.

V.1.1 Uniform Effective Viscosity Predictions

Initially the predictions were made with the k-ε turbulence model deactivated and a constant viscosity of 0.000797 Pa•s imposed throughout the flow field. These predictions were presented in Figures V.1 through V.4 for each of the four possible test section configurations. Each prediction was represented by plots at the axial midpoint and outlet. At each axial location two profiles were plotted, one through the center of each subchannel. The locations and normalizing velocities are given on the plots.

A viscosity of 0.000797 Pa•s merely represents the viscosity of water at 30 degrees Celsius (the water temperature during the experiment). Although it was not expected for these runs to properly model turbulent flow, they did prove valuable as a basis for comparison for the runs with the turbulence model activated. As a result of the "laminar flow" assumption the pressure gradients predicted by these runs were much lower than those observed in the experiment.

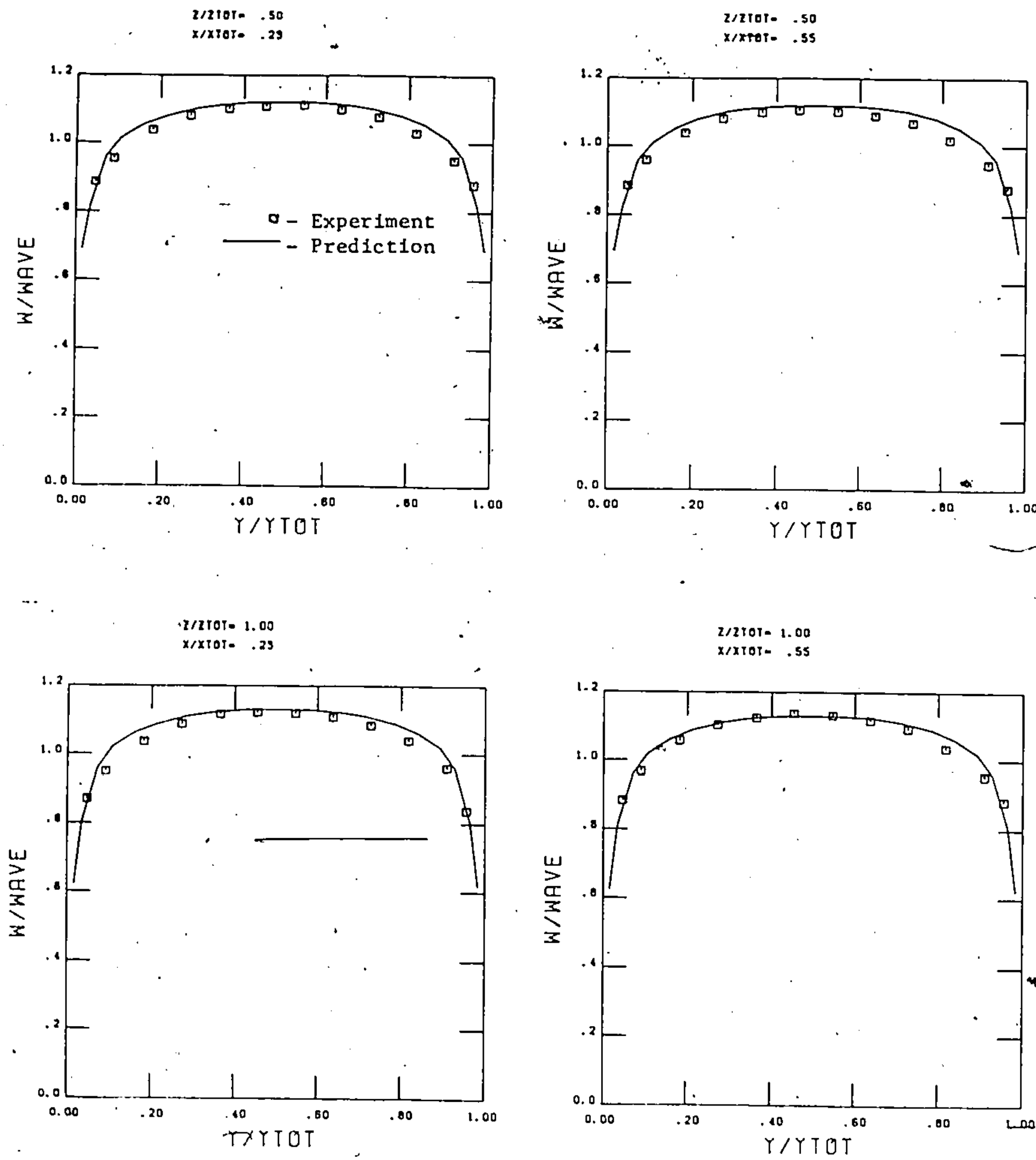

Figure V.1 Unequal Subchannel Predictions,
(μ=0.000797 Pa.s, W2/W1=1.0, R=180 000, W_{ave}=1.60 m/s)

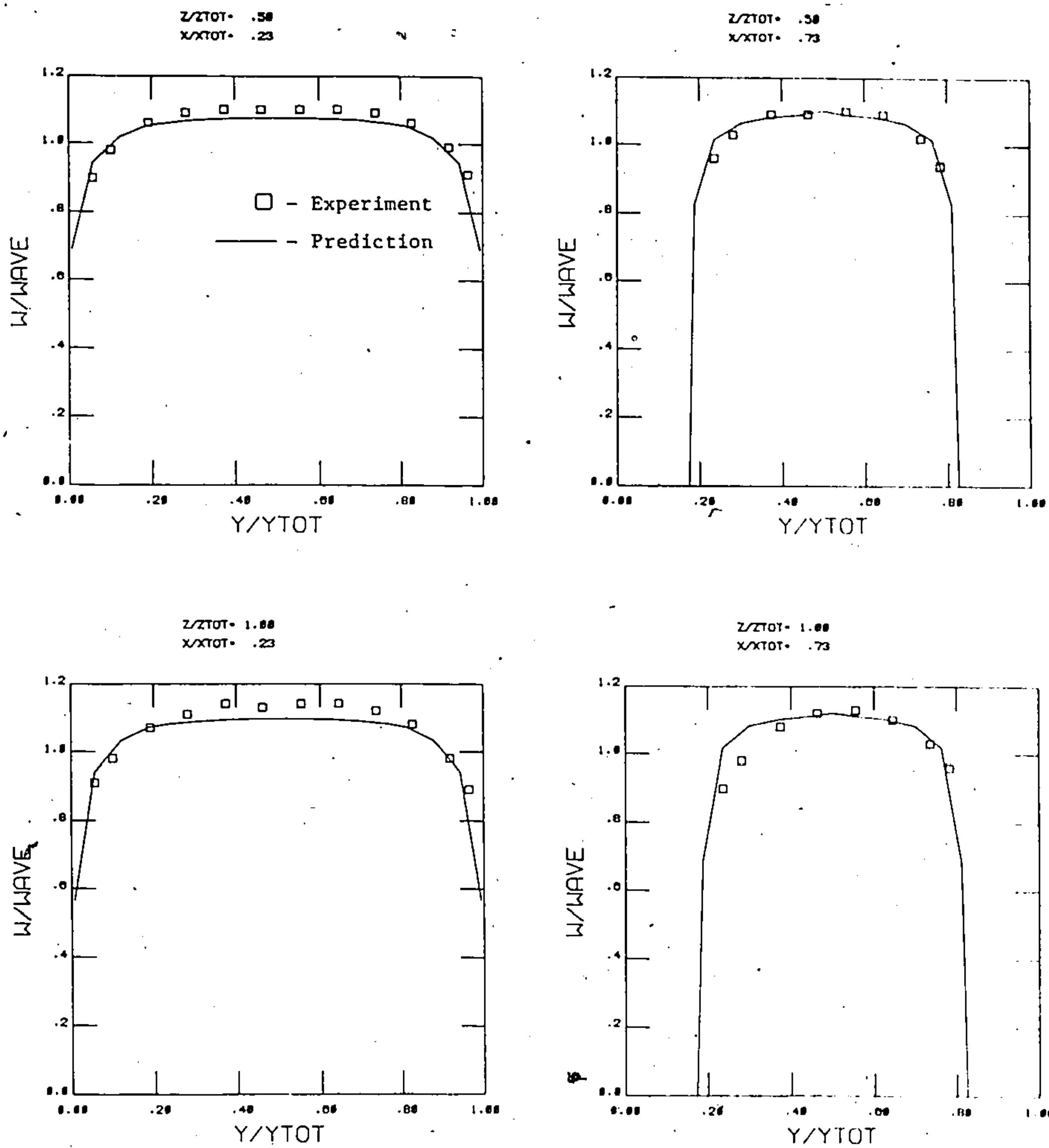

Figure V.2 Unequal Subchannel Predictions,
(μ=0.000797 Pa.s, W2/W1=0.68, R=180 000, W_{ave}=1.91 m/s)

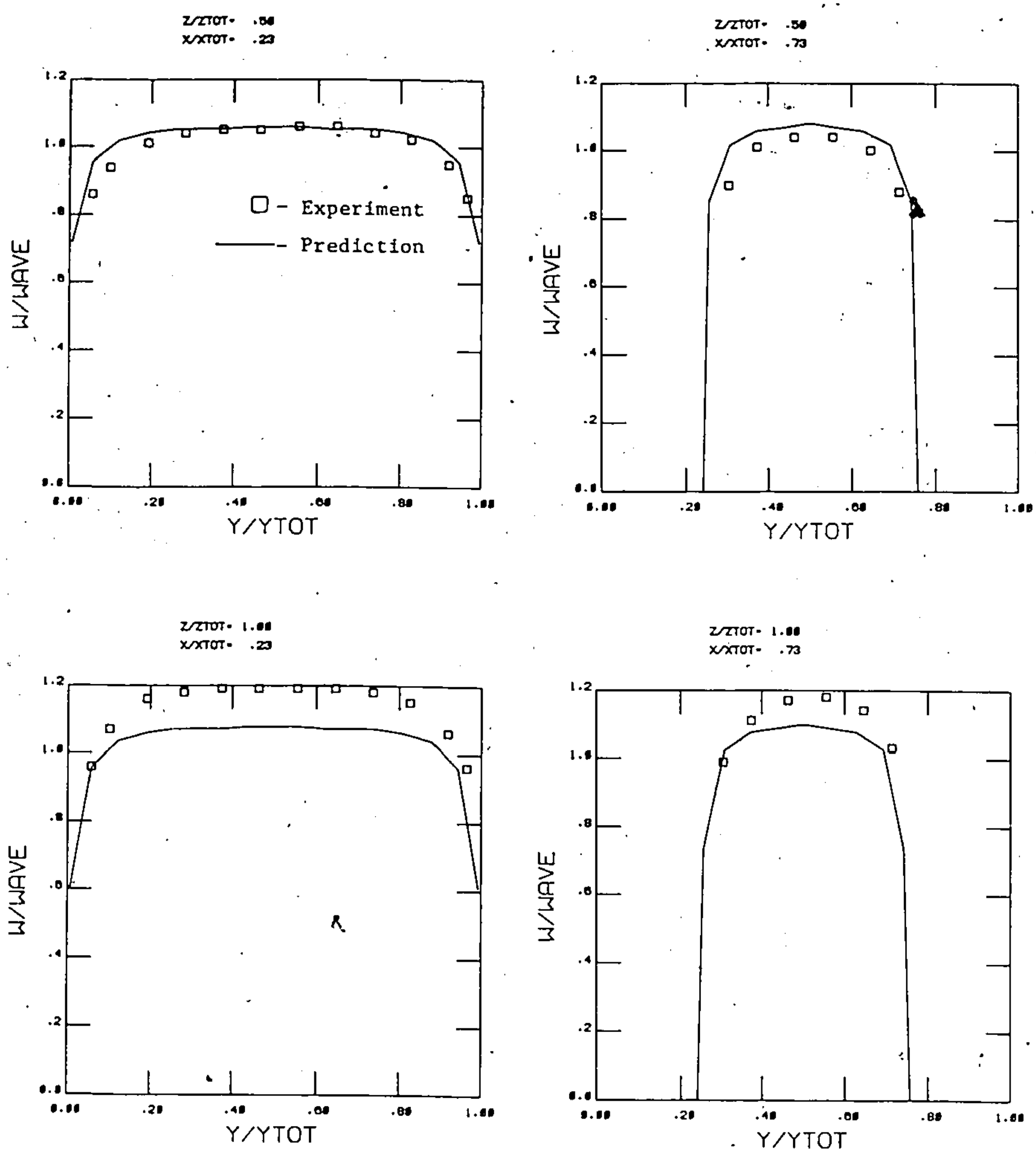

Figure V.3 Unequal Subchannel Predictions,
(μ=0.000797 Pa.s, W2/W1=0.50, R=180 000, W_{ave}=2.13 m/s)

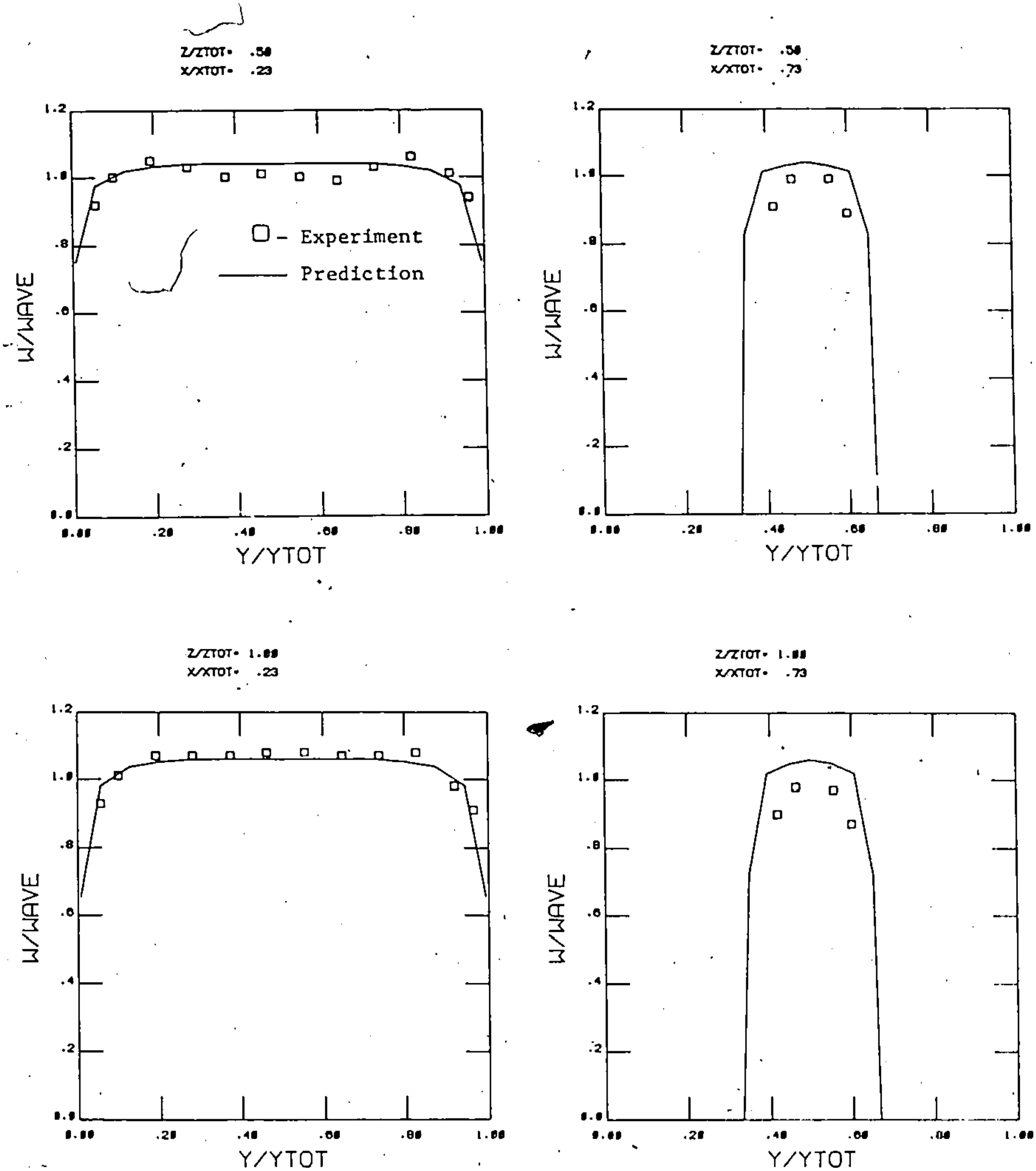

Figure V.4 Unequal Subchannel Predictions,
(μ=0.000797 Pa.s, W2/W1=0.32, R=180 000, W_{ave}=2.42 m/s)

The first observation when studying the velocity profiles for case W2/W1=1.0 was that the predictions appeared to be quite good with no turbulence model used. However, this initial impression was misleading since the channel inlet conditions were duplicated as a boundary condition to the model. The low viscosity used in the non-turbulent predictions (ie. viscosity = 0.000797 Pa·s) resulted in very little redistribution of the flow over the length of the test section. For the case W2/W1=1.0, the redistribution from z=0 onward was minimal because the inlet section had the same geometry as the test section (See Figures III.14 and III.18). This probably accounted for the good appearance of the velocity profiles, at least for the rectangular channel case. This could not be considered a highly successful prediction when the success appears to be due to the matched inlet condition.

For the other subchannel area ratios there obviously had to be more redistribution of the flow. For these cases it was apparent that the predictions were not as accurate as they had appeared for the rectangular channel case. The deficiencies were especially noticeable for the case of W2/W1=0.32. Because of the design of the transition pieces at the test section's inlet (see Section III.1.3), the velocity profile at the beginning of the small subchannel was rather flat. Although the experimental data shows significant development from this flat profile to a more parabolic one at downstream stations, the predicted profile stays essentially flat. Also, the predicted average velocity in the small subchannel does not decrease as much as the experiment by the time the flow gets to the test section outlet. In the model, the flow was not developing as quickly as observed in the experiment.

V.1.2 Turbulent Predictions

The velocity profile predictions with the k-ε model activated were presented in Figures V.5 through V.8. Immediately it was noticed that there was very little difference between these and the simple uniform effective viscosity predictions. This naturally led one to suspect the importance of the viscosity field in determining the flow distribution in this geometry. Although the effective viscosity calculated by the k-ε model was many times the nominal laminar value, the flow distribution did not seem to be affected much. The viscosity field was not as vital as was thought to the success of the prediction. The shear stresses in the fluid are proportional to the product of the local effective viscosity and the local mean velocity gradient. If the velocity gradient was small in a certain region of the fluid, the Reynolds stresses would have been small, and would not have contributed significantly to the forces on the fluid. Even in this geometry, the only large velocity gradients were near the wall where the model imposed the log law of the wall to predict the important wall shear stresses. As a result, the axial pressure profiles predicted with the k-ε model activated are much closer to the experiment than those without it.

An example of the pressure profile predictions is given in Figure V.9. Although the overall gradient appears to be predicted quite well, the inflection points and curvature of the experimental data are not predicted. These observations indicate that the code has probably been successful in predicting the overall average skin friction but has not reproduced the variation in static pressure associated with the development of the profiles observed in the experiment.

Since neither prediction gave satisfactory velocity profile results, there must have been a deficiency common to both of them that was significant. Close inspection of the experimental data gave some possible explanations. A comparison of the predicted and experimental contour plots presented in previous chapters showed some distinct features of the flow that were not modelled properly in either attempt. These features were believed to be due to the effect of secondary flows and are discussed below.

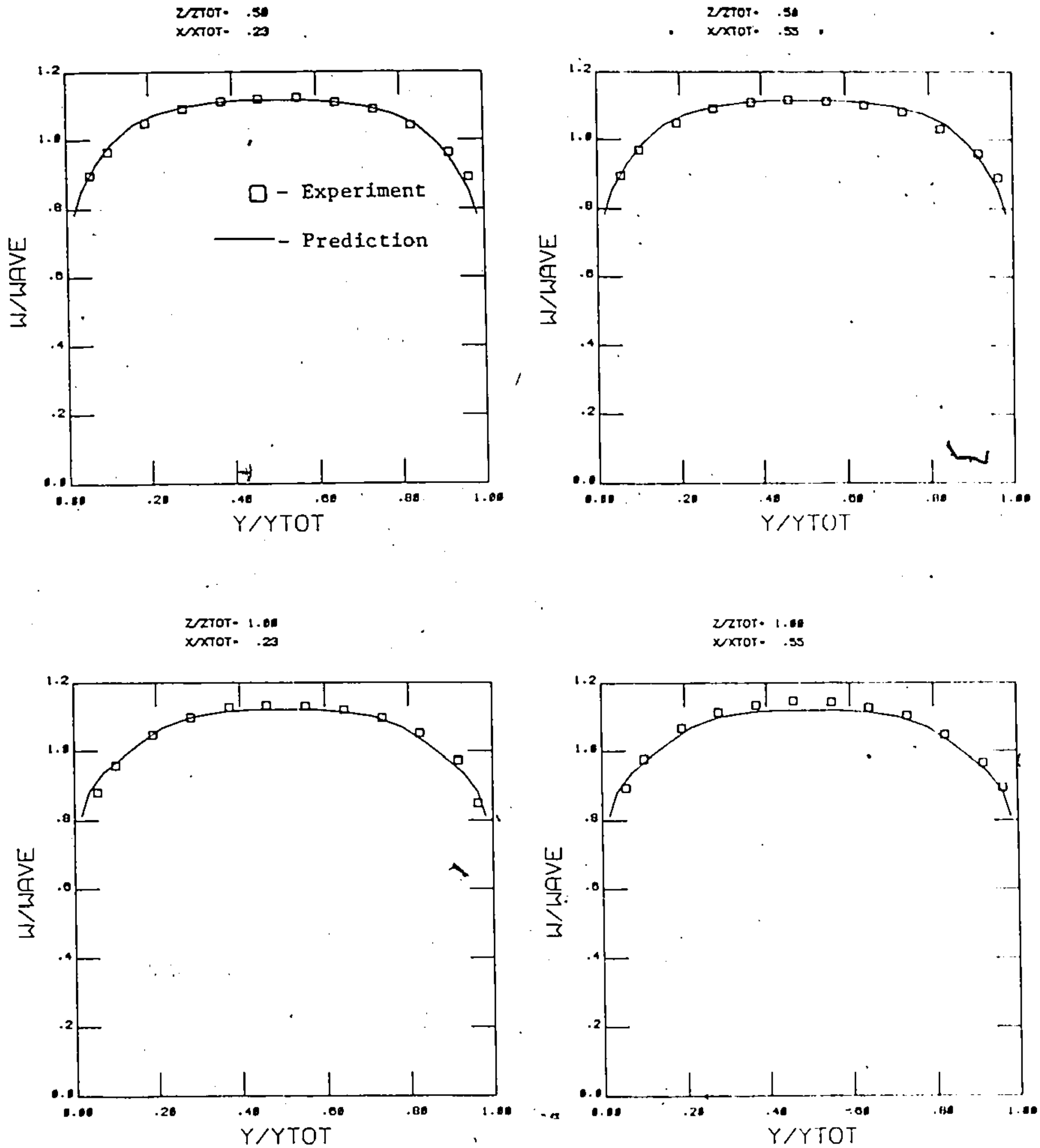

Figure V.5 Unequal Subchannel Predictions,
(k-ε Turbulence Model, W2/W1=1.0, R=180 000, W_{ave}=1.60 m/s)

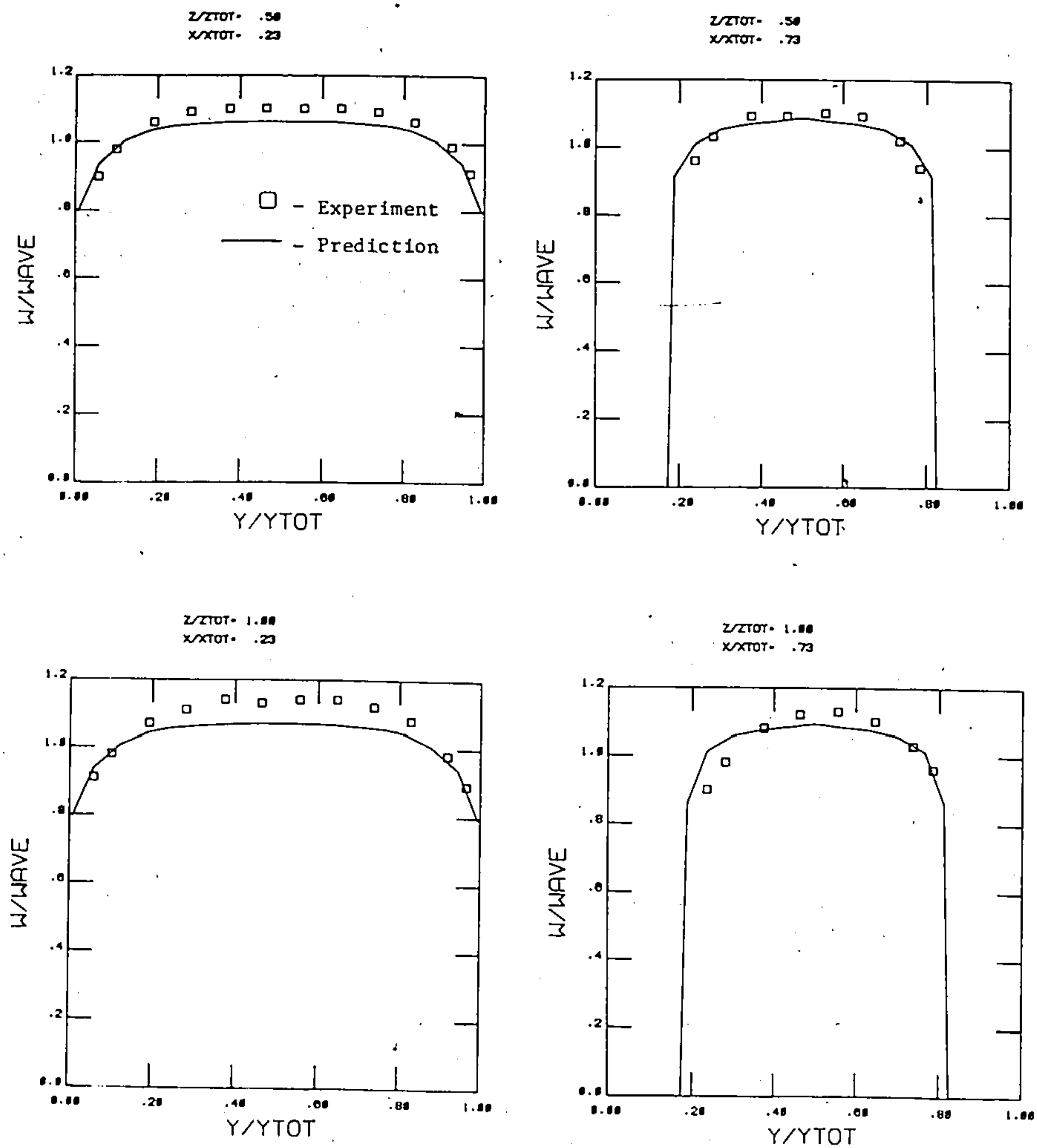

Figure V.6 Unequal Subchannel Predictions,
(k-ε Turbulence Model, W2/W1=0.68, R=180 000, W_{ave}=1.91 m/s)

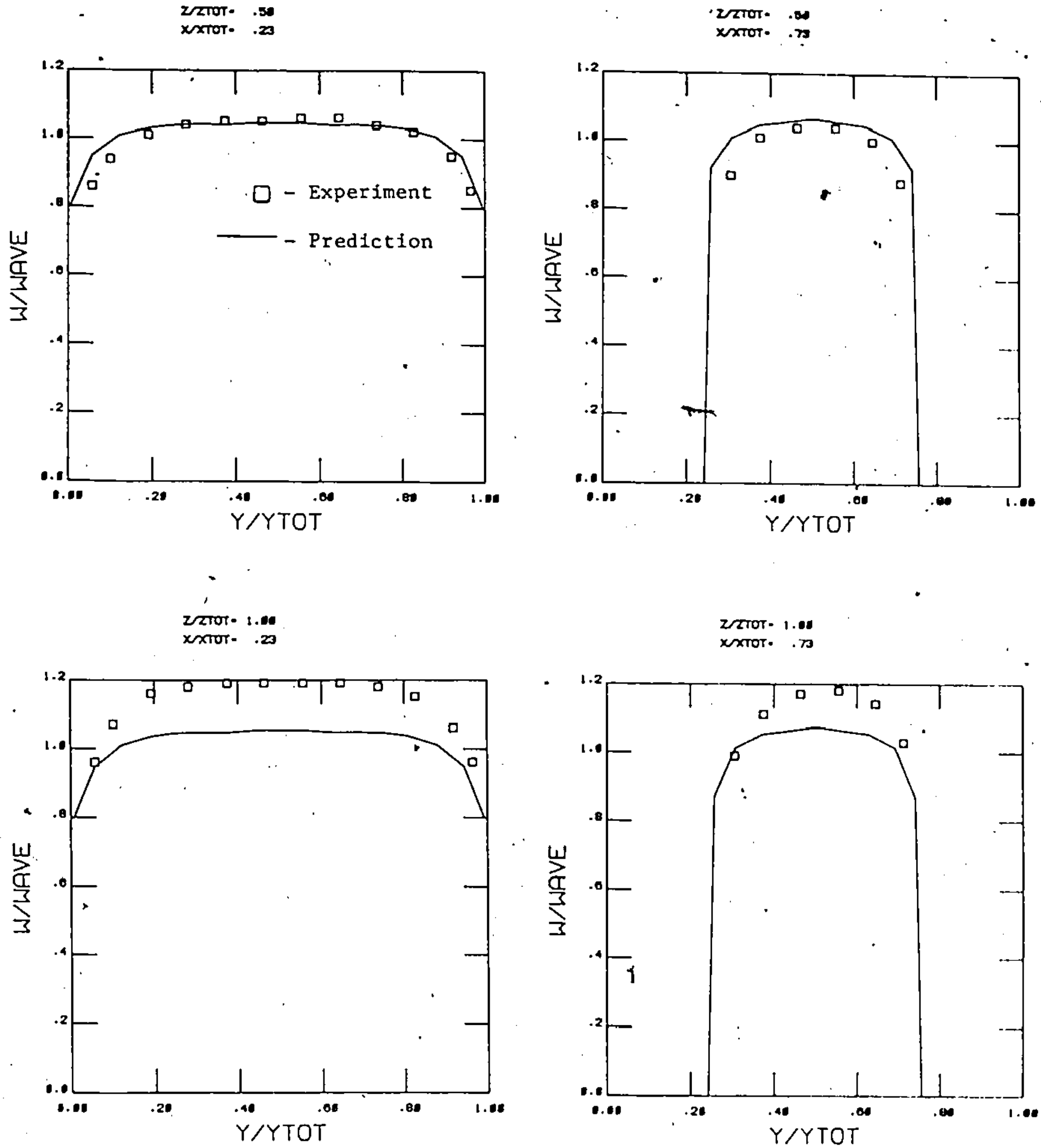

Figure V.7 Unequal Subchannel Predictions,
(k-ε Turbulence Model, W2/W1=0.50, R=180 000, W_{ave}=2.13 m/s)

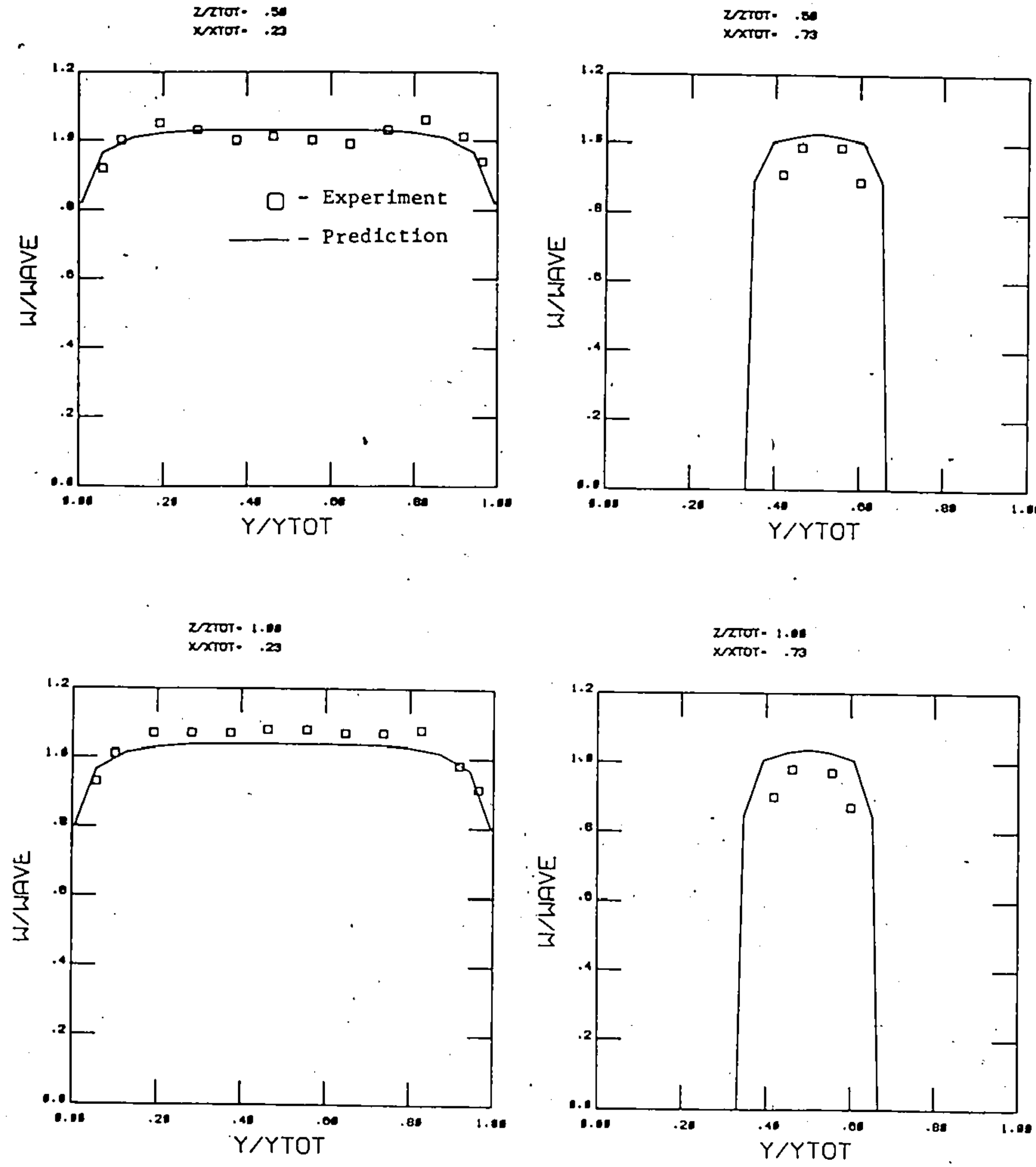

Figure V.8 Unequal Subchannel Predictions,
(k-ε Turbulence Model, W2/W1=0.32, R=180 000, W_{ave}=2.42 m/s)

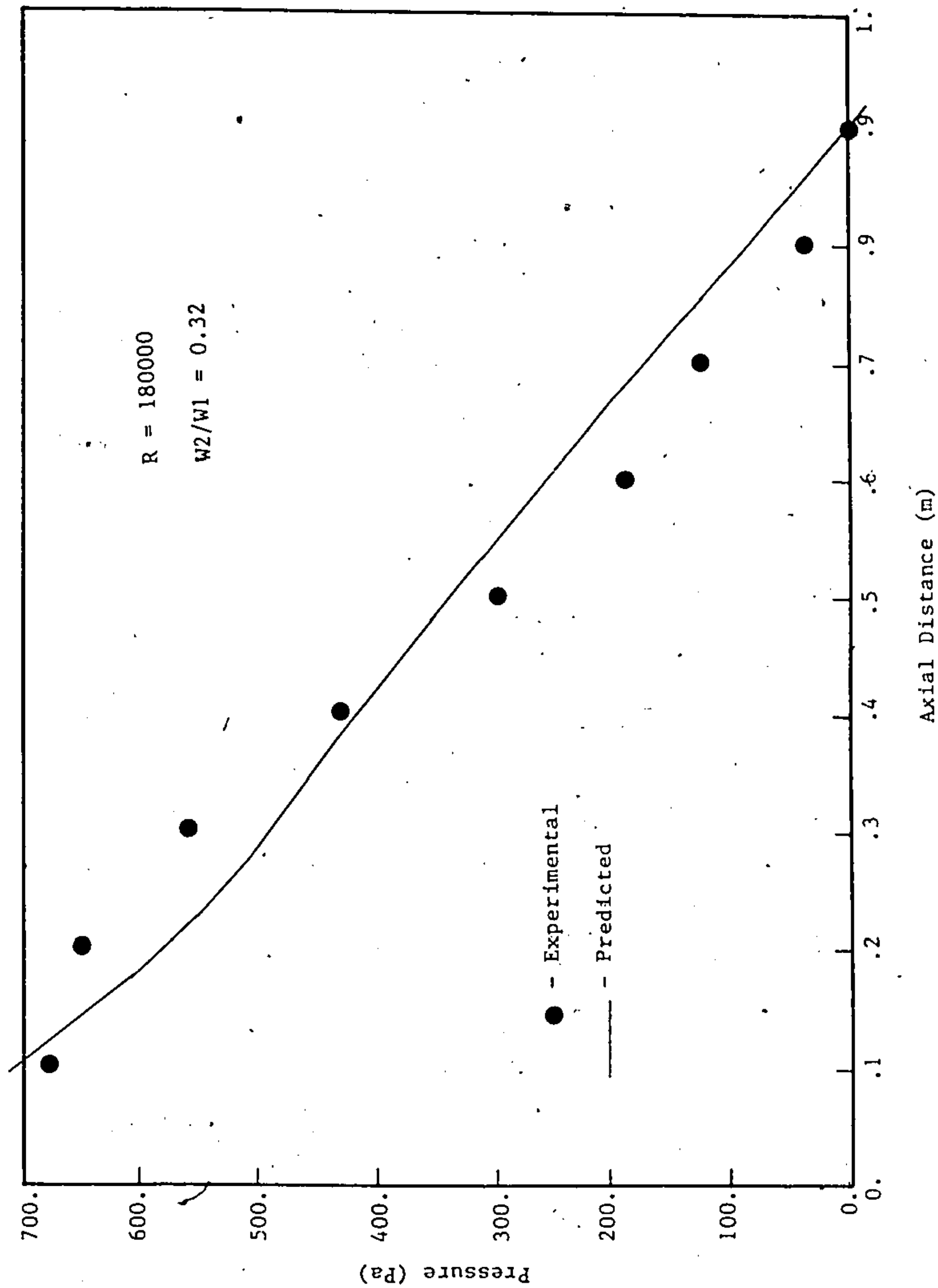

Figure V.9 Pressure Profile Comparison

V.1.3 Secondary Velocities

There was one mechanism present in turbulent flow in non-circular ducts which was not modelled by either the k-ε model or the laminar viscosity assumption. Even when turbulent flow in a rectangular duct is fully developed there exists secondary velocities caused by the turbulent stress field (Launder and Spalding [1974]). In rectangular ducts this results in a transfer of axial momentum away from the walls along the centerlines of the duct cross section and towards the walls along the diagonals. This effect was evident in the simple rectangular duct case and was seen quite clearly in the contour plots. Comparing Figure III.14 to Figure IV.10 it could be seen that the contours extended into the corners of the geometry much more in the experimental data. This was due to the high momentum fluid from the center of the duct being transported toward the corner by the secondary velocities. Because of the isotropic turbulence assumption inherent in the k-ε model, it is not able to predict this effect.

Another important feature in the experiment was the region of low velocity between the two subchannels. This was very evident in the experimental contour plots presented in Chapter III. The low velocity regions were more pronounced at the inlet plane and appeared as very sharp depressions in the axial velocity at two symmetrically opposed points near the corners of the opening between the two subchannels. Further downstream, there was still a very noticeable region of low momentum fluid near these two interior corners. They extended toward the centerline to create a low velocity region between the two subchannels such that each subchannel had its own distinct maximum velocity. A good example of this phenomenon was Figure III.19. This was also observed in work by Lyall [1973] in a similar geometry with air as the working fluid and was attributed to the effect of a secondary velocity away from the wall in this region. The low momentum fluid being transported from the wall would cause the velocity depression observed.

The model did not reproduce this effect. Although a low velocity region was evident at z/Z=0.5, this was merely due to the matched inlet conditions. At the outlet there was no apparent low velocity region in the model's predictions. The contour plots in Chapter IV showed that the predicted contours approach the two interior corners very closely at the opening between the two subchannels. The effect of a secondary velocity away from the wall and the resulting axial momentum flux depression between the two subchannels was not predicted.

An additional feature of the secondary velocities not predicted by the model but apparent in the experiment was the deviation of the axial velocity contours away from the short wall in the small subchannel. This secondary velocity appeared to be quite strong since it caused a significant deviation in the axial velocity contours in some cases. This effect was especially apparent in Figure III.16, but was not predicted by the model.

The secondary flow pattern implied by the shape of the axial velocity contours is given in Figure V.10. The momentum transport provided by this pattern was considered vital in determining the flow distribution in the unequal subchannels. If each of the two rectangular subchannels were considered separately, the expected secondary velocity pattern for a rectangular duct could be seen. However, the two rectangular ducts have one common wall and here the secondary flow towards the centerline had the effect of transporting low momentum fluid to the region between the two subchannels.

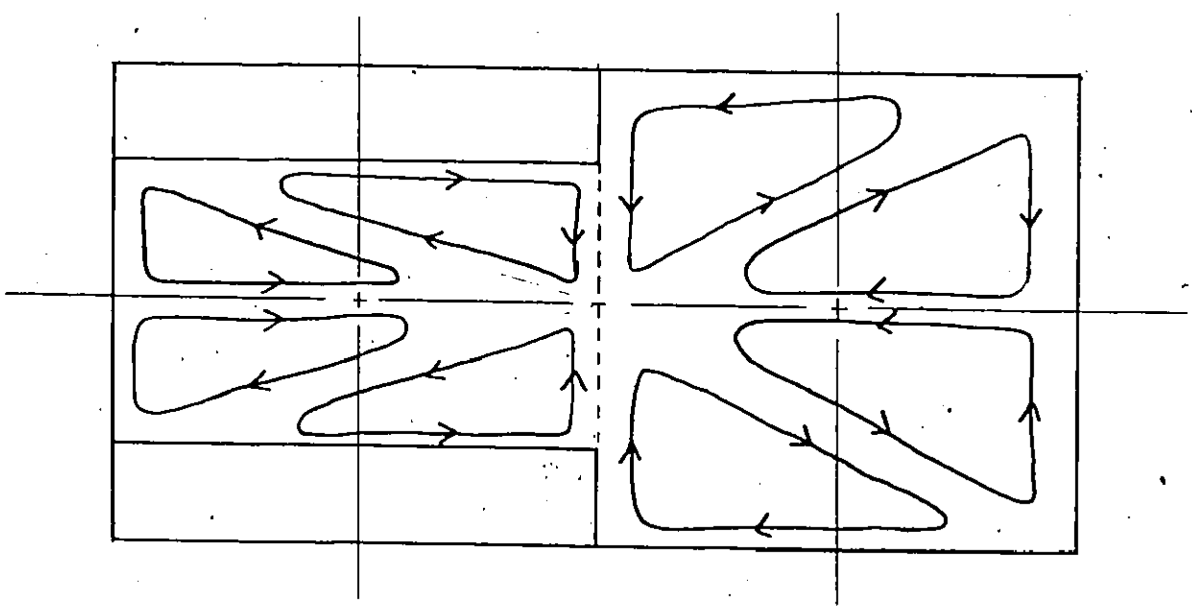

Figure V.10 Inferred Secondary Velocity Pattern

V.2 Tapucu Subchannel Experiments

No detailed point measurements of velocity were made during this set of experiments (Tapucu [1977]). However, the data available was very valuable in assessing the code's performance. This data consisted of axial pressure profiles, cross flow velocity between the subchannels, integral mass transfer along the subchannels and the mean axial velocity in each subchannel. To accomodate comparison with such data, the velocity fields predicted by the code were integrated over the appropriate areas to yield the required averages.

The Tapucu subchannel geometry has been presented previously in Section IV.4.2. For the purpose of the code predictions, the inlet velocity profiles to each subchannel were assumed to have been fully developed. These profiles were obtained by running the code with a single channel geometry and a flat inlet profile. The outlet profile from this run was then used as the inlet for the actual prediction.

The main prediction was done with the k-ε turbulence model activated and the laminar viscosity set at 0.001 Pa.s. To further investigate the predictions, several additional runs were done with no k-ε model and several different values for the effective viscosity. These runs are summarized in Table V.1.

Run No.	μ_{eff} (Pa·s)	k-ε Model
1	0.00100	Yes
2	0.00100	No
3	0.00162	No
4	0.01000	No

Table V.1 Tapucu Subchannel Runs

V.2.1 Discussion of the Code's Predictions

The code predictions were compared with the experimental data in Figure V.11 (repeat of Fig IV.19). Consider first the pressure profile prediction. The pressure gradients in the fully developed regions were properly predicted. This was seen in two locations; the high inlet flow subchannel before communication began and the interconnected subchannels far enough downstream that pressure differences between the subchannels had become minimal. Note that in this case there is zero inlet flow in one of the subchannels, as shown by the flat pressure profile.

While the fully developed pressure gradients were predicted successfully, the pressure recovery that occured at the beginning of the communicating section was not as accurately predicted. The mechanism producing this recovery was simply the deceleration of the fluid due to the suddenly larger flow area (recall that the inlet velocity in one of the subchannels was zero). Of greater importance than the pressure recovery was the pressure difference between the two subchannels. This was slightly underpredicted by the model, especially at the beginning of the communicating slot.

The cross flow velocity and integral mass transfer were plotted on common axes in Figure V.11. The integral mass transfer resulted from summing the flow through the communicating gap as given by the cross flow velocity. These predictions were quite good but there was a noticeable underprediction of cross flow velocity at the beginning of the slot. This corresponded to the underprediction of pressure difference pointed out earlier. Further down the subchannels, the cross flow velocity was predicted quite well.

Since continuity had to be respected the plot of mean axial velocity really provided no additional information than the cross flow velocity. However, the plot was included to illustrate a point. Note how accurate the plot of mean axial velocity appeared. Although the cross flow velocity was underpredicted at the beginning of the communicating region, there was no appreciable effect on the average axial velocity prediction because the gap was so narrow and the axial distance over which the prediction was poor was also small.

This illustrates the fact that bulk averages such as the mean axial velocities could be predicted very accurately while more detailed information such as the cross flow velocity was less accurately modelled. Although the cross flow velocity given here was not a single point value, the small communicating gap made it a much finer spatial average than the mean axial velocities.

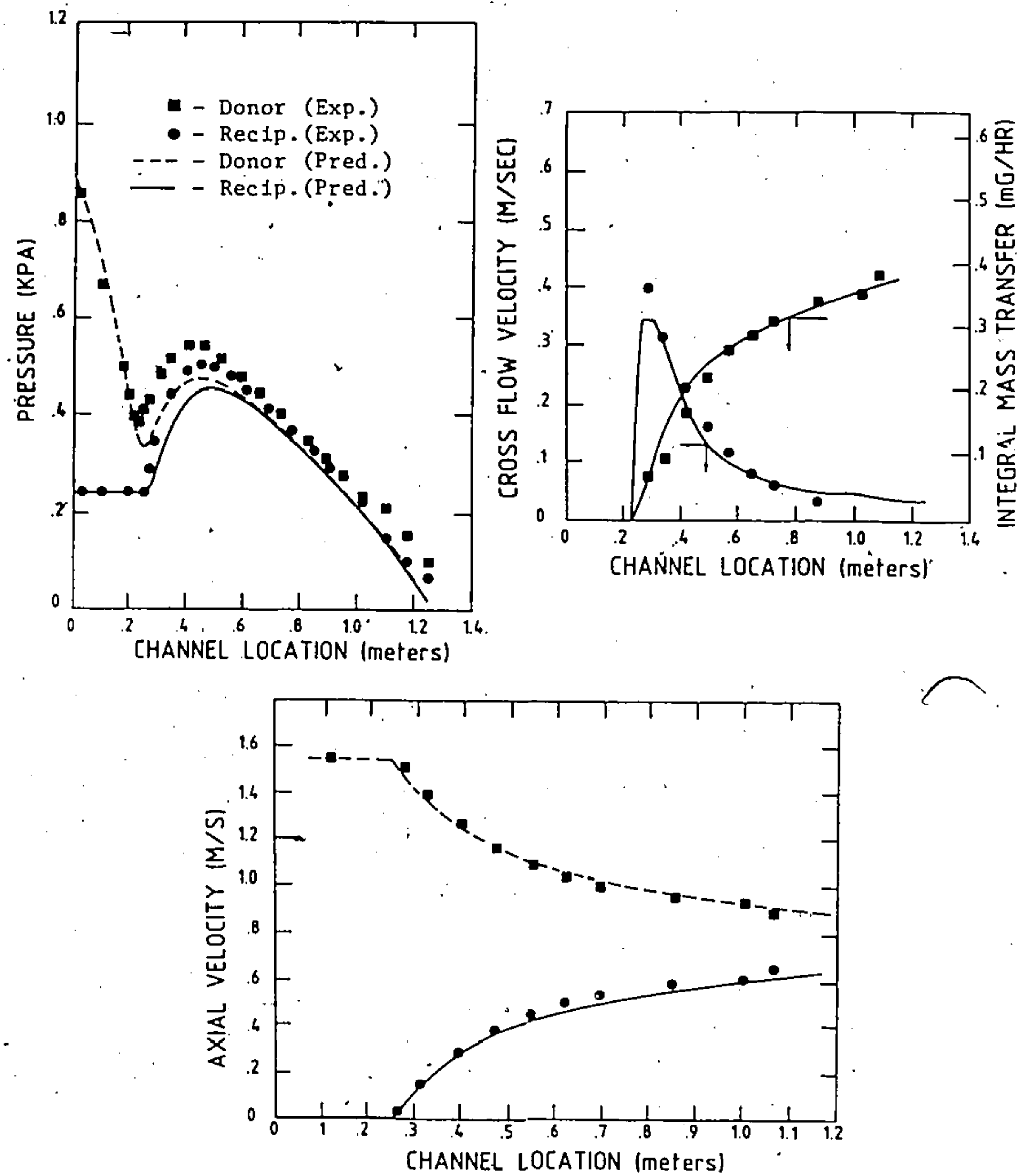

Figure V.11 Tapucu Subchannel Predictions (Run 1)
(k-ε Activated)

V.2.2 Discussion of the Turbulence Model

As listed in Table V.1, three additional runs were done to investigate the contribution of the k-ε model to the predictions shown in Figure V.11. Initially, the k-ε model was simply removed and the viscosity of the fluid left at the purely laminar value of 0.001 Pa.s. The results of this run were given in Figure V.12. The pressure gradient prior to the communicating slot was underpredicted by 38%. The most obvious discrepancy was the poor prediction of the pressure recovery, which was vastly underpredicted and occurred too far downstream. Also, the pressure difference between the two channels was badly underpredicted, especially at the beginning of the communicating slot. As a result, the cross flow velocity was also underpredicted. The integral mass transfer and mean axial velocity are consistent with the cross flow velocity.

Recall that the only link between the k-ε model and the solution of the Navier-Stokes equations was through the viscosity field. In general, the k-ε model increases the effective viscosity to model the increased diffusion of momentum due to turbulent fluctuations. The two runs discussed so far have definitely indicated that this elevated viscosity improved the prediction but there was no evidence that the elaborate field calculated by the k-ε model improved the prediction. Perhaps an artificially high effective viscosity throughout the flow field would have served just as well.

To see if there was a single viscosity which would give reasonable predictions, a run was done (Run No. 3) with an effective viscosity which would give the proper pressure gradient in the non-communicating region (μ = 0.00162 Pa.s). The results were given in Figure V.13. Note that the pressure gradient was matched but the pressure difference between the channels, as well as the pressure recovery and mass transfer predictions, did not show significant improvement.

Increasing the viscosity beyond that used in Run No. 3 would obviously result in an overprediction of the pressure gradient. However, this was done in Run No. 4 to see if the mass transfer prediction could be improved. The results were given in Figure V.14. The mass transfer was increased somewhat but still not near the experimental value. This slight improvement in mass transfer was gained at the expense of the pressure gradient which was then vastly overpredicted.

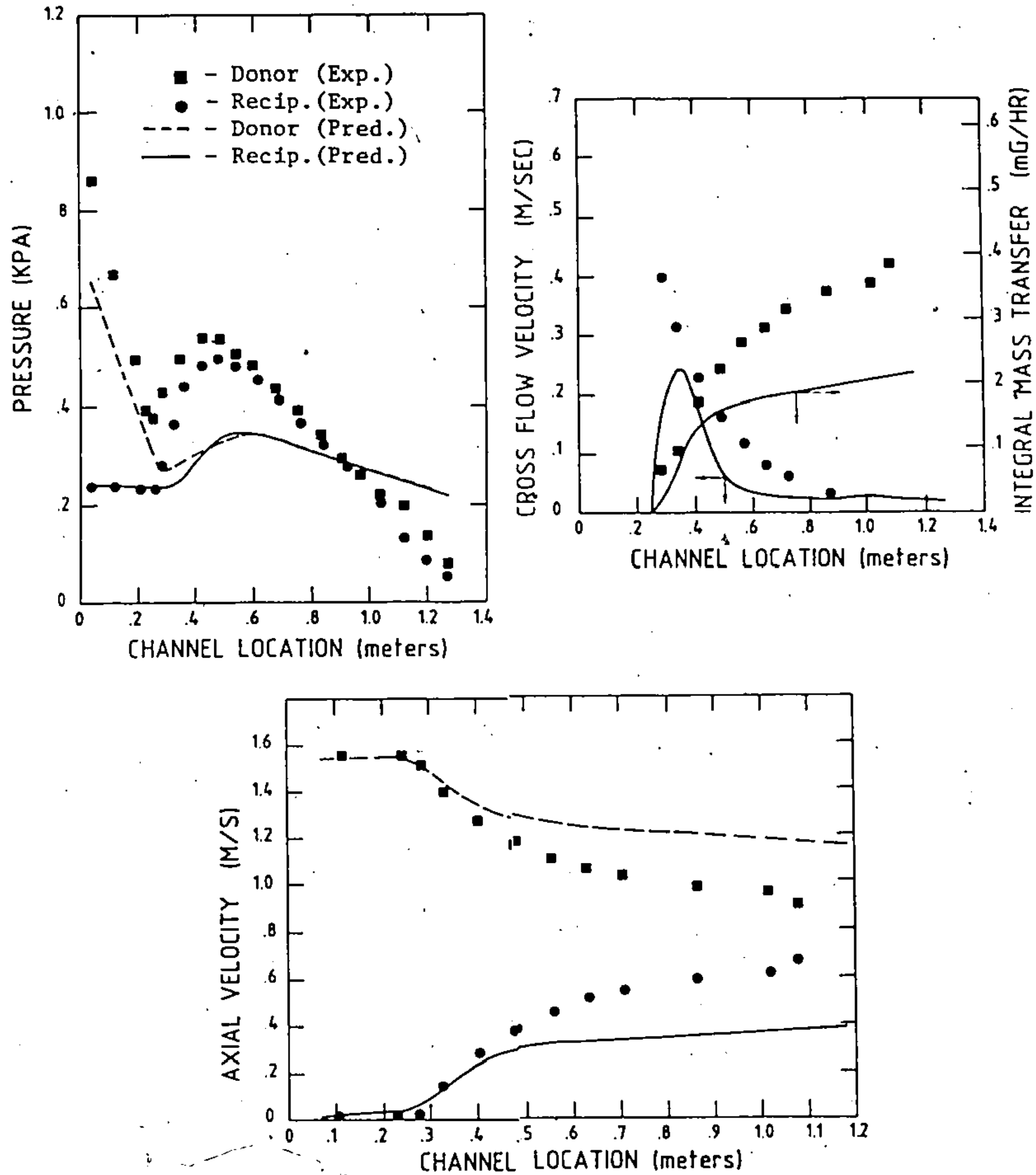

Figure V.12 , Tapucu Subchannel Predictions (Run 2)
(μ_{eff} = 0.001 Pa.s, k-ε off)

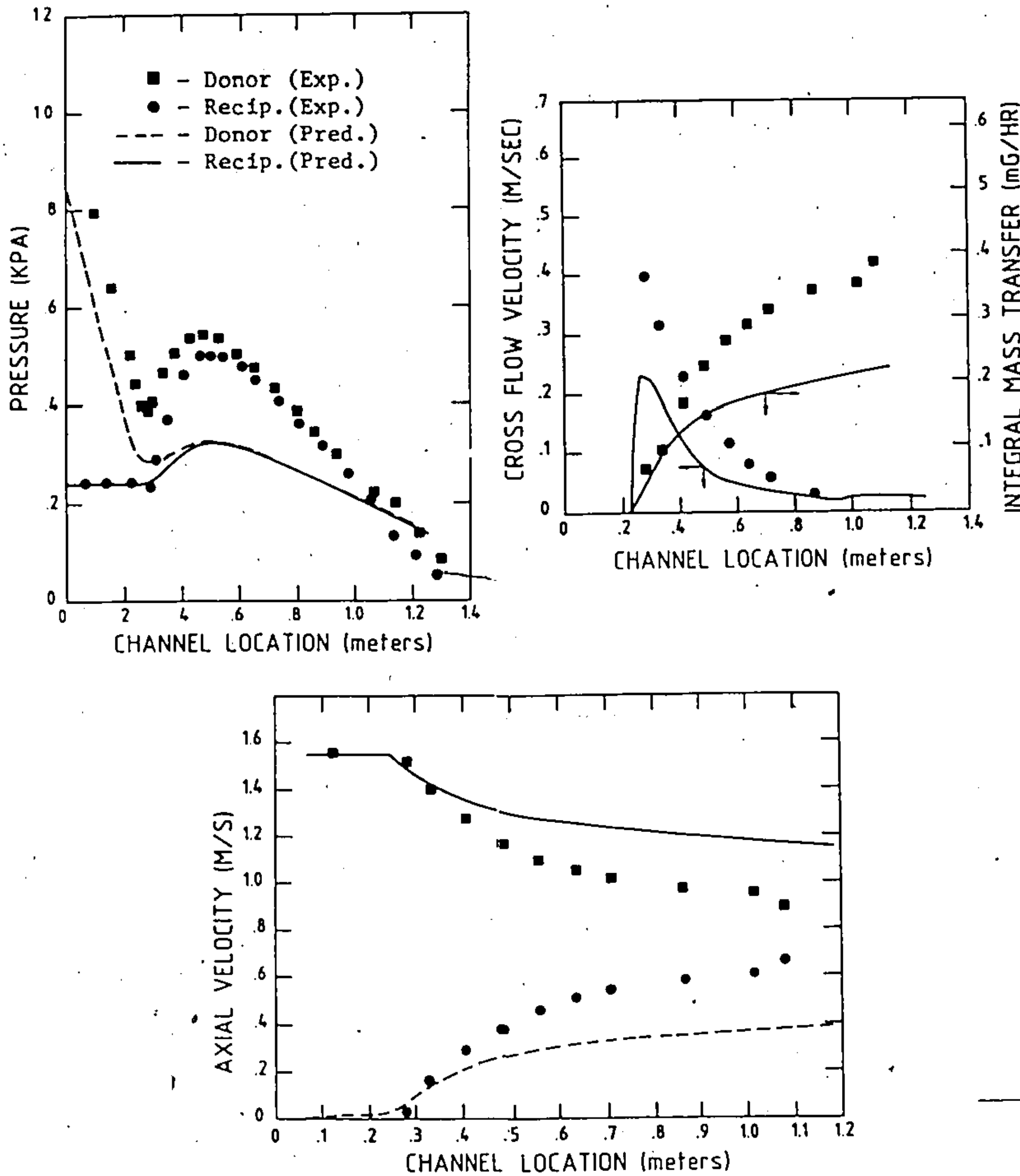

Figure V.13 Tapucu Subchannel Predictions (Run 3)
(μ_{eff} = 0.00162 Pa.s, k-ε off)

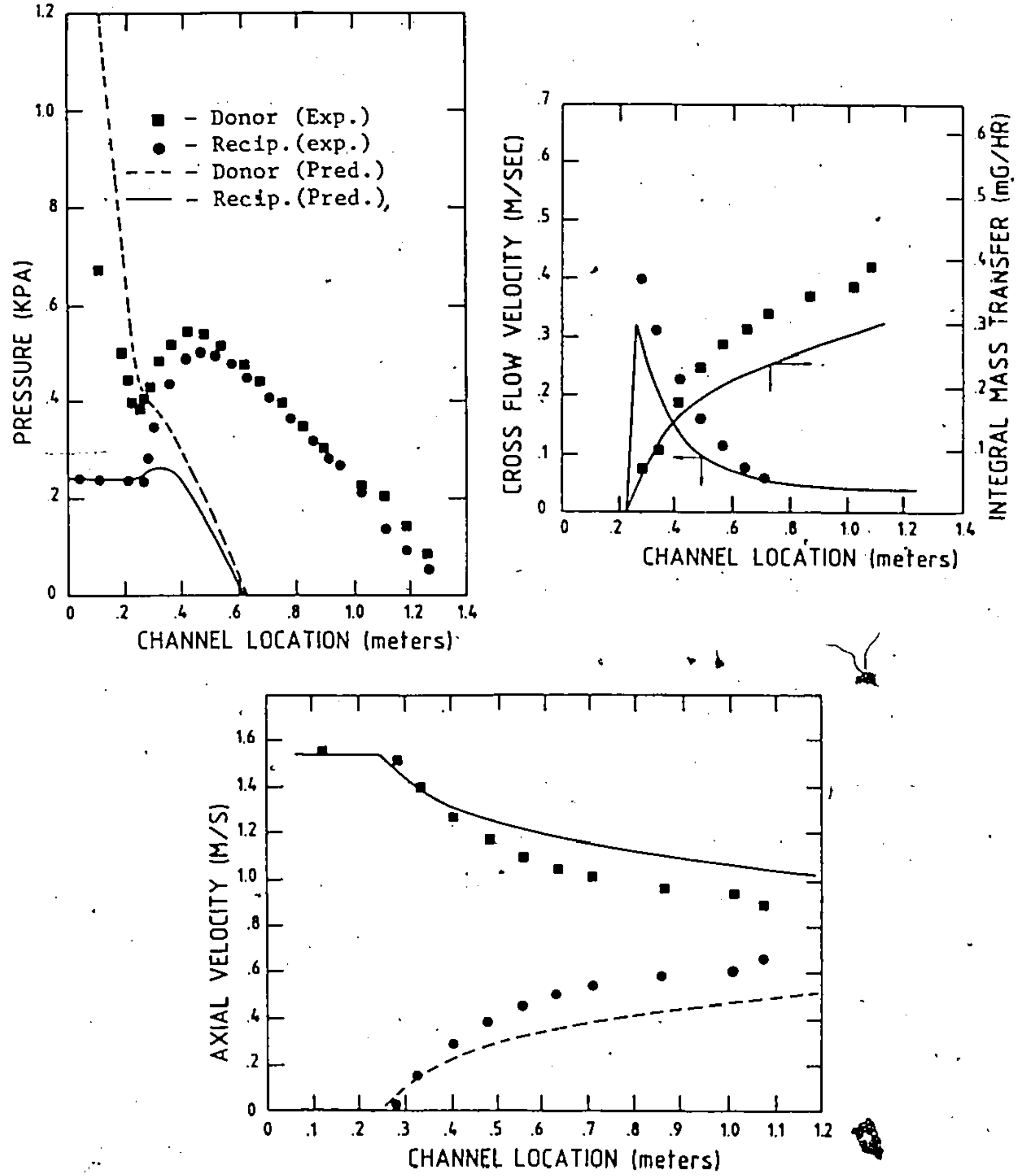

Figure V.14 Tapucu Subchannel Predictions (Run 4)
(μ_{eff} = 0.01 Pa.s, k-ε off)

The results of these runs had a clear interpretation when the transfer mechanisms involved were considered. Cross flow between the channels was induced by a pressure difference. Consider the two communicating subchannels with different flowrates. The subchannel with the higher flowrate had a larger pressure gradient. Since, at some downstream location, the pressure in the two subchannels had to be equal, the differing pressure gradients resulted in a pressure difference between the subchannels. It was this pressure difference which induced cross flow until the flowrates balanced causing the pressure gradients in both subchannels to be the same.

The effect of turbulent fluctuations between the subchannels was to enhance the pressure difference through their influence on the axial pressure gradients. The high flow subchannel received low momentum fluid via the turbulent fluctuations, which increased its axial pressure gradient. Meanwhile, the low flow subchannel received high momentum fluid via the turbulent fluctuations which decreased its pressure gradient. The net effect was a significantly enhanced pressure difference between the subchannels. It is important to note that since this was a single phase flow, the turbulent fluctuations themselves did not result in any net mass transfer. However, the effect they had on the pressure gradients did induce greater mass exchange.

Comparing Runs 1 and 2 showed the effect that the turbulent fluctuations had on the prediction. The pressure difference between the subchannels, and therefore the mass transfer, was underpredicted when the effects of turbulence were ignored. Near the beginning of the communicating slot a large portion of the pressure difference was due to the imbalance in pressure gradients in the non-communicating region. Although Run 2 also underpredicted in this region, it was even more inadequate further downstream where turbulent fluctuations between the subchannels were responsible for a higher fraction of the pressure imbalance.

The other runs done merely pointed out that a general elevation in the viscosity (even to the inflated value of 0.01 Pa.s) did not give good mass transfer predictions. The higher viscosity gave higher axial pressure gradients and therefore higher pressure differences between the subchannels and higher mass transfer. However, if the viscosity had been elevated to a point where the mass transfer had been adequately predicted by this mechanism alone, the pressure profile would have been very wrong. The ability to specify the viscosity in a more local manner was a great advantage in this prediction. This was because the level of turbulence varied a great deal throughout this geometry, from highly turbulent flow in the high flow subchannel, to laminar flow in the narrow communicating slot, to recirculating flow in the low flow subchannel. The addition of a local turbulence model was apparently quite effective in accounting for this.

VI. CONCLUSIONS

1. Successful single phase measurements of the fluid velocity in two adjacent subchannels of unequal size were made with a pitot tube and traversing device. Enough data points were taken to allow contour plots of velocity to be generated. The good symmetry of these plots as well as the close agreement between the flowrate measured in the pump supply line and the flowrate determined by integrating the pitot tube measurements indicates the accuracy of the data.

2. The experimental data indicates that two distinct relative maxima occur in the velocity contours; one in each subchannel.

3. As the area ratio is decreased (ie. size of small subchannel reduced) the velocity maximum in the small subchannel shifts toward the large subchannel (See Figures III.14 to III.21).

4. An area of low velocity exists between these two maxima in the region between the two subchannels. From the knowledge of the secondary flow pattern in rectangular ducts this low velocity can be attributed to a secondary flow away from the wall in that region.

5. Virtually no Reynolds number dependancy can be seen in the data over the range investigated. Compare, for example, Figures III.17 and III.21.

6. A three dimensional finite difference fluid flow code was modified to model the experiment. The code could assume a uniform effective viscosity or invoke the k-ε turbulence model.

7. There was no observable improvement in the predicted axial velocity field with or without the k-ε model activated. Neither method could predict the low velocity region between the subchannels and the resulting pair of axial velocity maxima (See Figures IV.10 to IV.13). Note how closely the contour lines approach the wall at the common corners between the two subchannels.

8. The k-ε turbulence model employs an isotropic turbulence assumption and was therefore unable to predict the secondary velocities present in flow through non-circular ducts. As a result, its predictions for the flow distribution in two adjacent subchannels of unequal size were quite poor. The elaborate viscosity field it specifies is of little importance because the velocity gradients are low everywhere except the wall, where the log law was imposed anyway.

9. The Tapucu [1977] subchannel experiments where modelled with the same code and for this case the k-ε turbulence model provided a very good prediction. Pressure differences between the subchannels, and not the secondary flows induced by Reynolds stresses, are the main mechanism creating cross flow between the subchannels. The very narrow communicating gap in this geometry led to a wide range of turbulence intensities and high velocity gradients in the freestream region. This made the local specification of viscosity very important to the solution.

BIBLIOGRAPHY

Acrivos,A., Schrader,L., [1982]. "Steady Flow in a Sudden Expansion at High Reynolds Numbers", Phys. Fluids , vol. 25, No. 6, pp.923-930.

Ahmed,S., Brundrett,E., [1971]. "Turbulent Flow in Non-Circular Ducts. Part 1: Mean Flow Properties in the Developing Region of a Square Duct", Int. J. Heat Mass Transfer, Vol.14, pp365-375.

Bradshaw,P., Dean,R.B., McEligot,D.M., [1973]. "Calculation of Interacting Turbulent Shear Layers: Duct Flow", Transactions of the ASME, June 1973, pp214-220.

Burden,R.L.., Faires,J.D., Reynolds,A.C. [1978]. Numerical Analysis, Second Edition, Prindle Weber and Schmidt, USA.

Byrne,J., Hatton,A.P., Marriott,P.G., [1970]. "Turbulent Flow and Heat Transfer in the Entrance Region of a Parallel Wall Passage", The Institution of Mechanical Engineers, Vol.184, Part 1, No.39.

Carver, M.B., [1983]. "Development and Application of Computer Codes for Multidimensional Analyses of Nuclear Reactor Components", CNS/ANS International Conference on Numerical Methods in Nuclear Engineering, Montreal, September 1983.

Carver,M.B., Tahir,A., Rowe,D.S., Tapucu,A., and Ahmad,S.Y., [1984]. "Computational Analysis of Two-Phase Flow in Horizontal Bundles", Nuclear Engineering and Design, Vol. 82, p12.

Chieng, C.C., Launder, B.E. [1980]. "On the Calculation of Turbulent Heat Transport Downstream from an Abrupt Pipe Expansion", The Winter Annual Meeting of the ASME, Chicago, Ill., Nov. 16-21.

Chue,S.H., [1975]. "Pressure Probes for Fluid Measurement", Prog. Aerospace Sci., Vol. 16, No. 2, pp147-223.

Courant,R., Isaacson,E., Rees,M., [1952]. "On the Solution of Non-linear Hyperbolic Differential Equations by Finite Differences", Comm. Pure Appl. Math., Vol.5, pp243.

Currie,I.G., [1974]. Fundamental Mechanics of Fluids, McGraw-Hill, USA.

Del Giudice,S., Strada,M., Comini,G., [1981]. "Three Dimensional Laminar Flow in Ducts", Numerical Heat Transfer, Vol.4, pp215-228.

Demuren,A.O., [1983]. "Prediction of Flow in Channels with Flood Planes", ASCE EMD Conf., Vol. 2, Lafayette, Indiana, May 1983.

Donea, J., [1984]. "Recent Advances in Computational Methods for Steady and Transient Transport Problems", Nuclear Engineering and Design, Vol. 80, pp141-162.

Fohs,H.P., Lyczkowski,R.W., Sha,W.T., [1981]. "A Three-Dimensional Simulation of Diversion Cross-Flow Between Two Parallel Channels Connected by a Narrow Lateral Slot Using the COMMIX-1A Computer Program", Argonne National Laboratory, ANL-CT-81-34.

Gessner,F.B., Jones,J.B., [1965]. "On Some Aspects of Fully Developed Turbulent Flow in Rectangular Channels", J.Fluid Mech., Vol.23, Part 4, pp689-713.

Hanjalic,K., Launder,B.E., [1972]. "A Reynolds Stress Model of Turbulence and its Application to Thin Shear Flow", J. Fluid Mech., Vol.52, part 4, pp.609-638.

Harlow,F.H., Nakayama,P.I., [1969]. "Transport of Turbulence Energy Decay Rate", Los Alamos Scientific Laboratory, LA-3854, Uc-34, Physics, TID-4500.

Harlow,F.H., Welch,J.E., [1965]. "Numerical Calculation of Time Dependant Viscous Incompressible Flow of Fluid with Free Surface", Phys. Fluids, Vol.8, pp2182.

Hartnett,J.P., Koh,J.C.Y., McComas,S.T., [1962]. "A Comparison of Predicted and Measured Friction Factors for Turbulent Flow Through Rectangular Ducts", Transactions of the ASME, Feb. 1962

Hinze,J.O., [1959]. Turbulence , Second Edition, McGraw-Hill,USA.

Knight,D.W., Lai,C.J., [1985]. "Turbulent Flow in Compound Channels and Ducts", Int. Symp. on Refined Flow Modeling and Turbulence Measurements, Iowa, Sept. 1985.

Kollmann,W., [1980]. Prediction Methods for Turbulent Flows, Hemisphere Publishing Corp., New York.

Kolmogorov,A.N., [1942]. "Equations of Turbulent Motion in an Incompressible Fluid", Izvestia Akademia Nauk SSSR, Seria fizicheska VI 1942, no. 1-2, pp56-58.

Laufer,J., [1951]. "Investigation of Turbulent Flow in a Two Dimensional Channel", NACA Report 1053.

Launder,B.E., Spalding,D.B., [1974]. "The Numerical Computation of Turbulent Flows", Computer Methods in Applied Mechanics and Engineering. Vol.3 pp 269-289.

Launder,B.E., Ying,W.M., [1973]. "Prediction of Flow and Heat Transfer in Ducts of Square Cross Section", Proc. Instn. Mech. Engrs., Vol. 187 37/73, pp455-461.

Leutheusser,H.J., [1963]. "Turbulent Flow in Rectangular Ducts", Journal of the Hydraulics Division, Proceedings of the American Society of Civil Engineers. Vol. 89.

Lumley, J.L., [1983]. "Turbulence Modelling", Journal of Applied Mechanics, Vol. 50, pp1097-1103.

Lundgren,T.S., Sparrow,E.M., Starr,J.B., [1964]. "Pressure Drop Due to the Entrance Region in Ducts of Arbitrary Cross Section", Transactions of the ASME, September 1964, pp620-626.

Lyall,H.G., [1973]. "Measurement of Flow Distribution and Secondary Flow in Ducts Composed of Two Interconnected Subchannels", Paper 33, Berkely Nuclear Laboratories.

MacMillan,F.A., [1956]. "Experiments on Pitot Tubes in Shear Flow", Brit. ARC R&M 3028.

Neti,S., Eichhorn,R., [1979]. "Comparison of Developing Turbulent Flow in a Square Duct", Proc. ASME Symp. Turbulent Boundary Layers, Niagara Falls.

Ng,K.H., Spalding,D.B., [1972]. "Turbulence Model for Boundary Layers near Walls", The Physics of Fluids, Vol. 15, No.1

Patankar,S.V., [1980]. Numerical Heat Transfer and Fluid Flow, McGraw-Hill, USA.

Prinos,P., Townsend,R., Tavoularis,S., [1985]. "Structure of Turbulence in Compound Channel Flows", Journal of Hydraulic Engineering, Vol. 111, No. 9.

Raithby,G.D., [1976a]. "A Critical Evaluation of Upstream Differencing Applied to Problems Involving Fluid Flow", Comp. Meth. App. Mech. and Eng., Vol.9, pp75-103.

Raithby,G.D., [1976b]. "Skew Upstream Differencing Schemes for Problems Involving Fluid Flow", Comp. Meth. App. Mech. and Eng., Vol.9, pp153-164.

Rapley,C.W., [1982]. "The Simulation of Secondary Flow Effects in Turbulent Non-Circular Passage Flows", International Journal for Numerical Methods in Fluids, Vol. 2, pp331-347.

Restivo,A.M.O. [1979]. "Turbulent Flow in Ventilated Rooms", Ph.D. Thesis, Imperial College, London.

Rhodes,D.B., Carlucci,L.N., [1983]. "Predicted and Measured Velocity Distributions in a Model Heat Exchanger", Atomic Energy of Canada Limited, AECL-8271.

Rogers,J.T., Tarasuk,W.R., [1968]. "A Generalized Correlation for Natural Mixing of Coolant in Fuel Bundles", Trans. Am. Nucl. Soc., Vol. 11, pp346-347.

Sami,S., [1967]. "The Pitit Tube in Turbulent Shear Flow", Proceedings of the 11th Midwestern Mechanicl Conference. Dev. in Mechanics, Vol. 5, pp 191-200.

Schlichting,Dr.H, [1955], Boundary-Layer Theory, Seventh Edition, McGraw-Hill, USA.

Slutsker,V.P.,Bolonov,E.P.,Tarasova,N.V., [1983]. "Experimental Investigation of the Intensity of Turbulent Cross-flow Transfer in Channels of Complex Shape", Thermal Engineering, Vol.30, No.2.

Spalding,D.B., [1972]. "A Novel Finite Difference Formulation for Differential Expressions Involving Both First and Second Derivatives", Int. J. Num. Methods Eng., Vol. 4, pp551.

Spalding,D.B., [1982]. Turbulence Models: A Lecture Course, Imperial College of Science and Technology, London.

Stephenson,P.L., [1975]. "A Theoretical Study of Heat Transfer in Two Dimensional Turbulent Flow in a Circular Pipe and Between Parallel and Diverging Plates", Int. J. Heat Mass Transfer, Vol. 19, pp413-423.

Tapucu,A. [1977]. "Studies on Diversion Cross-Flow Between Two Parallel Channels Communicating by a Lateral Slot. I: Transverse Flow Resistance Coefficient", Nuclear Engineering and Design. Vol. 42, pp297-306.

Tapucu,A., Merilo,M. [1977]. "Studies on Diversion Cross-Flow Between Two Parallel Channels Communicating by a Lateral Slot. II: Axial Pressure Variations", Nuclear Engineering and Design. Vol. 42, pp307-318.

Tapucu,A., Troche,N., [1982]. "Comparison of Subchannel Code COBRA-III-C with Experimental Data Obtained on Two Laterally Interconnected Flows", Ecole Polytechnique, Document IGN-465.

Tennekes,H.T., Lumley,J.L., [1972]. A First Course in Turbulence, MIT Press.

Tracey,H.J., [1976]. "The Structure of a Turbulent Flow in a Channel of Complex Shape", U.S. Geological Survey, Prof. Paper 983(1976).

Tsuge,A., Sakata,K., Hirao,Y., [1979]. "Abnormal Characteristics of Two-Phase Flow in Vertical Tube Banks", ASME Winter Annual Meeting, New York, Dec. 2-7, 1979.

van der Ros,T., Bogaardt,M., [1970]. "Mass and Heat Exchange Between Adjacent Channels in Liquid-Cooled Rod Bundles", Nuclear Engineering and Design. Vol. 12, pp259-268.

Verheugen,A.N.J., van der Ros,Th., van der Walle,F., Spight,C.L., Bogaardt,M., [1967]. "A Theoretical Model of Mixing Between Hydraulically Interconnected Channels", European Two Phase Heat Transfer Meeting, Bournemouth, June 12 - 16.

Wylie,C.R., [1966]. Advanced Engineering Mathematics, Fourth Edition, McGraw-Hill, USA.

APPENDIX A

PRESSURE PROFILE DATA

The measuring procedure used to obtain the pressure data presented here was explained in Section III.3.2. A short explanation of the layout of the tables on the following pages will now be given.

Each table contains all of the static wall pressure data taken for any of the four possible subchannel area ratios. The first column gives the axial location of the pressure tap in centimeters as measured from the test section inlet plane. Then, two sets of four columns each contain the various pressures at that axial location. Each set of four columns represents one of the two Reynolds numbers investigated. The four columns represent the four rows of pressure taps as depicted in Figure III.9. The reference location for the measurements is shown by the zero in the table. Note that the reference location was the most downstream tap on row A for all runs.

W2/W1=1.0

Axial Location (cm)	Pressure (Pa.)							
	R=180 000				R=108 000			
	A	B	C	D	A	B	C	D
10.0	163.7	168.5	169.9	158.5	65.4	77.8	62.9	69.9
20.0	143.8	148.7	150.1	138.6	57.5	69.9	55.0	62.0
30.0	125.0	129.9	131.4	119.7	50.0	62.6	47.4	54.5
40.0	103.8	108.7	110.1	98.5	41.5	54.1	38.9	46.0
50.0	81.0	85.7	87.1	75.8	32.4	44.6	29.9	36.8
60.0	61.5	66.3	67.7	56.3	24.6	37.0	22.1	29.1
70.0	41.3	46.1	47.5	36.0	16.5	29.0	14.0	21.0
80.0	20.5	25.3	26.7	15.3	8.2	20.6	5.7	12.7
90.0	0.0	4.8	6.2	-5.2	0.0	12.4	-2.5	4.5

W2/W1=0.68

Axial Location (cm)	Pressure (Pa.)							
	R=180 000				R=108 000			
	A	B	C	D	A	B	C	D
10.0	368.1	358.1	353.4	360.7	143.8	143.1	147.3	139.6
20.0	329.9	341.7	305.9	323.7	129.5	132.6	127.3	124.9
30.0	292.4	293.1	279.9	290.3	114.5	113.9	115.2	112.2
40.0	230.1	236.1	224.2	228.8	92.5	92.8	94.6	90.0
50.0	169.4	174.2	146.5	172.1	68.4	69.7	67.3	66.5
60.0	121.0	87.6	102.0	118.7	49.5	39.7	47.8	46.7
70.0	81.5	76.2	62.0	33.7	33.1	31.6	30.2	22.2
80.0	34.9	35.2	18.2	32.1	15.3	16.2	14.0	14.6
90.0	0.0	13.7	8.6	8.2	0.0	7.1	6.7	5.0

W2/W1=0.50

Axial Location (cm)	Pressure (Pa.)							
	R=180 000				R=108 000			
	A	B	C	D	A	B	C	D
10.0	491.5	516.3	513.7	484.0	171.8	184.0	188.6	182.2
20.0	476.4	491.9	469.7	464.9	164.7	173.8	172.8	172.8
30.0	418.5	424.6	426.2	422.1	143.8	149.3	155.1	156.0
40.0	348.6	348.3	352.6	336.8	119.0	122.1	127.8	126.1
50.0	263.2	259.5	265.4	261.8	88.1	90.0	94.8	95.9
60.0	183.4	144.1	183.9	171.9	59.8	49.8	64.8	64.5
70.0	103.8	101.4	117.7	114.5	31.8	33.2	39.0	40.4
80.0	14.6	31.3	66.0	29.4	1.1	6.3	64.9	9.2
90.0	0.0	-10.4	-8.1	-11.9	0.0	-10.1	-7.5	-6.5

W2/W1=0.32

Axial Location (cm)	Pressure (Pa.)							
	R=180 000				R=108 000			
	A	B	C	D	A	B	C	D
10.0	680.4	719.1	696.6	703.2	258.6	272.2	257.9	272.9
20.0	650.8	655.3	652.4	649.8	244.3	245.3	240.3	249.7
30.0	562.2	547.2	556.7	572.1	209.2	205.0	206.0	217.7
40.0	430.7	426.2	435.4	438.4	161.9	160.7	161.6	169.0
50.0	300.4	297.2	294.6	318.9	113.1	113.6	110.9	123.0
60.0	193.1	152.8	195.6	217.8	73.8	61.9	74.7	85.3
70.0	125.7	115.1	114.1	125.1	46.9	44.1	43.8	52.0
80.0	38.8	38.0	34.6	58.4	15.3	15.3	14.2	25.7
90.0	0.0	-17.2	1.7	10.2	0.0	-8.1	.3	7.1

APPENDIX B

AXIAL VELOCITY DATA

The velocity data tabulated here was presented in contour plot form in Section III.3.3. It was taken with a stagnation tube which was described in Section III.2.2. Each of the following pages contains the data for one axial location at a particular Reynolds number and subchannel area ratio. The locations are shown by the x and y coordinate values assigned to each row and column of the tables. The coordinate system to which these figures refer is established in Figure B.1.

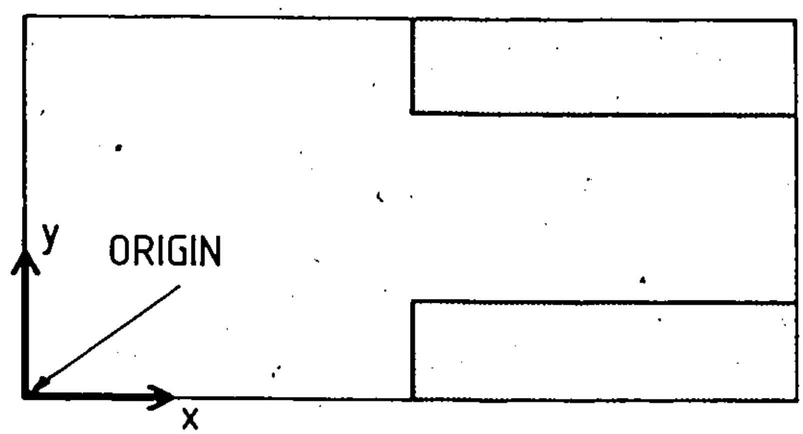

Figure B.1 Coordinate System for Axial Velocity Data

W2/W1=1.0

z/Z=0.0

R=180 000

Velocity in m/s ; Location in mm.

Y \ X	3.3	6.4	12.8	19.1	25.5	31.8	38.2	44.5	50.9	57.2	63.6	70.0
3.3	1.300	1.371	1.432	1.451	1.460	1.468	1.468	1.470	1.475	1.492	1.472	1.467
6.4	1.392	1.486	1.569	1.579	1.586	1.587	1.587	1.584	1.604	1.600	1.584	1.579
12.8	1.447	1.556	1.645	1.673	1.691	1.697	1.702	1.701	1.717	1.701	1.705	1.687
19.1	1.453	1.553	1.657	1.701	1.745	1.757	1.757	1.755	1.761	1.761	1.756	1.757
25.5	1.488	1.609	1.713	1.747	1.770	1.772	1.774	1.778	1.784	1.777	1.770	1.771
31.8	1.476	1.580	1.697	1.745	1.773	1.784	1.783	1.777	1.785	1.788	1.776	1.772
38.2	1.512	1.585	1.691	1.743	1.766	1.781	1.784	1.779	1.780	1.774	1.777	1.771
44.5	1.492	1.598	1.698	1.741	1.751	1.759	1.768	1.766	1.764	1.755	1.766	1.757
50.9	1.456	1.554	1.661	1.717	1.722	1.722	1.733	1.728	1.727	1.729	1.727	1.731
57.2	1.434	1.548	1.627	1.673	1.678	1.68[illegible]	1.673	1.678	1.672	1.676	1.682	1.690
63.6	1.362	1.450	1.522	1.558	1.567	1.574	1.563	1.560	1.562	1.560	1.564	1.568
66.8	1.[illegible]80	1.343	1.400	1.438	1.447	1.443	1.443	1.439	1.449	1.438	1.453	1.458

Y \ X	70.0	76.4	82.8	89.1	95.5	101.8	108.2	114.5	120.9	127.2	133.6	136.8
3.3	1.466	1.476	1.490	1.476	1.470	1.467	1.464	1.457	1.454	1.432	1.369	1.300
6.4	1.581	1.588	1.596	1.600	1.586	1.589	1.585	1.587	1.579	1.565	1.490	1.393
12.8	1.685	1.703	1.703	1.713	1.699	1.707	1.697	1.690	1.672	1.644	1.561	1.442
19.1	1.753	1.758	1.758	1.759	1.757	1.762	1.758	1.743	1.704	1.659	1.553	1.454
25.5	1.768	1.771	1.779	1.782	1.780	1.775	1.776	1.766	1.749	1.711	1.607	1.491
31.8	1.777	1.780	1.784	1.781	1.779	1.786	1.781	1.770	1.749	1.699	1.583	1.478
38.2	1.773	1.774	1.771	1.777	1.783	1.785	1.782	1.765	1.743	1.694	[illegible]	1.512
44.5	1.760	1.765	1.758	1.761	1.764	1.764	1.757	1.754	1.740	1.698	1.596	1.488
50.9	1.728	1.731	1.730	1.727	1.725	1.7[illegible]0	1.727	1.726	1.719	1.664	1.554	1.456
57.2	1.686	1.678	1.672	1.673	1.675	1.675	1.682	1.677	1.673	1.629	1.549	1.437
63.6	1.569	1.561	1.557	1.560	1.562	1.563	1.576	1.570	1.556	1.524	1.452	1.361
66.8	1.460	1.450	1.440	1.448	1.442	1.441	1.442	1.445	1.442	1.401	1.341	1.281

W2/W1=1.0

z/Z=0.5

R=180 000

Velocity in m/s ; Location in mm.

Y \ X	3.3	6.4	12.8	19.1	25.5	31.8	38.2	44.5	50.9	57.2	63.6	70.0
3.3	1.234	1.315	1.355	1.376	1.389	1.419	1.425	1.418	1.431	1.422	1.442	1.445
6.4	1.307	1.413	1.475	1.501	1.513	1.526	1.538	1.542	1.554	1.541	1.550	1.554
12.8	1.378	1.510	1.610	1.624	1.649	1.662	1.675	1.663	1.677	1.671	1.670	1.669
19.1	1.382	1.501	1.624	1.694	1.716	1.731	1.727	1.739	1.740	1.731	1.734	1.733
25.5	1.410	1.535	1.651	1.720	1.753	1.763	1.770	1.769	1.769	1.769	1.762	1.766
31.8	1.403	1.506	1.632	1.705	1.756	1.776	1.783	1.785	1.784	1.784	1.785	1.782
38.2	1.411	1.519	1.640	1.715	1.758	1.780	1.787	1.786	1.785	1.783	1.782	1.783
44.5	1.378	1.483	1.620	1.685	1.739	1.760	1.763	1.773	1.769	1.766	1.761	1.765
50.9	1.360	1.484	1.613	1.682	1.713	1.725	1.725	1.723	1.730	1.717	1.727	1.732
57.2	1.339	1.446	1.570	1.619	1.650	1.651	1.654	1.649	1.645	1.649	1.651	1.652
63.6	1.311	1.424	1.489	1.511	1.525	1.521	1.531	1.518	1.527	1.537	1.530	1.546
66.8	1.227	1.291	1.353	1.381	1.406	1.410	1.419	1.400	1.407	1.414	1.406	1.422

Y \ X	70.0	76.4	82.8	89.1	95.5	101.8	108.2	114.5	120.9	127.2	133.6	136.8
3.3	1.419	1.416	1.422	1.425	1.418	1.431	1.415	1.405	1.410	1.386	1.333	1.263
6.4	1.541	1.535	1.541	1.533	1.525	1.531	1.530	1.519	1.514	1.483	1.410	1.315
12.8	1.655	1.661	1.659	1.665	1.660	1.655	1.665	1.658	1.643	1.592	1.481	1.370
19.1	1.730	1.730	1.726	1.727	1.728	1.730	1.723	1.716	1.683	1.612	1.482	1.383
25.5	1.758	1.758	1.758	1.755	1.764	1.756	1.755	1.740	1.712	1.645	1.528	1.411
31.8	1.771	1.771	1.772	1.771	1.767	1.768	1.764	1.744	1.706	1.630	1.513	1.417
38.2	1.765	1.764	1.764	1.764	1.764	1.763	1.759	1.748	1.714	1.643	1.528	1.419
44.5	1.750	1.746	1.747	1.747	1.750	1.746	1.738	1.728	1.695	1.623	1.495	1.399
50.9	1.712	1.713	1.706	1.714	1.706	1.709	1.707	1.710	1.682	1.619	1.503	1.383
57.2	1.650	1.634	1.629	1.638	1.639	1.650	1.646	1.638	1.623	1.579	1.459	1.340
63.6	1.512	1.518	1.515	1.521	1.511	1.519	1.519	1.513	1.515	1.487	1.430	1.333
66.8	1.405	1.408	1.397	1.395	1.391	1.380	1.392	1.401	1.392	1.365	1.320	1.259

W2/W1=1.0

z/Z=1.0

R=180 000

Velocity in m/s ; Location in mm.

Y \ X	3.3	6.4	12.8	19.1	25.5	31.8	38.2	44.5	50.9	57.2	63.6	70.0
3.3	1.209	1.306	1.354	1.369	1.383	1.392	1.398	1.422	1.421	1.419	1.437	1.428
6.4	1.272	1.395	1.471	1.509	1.505	1.518	1.526	1.533	1.531	1.549	1.547	1.553
12.8	1.333	1.465	1.599	1.651	1.659	1.659	1.664	1.671	1.672	1.677	1.691	1.696
19.1	1.369	1.494	1.651	1.706	1.739	1.740	1.745	1.749	1.746	1.755	1.765	1.769
25.5	1.382	1.514	1.642	1.735	1.769	1.787	1.793	1.798	1.798	1.804	1.806	1.805
31.8	1.372	1.505	1.635	1.719	1.771	1.795	1.804	1.806	1.804	1.805	1.806	1.807
38.2	1.355	1.479	1.626	1.713	1.770	1.790	1.802	1.802	1.803	1.802	1.803	1.799
44.5	1.342	1.471	1.612	1.702	1.754	1.774	1.769	1.763	1.764	1.774	1.771	1.773
50.9	1.324	1.445	1.599	1.696	1.726	1.736	1.747	1.747	1.738	1.745	1.737	1.734
57.2	1.302	1.421	1.578	1.639	1.661	1.664	1.666	1.670	1.665	1.674	1.656	1.660
63.6	1.282	1.398	1.475	1.508	1.534	1.538	1.528	1.532	1.533	1.547	1.537	1.535
66.8	1.169	1.274	1.343	1.343	1.341	1.341	1.379	1.388	1.394	1.406	1.413	1.392

Y \ X	70.0	76.4	82.8	89.1	95.5	101.8	108.2	114.5	120.9	127.2	133.6	136.8
3.3	1.425	1.413	1.407	1.416	1.405	1.391	1.390	1.391	1.376	1.353	1.316	1.240
6.4	1.554	1.547	1.547	1.546	1.531	1.528	1.525	1.518	1.512	1.496	1.429	1.303
12.8	1.677	1.691	1.683	1.675	1.674	1.666	1.673	1.662	1.654	1.598	1.475	1.342
19.1	1.755	1.765	1.747	1.747	1.755	1.754	1.750	1.747	1.715	1.637	1.491	1.367
25.5	1.800	1.798	1.793	1.803	1.798	1.796	1.792	1.781	1.718	1.655	1.497	1.389
31.8	1.816	1.818	1.817	1.822	1.819	1.819	1.813	1.788	1.740	1.656	1.512	1.395
38.2	1.811	1.811	1.812	1.812	1.819	1.815	1.820	1.789	1.748	1.650	1.510	1.389
44.5	1.789	1.787	1.784	1.785	1.799	1.795	1.790	1.776	1.730	1.639	1.503	1.386
50.9	1.740	1.749	1.745	1.745	1.751	1.752	1.747	1.741	1.716	1.635	1.480	1.350
57.2	1.674	1.658	1.657	1.660	1.666	1.658	1.664	1.653	1.649	1.603	1.467	1.337
63.6	1.521	1.529	1.535	1.532	1.536	1.531	1.524	1.516	1.507	1.506	1.422	1.315
66.8	1.425	1.415	1.416	1.424	1.427	1.410	1.404	1.397	1.385	1.387	1.353	1.263

W2/W1=1.0

z/Z=0.0

R=108 000

Velocity in m/s ; Location in mm.

Y \ X	3.3	6.4	12.8	19.1	25.5	31.8	38.2	44.5	50.9	57.2	63.6	70.0
3.3	.686	.741	.788	.815	.842	.839	.847	.838	.820	.835	.831	.836
6.4	.744	.835	.885	.910	.926	.930	.934	.946	.943	.939	.930	.939
12.8	.797	.890	.967	.985	1.007	1.020	1.022	1.018	1.014	1.010	1.004	1.007
19.1	.806	.898	.980	1.021	1.031	1.046	1.044	1.045	1.038	1.034	1.031	1.035
25.5	.814	.915	1.001	1.038	1.052	1.057	1.059	1.061	1.055	1.056	1.048	1.050
31.8	.822	.901	.994	1.037	1.058	1.071	1.068	1.070	1.063	1.059	1.062	1.058
38.2	.823	.917	1.000	1.036	1.061	1.074	1.071	1.072	1.066	1.065	1.060	1.053
44.5	.799	.892	.987	1.031	1.060	1.068	1.070	1.067	1.062	1.059	1.054	1.054
50.9	.802	.900	.985	1.022	1.045	1.051	1.056	1.057	1.053	1.042	1.037	1.038
57.2	.779	.877	.957	.997	1.012	1.017	1.017	1.022	1.019	1.016	1.013	1.006
63.6	.765	.859	.926	.929	.933	.945	.943	.939	.943	.935	.934	.928
66.8	.716	.784	.820	.796	.843	.856	.864	.865	.859	.856	.854	.840

Y \ X	70.0	76.4	82.8	89.1	95.5	101.8	108.2	114.5	120.9	127.2	133.6	136.8
3.3	.842	.850	.843	.844	.834	.824	.840	.841	.832	.810	.783	.745
6.4	.932	.926	.932	.922	.918	.924	.918	.917	.908	.887	.847	.781
12.8	1.001	.995	1.001	1.000	.995	.992	.989	.983	.975	.954	.897	.817
19.1	1.035	1.026	1.026	1.023	1.022	1.018	1.018	1.012	.997	.963	.893	.805
25.5	1.053	1.043	1.042	1.036	1.032	1.032	1.032	1.024	1.008	.980	.916	.827
31.8	1.050	1.049	1.046	1.042	1.041	1.035	1.028	1.023	1.011	.978	.911	.840
38.2	1.056	1.050	1.044	1.043	1.036	1.038	1.032	1.024	1.015	.983	.922	.856
44.5	1.050	1.044	1.039	1.036	1.027	1.028	1.018	1.012	1.009	.969	.904	.842
50.9	1.035	1.031	1.023	1.022	1.014	1.013	1.008	1.002	.993	.966	.907	.835
57.2	1.011	1.007	.988	.987	.977	.977	.978	.973	.963	.935	.868	.805
63.6	.933	.930	.922	.917	.907	.910	.903	.919	.905	.890	.846	.782
66.8	.862	.860	.844	.835	.824	.828	.833	.832	.821	.810	.769	.715

W2/W1=1.0

z/Z=0.5

R=108 000

Velocity in m/s ; Location in mm.

Y \ X	3.3	6.4	12.8	19.1	25.5	31.8	38.2	44.5	50.9	57.2	63.6	70.0
3.3	.785	.824	.860	.858	.870	.882	.877	.880	.875	.877	.870	.878
6.4	.796	.847	.913	.920	.930	.927	.919	.918	.923	.933	.922	.918
12.8	.836	.894	.965	.994	1.005	1.005	1.006	1.011	1.002	.998	1.004	1.000
19.1	.826	.897	.975	1.021	1.047	1.049	1.046	1.051	1.055	1.056	1.052	1.051
25.5	.850	.923	.999	1.050	1.075	1.075	1.081	1.079	1.082	1.080	1.075	1.081
31.8	.842	.905	.988	1.036	1.080	1.091	1.087	1.090	1.096	1.095	1.087	1.087
38.2	.860	.925	1.004	1.058	1.081	1.087	1.089	1.086	1.093	1.096	1.094	1.086
44.5	.849	.912	.988	1.042	1.058	1.078	1.082	1.083	1.077	1.076	1.076	1.077
50.9	.847	.917	.989	1.031	1.040	1.037	1.047	1.053	1.054	1.044	1.042	1.060
57.2	.818	.880	.952	.990	.998	.993	.998	.996	.998	.998	1.007	1.011
63.6	.809	.863	.899	.906	.910	.912	.916	.915	.925	.919	.931	.932
66.8	.749	.784	.806	.846	.849	.851	.856	.848	.857	.843	.857	.861

Y \ X	70.0	76.4	82.8	89.1	95.5	101.8	108.2	114.5	120.9	127.2	133.6	136.8
3.3	.877	.874	.874	.876	.880	.876	.877	.866	.861	.859	.821	.784
6.4	.920	.926	.929	.919	.920	.922	.925	.931	.920	.908	.851	.796
12.8	.998	1.001	1.001	.997	1.009	1.011	1.005	1.004	.992	.964	.899	.830
19.1	1.047	1.054	1.052	1.053	1.053	1.051	1.050	1.045	1.025	.978	.897	.827
25.5	1.077	1.076	1.083	1.080	1.081	1.082	1.080	1.071	1.052	.997	.920	.853
31.8	1.092	1.091	1.091	1.092	1.092	1.090	1.088	1.076	1.040	.990	.909	.844
38.2	1.088	1.091	1.093	1.090	1.089	1.091	1.088	1.080	1.058	1.008	.930	.861
44.5	1.081	1.076	1.080	1.074	1.081	1.079	1.076	1.062	1.040	.988	.909	.845
50.9	1.056	1.046	1.046	1.053	1.050	1.043	1.041	1.045	1.033	.992	.917	.846
57.2	1.006	1.002	.993	.988	.993	.999	.995	.996	.990	.954	.881	.822
63.6	.932	.927	.916	.923	.917	.917	.913	.914	.903	.901	.866	.807
66.8	.863	.854	.845	.856	.852	.853	.849	.847	.850	.807	.783	.751

W2/W1=1.0

z/Z=1.0

R=108 000

Velocity in m/s ; Location in mm.

Y \ X	3.3	6.4	12.8	19.1	25.5	31.8	38.2	44.5	50.9	57.2	63.6	70.0
3.3	.695	.741	.786	.795	.793	.806	.810	.812	.810	.805	.824	.815
6.4	.743	.825	.880	.906	.913	.915	.925	.916	.920	.926	.935	.930
12.8	.785	.880	.965	.993	.999	1.004	1.001	1.002	1.007	1.011	1.016	1.017
19.1	.810	.896	.988	1.029	1.046	1.054	1.054	1.055	1.057	1.055	1.057	1.058
25.5	.827	.893	.994	1.053	1.088	1.084	1.081	1.087	1.087	1.090	1.087	1.086
31.8	.827	.894	.995	1.050	1.084	1.099	1.102	1.100	1.105	1.102	1.105	1.103
38.2	.823	.893	.993	1.054	1.089	1.107	1.109	1.106	1.107	1.106	1.104	1.100
44.5	.813	.887	.978	1.047	1.079	1.100	1.092	1.093	1.093	1.093	1.093	1.089
50.9	.813	.891	.977	1.038	1.057	1.061	1.068	1.066	1.062	1.066	1.064	1.064
57.2	.816	.889	.966	.992	1.004	.999	1.014	1.007	1.006	1.012	1.004	1.006
63.6	.780	.846	.887	.889	.902	.921	.910	.918	.927	.928	.926	.926
66.8	.729	.782	.800	.803	.811	.822	.835	.839	.846	.852	.845	.850

Y \ X	70.0	76.4	82.8	89.1	95.5	101.8	108.2	114.5	120.9	127.2	133.6	136.8
3.3	.833	.827	.834	.824	.829	.824	.826	.825	.819	.802	.775	.731
6.4	.907	.910	.911	.898	.905	.897	.902	.892	.879	.876	.827	.776
12.8	.995	.989	.996	.992	.989	.995	.988	.996	.982	.953	.875	.796
19.1	1.047	1.053	1.050	1.051	1.050	1.052	1.051	1.044	1.021	.968	.878	.803
25.5	1.079	1.082	1.081	1.085	1.084	1.084	1.078	1.067	1.040	.985	.896	.814
31.8	1.094	1.098	1.099	1.099	1.098	1.099	1.094	1.079	1.047	.990	.896	.834
38.2	1.099	1.096	1.093	1.101	1.101	1.098	1.094	1.077	1.048	.994	.899	.830
44.5	1.086	1.084	1.081	1.077	1.083	1.078	1.081	1.073	1.039	.988	.893	.824
50.9	1.059	1.061	1.052	1.048	1.054	1.050	1.044	1.047	1.025	.985	.896	.818
57.2	1.015	1.020	1.002	1.009	1.016	1.007	1.009	1.005	.993	.969	.900	.815
63.6	.944	.948	.938	.936	.935	.931	.925	.920	.922	.907	.872	.788
66.8	.872	.857	.864	.877	.867	.866	.855	.849	.842	.844	.787	.767

W2/W1=0.68

z/Z=0.0

R=180 000

Velocity in m/s ; Location in mm.

Y \ X	3.3	6.4	12.8	19.1	25.5	31.8	38.2	44.5	50.9	57.2	63.6	66.8
3.3	1.627	1.705	1.772	1.785	1.797	1.792	1.781	1.809	1.837	1.880	1.886	1.795
6.4	1.699	1.824	1.875	1.901	1.903	1.907	1.902	1.924	1.939	1.972	1.927	1.912
12.8	1.752	1.880	1.951	1.976	1.987	1.994	2.003	1.998	2.013	2.011	1.755	1.761
19.1	1.773	1.879	2.013	2.025	2.031	2.034	2.030	2.044	2.046	2.050	1.996	2.010
25.5	1.789	1.909	2.001	2.031	2.051	2.053	2.059	2.061	2.062	2.069	2.068	2.060
31.8	1.798	1.917	2.005	2.040	2.053	2.061	2.057	2.059	2.066	2.071	2.073	2.077
38.2	1.795	1.922	2.008	2.042	2.053	2.062	2.059	2.061	2.064	2.068	2.073	2.074
44.5	1.789	1.908	2.004	2.033	2.047	2.056	2.054	2.058	2.062	2.070	2.069	2.058
50.9	1.773	1.883	2.014	2.028	2.030	2.031	2.036	2.038	2.048	2.048	1.996	2.009
57.2	1.755	1.877	1.955	1.976	1.989	1.995	2.001	1.998	2.012	2.007	1.753	1.757
63.6	1.699	1.821	1.873	1.898	1.900	1.905	1.901	1.925	1.941	1.970	1.931	1.913
66.8	1.625	1.708	1.775	1.785	1.794	1.795	1.783	1.808	1.837	1.878	1.888	1.793

Y \ X	66.8	70.0	73.3	76.4	82.8	89.1	95.5	101.8	108.2	114.5	120.9	127.2	133.6	136.8
15.9	1.823	1.835	1.929	1.935	1.933	1.933	1.935	1.930	1.936	1.930	1.927	1.910	1.845	1.766
19.1	1.992	1.990	2.017	2.018	2.014	2.011	2.011	2.006	2.005	1.998	1.987	1.968	1.885	1.816
25.5	2.075	2.076	2.069	2.071	2.069	2.067	2.068	2.071	2.058	2.057	2.030	1.980	1.888	1.797
31.8	2.086	2.088	2.089	2.094	2.100	2.095	2.094	2.097	2.093	2.085	2.055	1.992	1.887	1.800
38.2	2.087	2.089	2.095	2.092	2.100	2.095	2.095	2.096	2.090	2.081	2.054	1.995	1.888	1.799
44.5	2.071	2.075	2.068	2.070	2.071	2.064	2.068	2.071	2.059	2.057	2.029	1.979	1.891	1.794
50.9	1.992	1.985	2.014	2.022	2.018	2.012	2.012	2.004	2.004	1.999	1.987	1.963	1.889	1.815
54.2	[illegible]	1.829	1.931	1.935	1.934	1.934	1.933	1.920	1.939	1.933	1.926	1.910	1.843	1.767

W2/W1=0.68

z/Z=0.5

R=180 000

Velocity in m/s ; Location in mm.

Y \ X	3.3	6.4	12.8	19.1	25.5	31.8	38.2	44.5	50.9	57.2	63.6	66.8
3.3	1.553	1.630	1.689	1.726	1.728	1.731	1.760	1.795	1.787	1.753	1.619	1.551
6.4	1.634	1.781	1.836	1.855	1.874	1.885	1.896	1.918	1.943	1.917	1.818	1.690
12.8	1.719	1.864	1.990	2.022	2.027	2.044	2.058	2.065	2.054	2.020	1.922	1.775
19.1	1.738	1.894	2.028	2.078	2.095	2.107	2.115	2.108	2.076	2.033	1.964	1.917
25.5	1.768	1.905	2.033	2.095	2.115	2.128	2.130	2.128	2.102	2.073	2.038	2.033
31.8	1.769	1.897	2.047	2.106	2.120	2.136	2.141	2.136	2.116	2.097	2.088	2.084
38.2	1.760	1.913	2.047	2.104	2.124	2.132	2.138	2.135	2.119	2.094	2.082	2.078
44.5	1.739	1.871	2.026	2.095	2.131	2.133	2.143	2.135	2.108	2.076	2.041	2.038
50.9	1.734	1.888	2.034	2.093	2.114	2.115	2.123	2.113	2.085	2.047	1.962	1.923
57.2	1.705	1.844	1.993	2.040	2.056	2.052	2.053	2.059	2.051	2.015	1.924	1.791
63.6	1.680	1.804	1.887	1.904	1.912	1.910	1.927	1.927	1.914	1.866	1.802	1.650
66.8	1.591	1.673	1.728	1.729	1.753	1.755	1.763	1.783	1.781	1.722	1.615	1.516

Y \ X	66.8	70.0	73.3	76.4	82.8	89.1	95.5	101.8	108.2	114.5	120.9	127.2	133.6	136.8
15.9	1.836	1.784	1.854	1.886	1.908	1.855	1.876	1.863	1.858	1.857	1.851	1.815	1.739	1.660
19.1	1.920	1.909	1.951	1.986	2.018	2.013	1.999	1.992	1.983	1.986	1.966	1.9[illegible]	1.819	1.711
25.5	2.019	2.031	2.047	2.066	2.095	2.10[illegible]	2.100	2.105	2.092	2.073	2.045	1.939	1.798	1.668
31.8	2.0[illegible]2	2.076	2.079	2.079	2.101	2.108	2.119	2.117	2.104	2.090	2.030	1.917	1.749	1.622
38.2	2.06[illegible]	2.068	2.077	2.084	2.109	2.127	2.129	2.124	2.129	2.131	2.078	1.958	1.816	1.689
44.5	2.0[illegible]5	2.031	2.041	2.051	2.080	2.108	2.106	2.101	2.092	2.085	2.043	1.959	1.836	1.722
50.9	1.[illegible]13	1.893	1.910	1.960	1.979	1.984	1.968	1.966	1.960	1.943	1.921	1.888	1.790	1.698
54.2	1.[illegible]53	1.799	1.832	1.847	1.875	1.850	1.830	1.813	1.829	1.777	1.747	1.698	1.623	1.582

W2/W1=0.68

z/Z=1.0

R=180 000

Velocity in m/s ; Location in mm.

Y \ X	3.3	6.4	12.8	19.1	25.5	31.8	38.2	44.5	50.9	57.2	63.6	66.8
3.3	1.517	1.634	1.680	1.710	1.715	1.734	1.772	1.786	1.7[illegible]1	1.693	1.575	1.52[illegible]
6.4	1.600	1.751	1.852	1.866	1.879	1.880	1.899	1.909	1.901	1.857	1.756	1.672
12.8	1.653	1.815	1.985	2.027	2.037	2.052	2.057	2.065	2.047	2.011	1.898	1.769
19.1	1.689	1.844	2.014	2.092	2.130	2.130	2.138	2.128	2.101	2.044	1.938	1.886
25.5	1.722	1.872	2.051	2.123	2.156	2.176	2.172	2.154	2.126	2.088	2.036	2.027
31.8	1.730	1.882	2.046	2.121	2.157	2.170	2.171	2.153	2.130	2.108	2.091	2.091
38.2	1.740	1.883	2.049	2.129	2.164	2.181	2.176	2.160	2.136	2.110	2.089	2.080
44.5	1.709	1.860	2.034	2.134	2.171	2.183	2.181	2.165	2.138	2.099	2.048	2.028
50.9	1.684	1.841	2.017	2.108	2.142	2.145	2.154	2.139	2.103	2.043	1.945	1.881
57.2	1.652	1.816	1.976	2.037	2.053	2.063	2.069	2.065	2.038	1.996	1.897	1.783
63.6	1.619	1.752	1.839	1.862	1.869	1.875	1.884	1.890	1.853	1.826	1.758	1.650
66.8	1.489	1.562	1.636	1.679	1.683	1.701	1.710	1.721	1.715	1.639	1.559	1.503

Y \ X	66.8	70.0	73.3	76.4	82.8	89.[illegible]	95.5	101.8	108.2	114.5	120.9	127.2	133.6	136.8
15.9	1.779	1.730	1.795	1.835	1.838	1.800	1.771	1.737	1.724	1.713	1.700	1.644	1.585	1.510
19.1	1.872	1.868	1.908	1.956	1.971	1.960	1.913	1.894	1.879	1.869	1.850	1.801	1.714	1.600
25.5	2.017	2.011	2.038	2.058	2.101	2.111	2.110	2.094	2.072	2.067	2.023	1.936	1.783	1.642
31.8	2.097	2.093	2.105	2.112	2.142	2.165	2.17[illegible]	2.162	2.155	2.115	2.043	1.928	1.747	1.628
38.2	2.091	2.097	2.096	2.110	2.140	2.161	2.172	2.183	2.167	2.134	2.061	1.939	1.784	1.635
44.5	2.009	2.019	2.028	2.058	2.111	2.129	2.127	2.127	2.115	2.101	2.045	1.951	1.808	1.669
50.9	1.877	1.899	1.907	1.958	2.003	2.008	2.014	1.997	1.975	1.955	1.939	1.887	1.794	1.651
54.2	1.798	1.730	1.799	1.845	1.887	1.882	1.863	1.854	1.845	1.833	1.792	1.749	1.696	1.599

W2/W1=0.68

z/Z=0.0

R=108 000

Velocity in m/s ; Location in mm.

Y \ X	3.3	6.4	12.8	19.1	25.5	31.8	38.2	44.5	50.9	57.2	63.6	66.8
3.3	.949	1.005	1.039	1.056	1.059	1.059	1.050	1.063	1.070	1.111	1.107	1.073
6.4	1.009	1.080	1.114	1.127	1.135	1.132	1.133	1.147	1.150	1.171	1.141	1.129
12.8	1.032	1.124	1.178	1.187	1.205	1.212	1.207	1.200	1.201	1.207	1.047	1.031
19.1	1.050	1.112	1.202	1.216	1.219	1.229	1.209	1.215	1.234	1.230	1.195	1.181
25.5	1.067	1.126	1.206	1.230	1.231	1.232	1.221	1.244	1.249	1.225	1.233	1.236
31.8	1.058	1.141	1.205	1.222	1.234	1.233	1.237	1.234	1.240	1.234	1.239	1.234
38.2	1.059	1.135	1.204	1.223	1.237	1.239	1.236	1.234	1.241	1.233	1.236	1.235
44.5	1.068	1.130	1.206	1.229	1.234	1.231	1.221	1.241	1.247	1.225	1.235	1.238
50.9	1.052	1.113	1.200	1.214	1.222	1.230	1.213	1.218	1.234	1.233	1.192	1.180
57.2	1.027	1.125	1.178	1.183	1.208	1.214	1.209	1.200	1.199	1.205	1.042	1.033
63.6	1.007	1.079	1.118	1.125	1.133	1.130	1.138	1.148	1.152	1.171	1.140	1.133
66.8	.947	1.008	1.044	1.061	1.058	1.057	1.050	1.064	1.070	1.111	1.105	1.073

Y \ X	66.8	70.0	73.3	76.4	82.8	89.1	95.5	101.8	108.2	114.5	120.9	127.2	133.6	136.8
15.9	1.039	1.046	1.132	1.132	1.127	1.111	1.120	1.107	1.112	1.109	1.098	1.083	1.052	.998
19.1	1.165	1.163	1.167	1.175	1.172	1.172	1.167	1.161	1.160	1.153	1.146	1.125	1.084	[illegible]
25.5	1.218	1.211	1.211	1.210	1.212	1.214	1.214	1.213	1.205	1.201	1.184	1.148	1.086	[illegible]
31.8	1.221	1.220	1.225	1.226	1.229	1.227	1.225	1.224	1.225	1.217	1.193	1.156	1.083	1.031
38.2	1.223	1.220	1.226	1.226	1.225	1.226	1.227	1.226	1.222	1.216	1.193	1.158	1.078	1.031
44.5	1.218	1.214	1.211	1.213	1.211	1.215	1.213	1.215	1.206	1.205	1.185	1.150	1.089	1.028
50.9	1.159	1.160	1.170	1.175	1.174	1.170	1.162	1.160	1.155	1.156	1.143	1.128	1.081	1.030
54.2	1.035	1.043	1.132	1.133	1.129	1.113	1.120	1.109	1.106	1.110	1.103	1.087	1.050	.995

W2/W1=0.68

z/Z=0.5

R=108 000

Velocity in m/s ; Location in mm.

Y \ X	3.3	6.4	12.8	19.1	25.5	31.8	38.2	44.5	50.9	57.2	63.6	66.8
3.3	.932	.974	1.008	1.020	1.021	1.025	1.038	1.062	1.073	1.035	.981	.932
6.4	.998	1.073	1.122	1.126	1.128	1.134	1.154	1.167	1.172	1.148	1.092	1.018
12.8	1.031	1.115	1.204	1.222	1.230	1.233	1.240	1.252	1.241	1.216	1.163	1.076
19.1	1.038	1.136	1.234	1.264	1.277	1.281	1.288	1.281	1.260	1.233	1.170	1.152
25.5	1.063	1.144	1.243	1.281	1.298	1.301	1.303	1.296	1.277	1.257	1.233	1.230
31.8	1.059	1.159	1.249	1.288	1.300	1.311	1.310	1.305	1.295	1.281	1.269	1.267
38.2	1.062	1.148	1.240	1.285	1.297	1.307	1.306	1.308	1.294	1.281	1.268	1.266
44.5	1.055	1.152	1.240	1.280	1.296	1.302	1.303	1.297	1.280	1.260	1.236	1.223
50.9	1.036	1.170	1.224	1.268	1.280	1.284	1.287	1.279	1.267	1.235	1.192	1.149
57.2	1.025	1.116	1.212	1.234	1.240	1.245	1.247	1.241	1.237	1.221	1.168	1.088
63.6	1.003	1.082	1.120	1.141	1.136	1.139	1.150	1.149	1.155	1.136	1.081	1.002
66.8	.952	.999	1.020	1.030	1.034	1.041	1.038	1.065	1.054	1.035	.960	.911

Y \ X	66.8	70.0	73.3	76.4	82.8	89.1	95.5	101.8	108.2	114.5	120.9	127.2	133.6	136.8
15.9	1.087	1.048	1.084	1.096	1.103	1.102	1.100	1.087	1.087	1.085	1.085	1.056	1.006	.971
19.1	1.143	1.132	1.156	1.180	1.204	1.197	1.191	1.179	1.163	1.168	1.161	1.136	1.078	1.016
25.5	1.222	1.220	1.235	1.248	1.270	1.280	1.271	1.269	1.264	1.253	1.227	1.168	1.081	1.002
31.8	1.261	1.262	1.267	1.275	1.284	1.293	1.295	1.292	1.289	1.273	1.237	1.162	1.055	.974
38.2	1.263	1.266	1.267	1.273	1.288	1.295	1.297	1.293	1.291	1.276	1.239	1.154	1.052	.993
44.5	1.229	1.223	1.232	1.245	1.264	1.271	1.275	1.271	1.267	1.260	1.230	1.184	1.100	1.020
50.9	1.157	1.153	1.166	1.185	1.198	1.200	1.187	1.188	1.185	1.177	1.156	1.126	1.077	1.013
54.2	1.112	1.085	1.109	1.118	1.128	1.112	1.104	1.096	1.081	1.083	1.069	1.049	1.012	.967

W2/W1=0.68

z/Z=1.0

R=108 000

Velocity in m/s ; Location in mm.

Y \ X	3.3	6.4	12.8	19.1	25.5	31.8	38.2	44.5	50.9	57.2	63.6	66.8
3.3	.889	.954	.986	.982	.997	1.011	1.019	1.033	1.033	.994	.929	.903
6.4	.947	1.033	1.089	1.098	1.097	1.116	1.125	1.134	1.137	1.101	1.011	.992
12.8	.971	1.069	1.166	1.199	1.210	1.218	1.221	1.226	1.225	1.200	1.131	1.061
19.1	.989	1.096	1.203	1.256	1.279	1.279	1.280	1.275	1.255	1.217	1.160	1.123
25.5	1.010	1.107	1.212	1.273	1.294	1.305	1.300	1.296	1.276	1.250	1.277	1.210
31.8	1.024	1.110	1.224	1.284	1.308	1.316	1.311	1.305	1.286	1.267	1.257	1.251
38.2	1.014	1.101	1.217	1.278	1.304	1.315	1.314	1.306	1.293	1.274	1.254	1.248
44.5	1.011	1.113	1.219	1.276	1.303	1.310	1.310	1.296	1.275	1.250	1.215	1.193
50.9	.989	1.089	1.202	1.256	1.276	1.285	1.290	1.279	1.262	1.226	1.159	1.123
57.2	.987	1.085	1.179	1.217	1.222	1.224	1.230	1.236	1.225	1.194	1.140	1.065
63.6	.969	1.043	1.095	1.112	1.123	1.125	1.127	1.130	1.122	1.095	1.043	.981
66.8	.891	.937	.983	.981	1.008	.995	1.027	1.027	1.032	.993	.942	.906

Y \ X	66.8	70.0	73.3	76.4	82.8	89.1	95.5	101.8	108.2	114.5	120.9	127.2	133.6	136.8
15.9	1.062	1.047	1.071	1.096	1.093	1.072	1.051	1.030	1.028	1.018	.995	.973	.930	.890
19.1	1.125	1.117	1.150	1.169	1.182	1.170	1.153	1.136	1.122	1.114	1.106	1.074	1.022	.942
25.5	1.210	1.206	1.222	1.240	1.266	1.271	1.267	1.255	1.242	1.233	1.198	1.134	1.041	.953
31.8	1.261	1.260	1.261	1.271	1.287	1.302	1.304	1.301	1.295	1.274	1.228	1.138	1.028	.946
38.2	1.259	1.261	1.264	1.273	1.293	1.308	1.315	1.297	1.306	1.286	1.236	1.142	1.028	.946
44.5	1.191	1.193	1.197	1.222	1.257	1.267	1.274	1.268	1.259	1.242	1.239	1.169	1.070	.974
50.9	1.099	1.100	1.127	1.151	1.193	1.186	1.179	1.165	1.165	1.142	1.125	1.103	1.038	.955
54.2	1.035	1.011	1.053	1.084	1.102	1.095	1.097	1.080	1.064	1.049	1.039	1.020	.990	.921

W2/W1=0.50

z/Z=0.0

R=180 000

Velocity in m/s ; Location in mm.

Y \ X	3.3	6.4	12.8	19.1	25.5	31.8	38.2	44.5	50.9	57.2	63.6	66.8
3.3	1.903	1.957	1.997	2.017	2.020	2.037	2.033	2.065	2.100	2.118	2.056	1.968
6.4	1.986	2.068	2.110	2.121	2.130	2.136	2.150	2.164	2.185	2.207	2.189	2.145
12.8	2.034	2.127	2.180	2.200	2.207	2.216	2.225	2.228	2.243	2.193	2.081	2.165
19.1	2.042	2.145	2.206	2.235	2.247	2.252	2.252	2.251	2.259	2.107	1.742	2.042
25.5	2.058	2.199	2.220	2.255	2.254	2.260	2.259	2.265	2.265	2.252	2.167	2.175
31.8	2.065	2.160	2.229	2.258	2.268	2.260	2.271	2.271	2.278	2.282	2.278	2.281
38.2	2.063	2.155	2.224	2.253	2.263	2.264	2.271	2.275	2.272	2.281	2.280	2.277
44.5	2.055	2.199	2.223	2.255	2.253	2.262	2.262	2.264	2.267	2.246	2.167	2.171
50.9	2.045	2.147	2.212	2.232	2.247	2.253	2.255	2.255	2.257	2.105	1.744	2.037
57.2	2.031	2.129	2.184	2.198	2.209	2.211	2.223	2.227	2.243	2.193	2.079	2.165
63.6	1.988	2.071	2.113	2.118	2.127	2.136	2.153	2.161	2.191	2.210	2.190	2.148
66.8	1.898	1.959	2.002	2.019	2.022	2.034	2.034	2.062	2.101	2.117	2.055	1.968

Y \ X	66.8	70.0	73.3	76.4	82.8	89.1	95.5	101.8	108.2	114.5	120.9	127.2	133.6	136.8
20.7	1.980	2.180	2.139	2.169	2.171	2.171	2.173	2.176	2.172	2.171	2.169	2.143	2.086	2.131
25.5	2.188	2.221	2.261	2.266	2.265	2.271	2.264	2.260	2.254	2.248	2.226	2.187	2.103	2.052
31.8	2.297	2.297	2.291	2.293	2.296	2.291	2.287	2.286	2.280	2.262	2.229	2.172	2.060	1.976
38.2	2.298	[illegible]	2.293	2.293	2.293	2.291	2.283	2.287	2.276	2.263	2.235	2.168	2.062	1.977
44.5	2.190	2.220	2.261	2.264	2.269	2.271	2.264	2.257	2.253	2.247	2.225	2.188	2.108	2.057
49.3	1.981	2.181	2.140	2.166	2.174	2.173	2.172	2.182	2.170	2.176	2.168	2.139	2.088	2.134

W2/W1=0.50

z/Z=0.5

R=180 000

Velocity in m/s ; Location in mm.

Y \ X	3.3	6.4	12.8	19.1	25.5	31.8	38.2	44.5	50.9	57.2	63.6	66.8
3.3	1.674	1.773	1.796	1.818	1.843	1.859	1.892	1.939	1.915	1.839	1.712	1.615
6.4	1.763	1.933	2.000	2.007	2.011	2.043	2.082	2.116	2.113	2.046	1.939	1.771
12.8	1.826	2.019	2.160	2.165	2.177	2.190	2.225	2.232	2.213	2.190	2.127	1.931
19.1	1.865	2.049	2.179	2.222	2.242	2.253	2.260	2.232	2.171	2.153	2.118	1.941
25.5	1.887	2.065	2.198	2.244	2.261	2.271	2.260	2.208	2.129	2.096	2.068	2.047
31.8	1.879	2.062	2.199	2.264	2.277	2.285	2.273	2.222	2.158	2.121	2.118	2.131
38.2	1.894	2.075	2.228	2.269	2.289	2.295	2.285	2.221	2.146	2.114	2.111	2.115
44.5	1.879	2.051	2.221	2.259	2.284	2.289	2.279	2.232	2.151	2.118	2.075	2.034
50.9	1.849	2.040	2.174	2.229	2.248	2.255	2.255	2.229	2.171	2.154	2.100	1.878
57.2	1.814	1.994	2.138	2.172	2.187	2.202	2.206	2.202	2.182	2.173	2.104	1.824
63.6	1.799	1.950	2.021	2.014	2.030	2.047	2.060	2.071	2.064	1.988	1.893	1.661
66.8	1.680	1.755	1.810	1.845	1.828	1.842	1.867	1.884	1.869	1.780	1.712	1.522

Y \ X	66.8	70.0	73.3	76.4	82.8	89.1	95.5	101.8	108.2	114.5	120.9	127.2	133.6	136.8
20.7	1.974	1.894	2.003	2.032	2.007	1.963	1.935	1.940	1.948	1.962	1.963	1.905	1.735	1.674
25.5	2.057	2.071	2.140	2.196	2.220	2.191	2.190	2.179	2.136	2.134	2.079	2.014	1.937	1.846
31.8	2.131	2.149	2.186	2.226	2.266	2.271	2.267	2.260	2.243	2.202	2.073	1.942	1.833	1.727
38.2	2.120	2.142	2.168	2.211	2.270	2.275	2.269	2.259	2.249	2.191	2.073	1.927	1.840	1.731
44.5	2.038	2.043	2.107	2.172	2.203	2.181	2.159	2.164	2.158	2.157	2.106	2.019	1.942	1.833
49.3	1.940	1.882	1.984	2.006	1.985	1.946	1.920	1.914	1.933	1.946	1.952	1.875	1.686	1.624

W2/W1=0.50

z/Z=1.0

R=180 000

Velocity in m/s ; Location in mm.

Y \ X	3.3	6.4	12.8	19.1	25.5	31.8	38.2	44.5	50.9	57.2	63.6	66.8
3.3	1.982	2.107	2.155	2.142	2.161	2.073	2.226	2.215	2.189	2.108	1.954	1.923
6.4	2.017	2.197	2.298	2.280	2.295	2.323	2.351	2.340	2.338	2.258	2.115	2.046
12.8	2.059	2.230	2.417	2.468	2.493	2.509	2.523	2.511	2.499	2.451	2.360	2.230
19.1	2.098	2.276	2.461	2.538	2.561	2.569	2.556	2.531	2.525	2.502	2.470	2.416
25.5	2.118	2.297	2.477	2.569	2.588	2.585	2.558	2.519	2.495	2.474	2.431	2.399
31.8	2.124	2.298	2.473	2.569	2.597	2.590	2.551	2.511	2.479	2.460	2.441	2.427
38.2	2.140	2.304	2.484	2.563	2.591	2.589	2.556	2.516	2.485	2.467	2.441	2.422
44.5	2.115	2.280	2.463	2.560	2.590	2.595	2.571	2.542	2.517	2.499	2.446	2.400
50.9	2.084	2.252	2.449	2.535	2.570	2.573	2.570	2.553	2.536	2.504	2.457	2.400
57.2	2.051	2.219	2.407	2.470	2.489	2.494	2.502	2.498	2.484	2.429	2.327	2.183
63.6	2.032	2.150	2.227	2.260	2.291	2.299	2.302	2.305	2.278	2.199	2.099	2.010
66.8	1.863	1.951	2.003	2.039	2.077	2.091	2.125	2.129	2.102	2.030	1.932	1.886

Y \ X	66.8	70.0	73.3	76.4	82.8	89.1	95.5	101.8	108.2	114.5	120.9	127.2	133.6	136.8
20.7	2.430	2.371	2.195	2.112	2.272	2.240	2.179	2.143	2.121	2.108	2.083	2.051	1.901	1.834
25.5	2.403	2.362	2.311	2.308	2.442	2.474	2.437	2.401	2.408	2.394	2.358	2.299	2.161	2.079
31.8	2.433	2.425	2.412	2.420	2.480	2.544	2.554	2.544	2.500	2.491	2.429	2.315	2.177	2.036
38.2	2.446	2.429	2.425	2.437	2.509	2.573	2.591	2.554	2.540	2.500	2.416	2.307	2.153	2.040
44.5	2.435	2.381	2.320	2.313	2.469	2.508	2.493	2.474	2.462	2.443	2.418	2.342	2.215	2.113
49.3	2.446	2.344	2.137	2.120	2.307	2.304	2.251	2.229	2.224	2.206	2.194	2.149	2.030	1.960

W2/W1=0.50

z/Z=0.0

R=108 000

Velocity in m/s ; Location in mm.

Y \ X	3.3	6.4	12.8	19.1	25.5	31.8	38.2	44.5	50.9	57.2	63.6	66.8
3.3	1.132	1.163	1.192	1.206	1.208	1.219	1.218	1.233	1.255	1.268	1.234	1.184
6.4	1.173	1.226	1.253	1.263	1.266	1.269	1.282	1.285	1.302	1.315	1.301	1.280
12.8	1.208	1.270	1.309	1.325	1.329	1.334	1.334	1.341	1.343	1.314	1.226	1.273
19.1	1.221	1.288	1.333	1.345	1.349	1.352	1.357	1.357	1.353	1.266	1.053	1.193
25.5	1.230	1.294	1.336	1.359	1.361	1.364	1.364	1.364	1.366	1.351	1.297	1.300
31.8	1.232	1.295	1.342	1.362	1.367	1.369	1.368	1.363	1.367	1.364	1.366	1.365
38.2	1.233	1.297	1.344	1.362	1.365	1.367	1.363	1.362	1.369	1.363	1.368	1.368
44.5	1.227	1.290	1.342	1.360	1.362	1.361	1.363	1.365	1.364	1.346	1.294	1.299
50.9	1.226	1.286	1.332	1.342	1.345	1.350	1.356	1.357	1.352	1.265	1.052	1.194
57.2	1.207	1.268	1.315	1.323	1.327	1.329	1.335	1.343	1.342	1.310	1.225	1.274
63.6	1.178	1.229	1.254	1.261	1.369	1.268	1.278	1.286	1.299	1.315	1.301	1.277
66.8	1.132	1.163	1.194	1.205	1.205	1.220	1.221	1.238	1.250	1.269	1.232	1.186

Y \ X	66.8	70.0	73.3	76.4	82.8	89.1	95.5	101.8	108.2	114.5	120.9	127.2	133.6	136.8
20.7	1.193	1.183	1.280	1.279	1.277	1.281	1.273	1.272	1.274	1.271	1.263	1.254	1.210	1.133
25.5	1.322	1.334	1.351	1.360	1.353	1.350	1.346	1.345	1.340	1.333	1.319	1.289	1.250	1.206
31.8	1.381	1.375	1.379	1.379	1.375	1.381	1.372	1.370	1.370	1.354	1.333	1.289	1.222	1.183
38.2	1.377	1.380	1.381	1.373	1.375	1.381	1.373	1.373	1.368	1.355	1.336	1.289	1.223	1.184
44.5	1.318	1.334	1.354	1.356	1.354	1.350	1.350	1.347	1.343	1.337	1.324	1.292	1.250	1.204
49.3	1.194	1.189	1.279	1.278	1.277	1.279	1.273	1.266	1.273	1.266	1.265	1.254	1.214	1.134

W2/W1=0.50

z/Z=0.5

R=108 000

Velocity in m/s ; Location in mm.

X / Y	3.3	6.4	12.8	19.1	25.5	31.8	38.2	44.5	50.9	57.2	63.6	66.8
3.3	.857	.949	.974	.975	.944	.945	.986	1.002	1.001	.949	.864	.789
6.4	.898	1.040	1.095	1.104	1.090	1.104	1.126	1.143	1.145	1.112	1.043	.935
12.8	.946	1.069	1.172	1.197	1.204	1.213	1.225	1.224	1.203	1.188	1.155	1.050
19.1	.975	1.099	1.201	1.228	1.241	1.250	1.250	1.223	1.177	1.151	1.128	1.026
25.5	.978	1.100	1.209	1.245	1.260	1.260	1.258	1.221	1.167	1.136	1.115	1.101
31.8	.977	1.109	1.211	1.252	1.266	1.268	1.258	1.223	1.172	1.147	1.144	1.146
38.2	.983	1.096	1.215	1.256	1.265	1.269	1.263	1.224	1.172	1.148	1.134	1.139
44.5	.979	1.100	1.217	1.251	1.262	1.265	1.260	1.227	1.174	1.142	1.114	1.081
50.9	.950	1.081	1.198	1.237	1.248	1.250	1.254	1.238	1.203	1.188	1.152	1.008
57.2	.938	1.080	1.174	1.196	1.209	1.209	1.221	1.222	1.210	1.183	1.131	.958
63.6	.910	1.028	1.064	1.064	1.077	1.093	1.098	1.115	1.112	1.048	.996	.834
66.8	.826	.890	.906	.925	.927	.955	.965	.971	.957	.911	.853	.760

X / Y	66.8	70.0	73.3	76.4	82.8	89.1	95.5	101.8	108.2	114.5	120.9	127.2	133.6	136.8
20.7	1.043	1.022	1.089	1.114	1.091	1.062	1.046	1.037	1.041	1.057	1.046	.998	.902	1.451
25.5	1.109	1.116	1.160	1.200	1.215	1.208	1.189	1.192	1.190	1.180	1.144	1.087	1.031	.946
31.8	1.168	1.177	1.203	1.229	1.255	1.258	1.256	1.251	1.240	1.203	1.114	1.025	.937	.843
38.2	1.158	1.170	1.193	1.218	1.252	1.256	1.251	1.248	1.239	1.206	1.120	1.034	.951	.860
44.5	[illegible]	[illegible]	1.155	1.185	1.198	1.186	1.167	1.170	1.166	1.164	1.135	1.075	1.009	.935
49.3	1.014	[illegible]	1.057	1.069	1.049	1.019	.999	.994	1.000	1.004	1.001	.961	.849	.805

W2/W1=0.50

z/Z=1.0

R=108 000

Velocity in m/s ; Location in mm.

Y \ X	3.3	6.4	12.8	19.1	25.5	31.8	38.2	44.5	50.9	57.2	63.6	66.8
3.3	1.169	1.240	1.270	1.262	1.268	1.289	1.297	1.303	1.278	1.231	1.138	1.114
6.4	1.203	1.302	1.327	1.340	1.365	1.381	1.384	1.375	1.367	1.316	1.281	1.215
12.8	1.211	1.316	1.437	1.474	1.485	1.498	1.495	1.501	1.496	1.470	1.404	1.341
19.1	1.236	1.349	1.471	1.525	1.543	1.544	1.539	1.527	1.513	1.498	1.475	1.437
25.5	1.249	1.347	1.468	1.521	1.541	1.542	1.524	1.500	1.483	1.478	1.451	1.423
31.8	1.259	1.357	1.476	1.528	1.552	1.500	1.528	1.499	1.476	1.459	1.443	1.437
38.2	1.262	1.356	1.473	1.540	1.563	1.558	1.536	1.508	1.482	1.467	1.448	1.435
44.5	1.252	1.346	1.477	1.533	1.559	1.558	1.548	1.526	1.509	1.493	1.454	1.429
50.9	1.225	1.327	1.460	1.516	1.538	1.547	1.544	1.535	1.518	1.506	1.469	1.428
57.2	1.212	1.320	1.434	1.473	1.486	1.491	1.493	1.495	1.484	1.453	1.392	1.300
63.6	1.196	1.273	1.322	1.334	1.355	1.362	1.382	1.370	1.361	1.306	1.249	1.194
66.8	1.106	1.151	1.180	1.199	1.221	1.246	1.247	1.252	1.245	1.206	1.142	1.113

Y \ X	66.8	70.0	73.3	76.4	82.8	89.1	95.5	101.8	108.2	114.5	120.9	127.2	133.6	136.8
20.7	1.437	1.387	1.259	1.258	1.351	1.322	1.282	1.257	1.255	1.245	1.217	1.196	1.119	1.086
25.5	1.419	1.390	1.365	1.372	1.461	1.478	1.442	1.429	1.422	1.416	1.393	1.351	1.275	1.220
31.8	1.448	1.438	1.440	1.445	1.488	1.519	1.531	1.521	1.509	1.487	1.441	1.371	1.268	1.189
38.2	1.440	1.432	1.433	1.443	1.488	1.528	1.534	1.531	1.525	1.494	1.442	1.369	1.262	1.189
44.5	1.430	1.391	1.352	1.372	1.467	1.478	1.465	1.456	1.451	1.431	1.408	1.364	1.288	1.221
49.3	1.450	1.368	1.236	1.259	1.351	1.339	1.325	1.321	1.297	1.292	1.291	1.249	1.178	1.145

W2/W1=0.32

z/Z=0.0

R=180 000

Velocity in m/s ; Location in mm.

Y \ X	3.3	6.4	12.8	19.1	25.5	31.8	38.2	44.5	50.9	57.2	63.6	66.8
3.3	2.260	2.304	2.350	2.367	2.374	2.396	2.394	2.440	2.465	2.478	2.413	2.328
6.4	2.325	2.401	2.428	2.439	2.459	2.463	2.481	2.511	2.526	2.540	2.528	2.489
12.8	2.357	2.439	2.494	2.504	2.513	2.529	2.540	2.554	2.564	2.521	2.494	2.545
19.1	2.376	2.462	2.525	2.537	2.543	2.552	2.566	2.576	2.570	2.271	2.089	2.391
25.5	2.400	2.485	2.543	2.557	2.561	2.568	2.571	2.581	2.576	2.307	2.290	2.310
31.8	2.408	2.487	2.544	2.552	2.556	2.565	2.563	2.573	2.580	2.561	2.554	2.573
38.2	2.409	2.486	2.544	2.552	2.555	2.565	2.564	2.571	2.577	2.564	2.554	2.574
44.5	2.400	2.486	2.542	2.555	2.568	2.567	2.568	2.580	2.574	2.306	2.288	2.314
50.9	2.374	2.465	2.520	2.532	2.545	2.554	2.566	2.577	2.566	2.272	2.092	2.387
57.2	2.355	2.445	2.491	2.505	2.513	2.530	2.536	2.554	2.567	2.519	2.496	2.544
63.6	2.331	2.399	2.430	2.443	2.460	2.469	2.483	2.511	2.525	2.538	2.529	2.495
66.8	2.263	2.305	2.351	2.363	2.373	2.392	2.397	2.438	2.463	2.475	2.418	2.325

Y \ X	66.8	70.0	73.3	76.4	82.8	89.1	95.5	101.8	108.2	114.5	120.9	127.2	133.6	136.8
28.6	2.316	2.411	2.515	2.526	2.521	2.521	2.521	2.510	2.510	2.496	2.472	2.442	2.386	2.240
31.8	2.493	2.541	2.547	2.551	2.550	2.552	2.543	2.535	2.521	2.516	2.479	2.427	2.342	2.245
38.2	2.496	2.539	2.551	2.550	2.551	2.550	2.541	2.537	2.528	2.517	2.481	2.430	2.341	2.244
41.4	2.320	2.407	2.515	2.525	2.520	2.520	2.522	2.515	2.511	2.494	2.477	2.449	2.383	2.242

W2/W1=0.32

z/Z=0.5

R=180 000

Velocity in m/s ; Location in mm.

Y \ X	3.3	6.4	12.8	19.1	25.5	31.8	38.2	44.5	50.9	57.2	63.6	66.8
3.3	1.977	2.087	2.171	2.189	2.238	2.298	2.305	2.257	2.187	2.087	2.048	1.885
6.4	2.104	2.292	2.408	2.448	2.473	2.491	2.475	2.433	2.359	2.268	2.202	1.987
12.8	2.191	2.385	2.549	2.602	2.635	2.630	2.619	2.604	2.585	2.519	2.443	2.145
19.1	2.263	2.459	2.609	2.648	2.621	2.565	2.528	2.576	2.606	2.595	2.488	2.187
25.5	2.301	2.494	2.356	2.655	2.591	2.499	2.464	2.540	2.612	2.582	2.384	2.190
31.8	2.325	2.539	2.649	2.638	2.565	2.528	2.549	2.584	2.592	2.544	2.474	2.479
38.2	2.297	2.482	2.611	2.617	2.551	2.500	2.493	2.548	2.578	2.557	2.483	2.489
44.5	2.283	2.478	2.620	2.624	2.559	2.466	2.423	2.509	2.592	2.571	2.357	2.184
50.9	2.238	2.416	2.595	2.644	2.619	2.561	2.531	2.558	2.593	2.596	2.505	2.198
57.2	2.179	2.377	2.573	2.625	2.643	2.637	2.627	2.607	2.562	2.502	2.423	2.132
63.6	2.119	2.299	2.449	2.493	2.521	2.530	2.517	2.472	2.395	2.271	2.224	2.005
66.8	2.090	2.211	2.284	2.305	2.336	2.333	2.300	2.265	2.155	2.051	2.023	1.827

Y \ X	66.8	70.0	73.3	76.4	82.8	89.1	95.5	101.8	108.2	114.5	120.9	127.2	133.6	136.8
28.6	2.317	2.324	2.400	2.388	2.330	2.284	2.258	2.259	2.243	2.234	2.217	2.154	2.008	1.911
31.8	2.412	2.431	2.483	2.522	2.511	2.495	2.477	2.466	2.451	2.439	2.375	2.269	2.108	2.000
38.2	2.382	2.417	2.495	2.532	2.519	2.467	2.455	2.456	2.461	2.428	2.386	2.268	2.093	1.970
41.4	2.258	2.246	2.347	2.357	2.273	2.216	2.204	2.212	2.214	2.225	2.198	2.108	1.963	1.888

W2/W1=0.32

z/Z=1.0

R=180 000

Velocity in m/s ; Location in mm.

Y \ X	3.3	6.4	12.8	19.1	25.5	31.8	38.2	44.5	50.9	57.2	63.6	66.8
3.3	1.967	2.118	2.255	2.320	2.320	2.307	2.243	2.140	2.038	1.943	2.013	1.882
6.4	2.041	2.238	2.453	2.542	2.543	2.515	2.451	2.355	2.247	2.170	2.200	2.013
12.8	2.109	2.328	2.593	2.672	2.695	2.676	2.647	2.578	2.495	2.448	2.414	2.191
19.1	2.226	2.443	2.652	2.678	2.662	2.670	2.677	2.658	2.632	2.598	2.505	2.291
25.5	2.340	2.537	2.686	2.673	2.656	2.666	2.690	2.691	2.663	2.579	2.379	2.207
31.8	2.376	2.579	2.689	2.683	2.681	2.696	2.703	2.695	2.659	2.582	2.474	2.446
38.2	2.393	2.587	2.692	2.680	2.672	2.687	2.707	2.697	2.653	2.569	2.475	2.456
44.5	2.332	2.533	2.679	2.675	2.649	2.659	2.692	2.703	2.671	2.597	2.388	2.197
50.9	2.242	2.445	2.645	2.684	2.668	2.677	2.686	2.678	2.628	2.589	2.489	2.269
57.2	2.096	2.304	2.555	2.662	2.685	2.690	2.661	2.585	2.514	2.441	2.395	2.179
63.6	2.048	2.240	2.442	2.522	2.531	2.433	2.450	2.355	2.238	2.154	2.175	1.964
66.8	1.947	2.058	2.203	2.270	2.282	2.271	2.219	2.137	1.907	1.975	2.038	1.877

Y \ X	66.8	70.0	73.3	76.4	82.8	89.1	95.5	101.8	108.2	114.5	120.9	127.2	133.6	136.8
28.6	1.993	2.305	2.395	2.395	2.338	2.292	2.267	2.253	2.227	2.181	2.131	2.066	1.964	1.860
31.8	2.428	2.438	2.511	2.554	2.539	2.495	2.474	2.446	2.428	2.391	2.380	2.262	2.086	1.908
38.2	2.361	2.395	2.497	2.537	2.507	2.451	2.427	2.425	2.406	2.364	2.320	2.227	2.066	1.906
41.4	2.225	2.223	2.318	2.318	2.240	2.183	2.161	2.165	2.135	2.103	2.054	1.993	1.918	1.831

W2/W1=0.32

z/Z=0.0

R=108 000

Velocity in m/s ; Location in mm.

Y \ X	3.3	6.4	12.8	19.1	25.5	31.8	38.2	44.5	50.9	57.2	63.6	66.8
3.3	1.356	1.392	1.414	1.422	1.360	1.438	1.441	1.463	1.477	1.492	1.448	1.399
6.4	1.404	1.452	1.473	1.485	1.483	1.496	1.500	1.521	1.538	1.538	1.531	1.508
12.8	1.432	1.486	1.516	1.522	1.526	1.535	1.538	1.549	1.556	1.514	1.504	1.536
19.1	1.439	1.496	1.530	1.545	1.544	1.549	1.550	1.553	1.546	1.439	1.303	1.314
25.5	1.442	1.502	1.542	1.552	1.551	1.552	1.552	1.548	1.477	1.387	1.381	1.385
31.8	1.446	1.501	1.536	1.551	1.556	1.556	1.557	1.558	1.555	1.546	1.534	1.549
38.2	1.447	1.500	1.537	1.550	1.553	1.555	1.556	1.554	1.552	1.544	1.533	1.547
44.5	1.442	1.501	1.544	1.555	1.553	1.553	1.550	1.550	1.478	1.392	1.376	1.383
50.9	1.439	1.494	1.531	1.544	1.542	1.547	1.548	1.553	1.543	1.439	1.301	1.318
57.2	1.432	1.486	1.511	1.521	1.526	1.534	1.537	1.547	1.554	1.518	1.501	1.538
63.6	1.408	1.455	1.474	1.485	1.487	1.497	1.503	1.520	1.532	1.535	1.529	1.503
66.8	1.360	1.387	1.415	1.422	1.359	1.437	1.440	1.464	1.482	1.492	1.449	1.400

Y \ X	66.8	70.0	73.3	76.4	82.8	89.1	95.5	101.8	108.2	114.5	120.9	127.2	133.6	136.8
28.6	1.399	1.483	1.511	1.514	1.513	1.513	1.510	1.509	1.503	1.495	1.479	1.458	1.418	1.340
31.8	1.487	1.529	1.530	1.531	1.531	1.530	1.522	1.519	1.514	1.506	1.486	1.451	1.402	1.309
38.2	1.490	1.526	1.532	1.533	1.530	1.532	1.526	1.520	1.516	1.502	1.481	1.450	1.406	1.304
41.4	1.396	1.478	1.510	1.516	1.516	1.511	1.512	1.510	1.501	1.492	1.479	1.455	1.420	1.344

W2/W1=0.32

z/Z=0.5

R=108 000

Velocity in m/s ; Location in mm.

Y \ X	3.3	6.4	12.8	19.1	25.5	31.8	38.2	44.5	50.9	57.2	63.6	66.8
3.3	1.175	1.243	1.286	1.318	1.328	1.351	1.353	1.328	1.298	1.217	1.167	1.109
6.4	1.240	1.339	1.412	1.444	1.471	1.490	1.481	1.477	1.416	1.355	1.310	1.204
12.8	1.294	1.423	1.530	1.559	1.574	1.576	1.563	1.551	1.532	1.498	1.434	1.290
19.1	1.321	1.439	1.544	1.586	1.578	1.547	1.508	1.516	1.547	1.553	1.498	1.363
25.5	1.352	1.468	1.570	1.585	1.550	1.497	1.458	1.488	1.537	1.533	1.411	1.298
31.8	1.360	1.468	1.569	1.582	1.547	1.507	1.498	1.515	1.523	1.499	1.451	1.448
38.2	1.366	1.479	1.574	1.585	1.542	1.499	1.485	1.512	1.530	1.500	1.447	1.451
44.5	1.342	1.454	1.561	1.587	1.560	1.503	1.455	1.470	1.543	1.557	1.433	1.304
50.9	1.327	1.443	1.556	1.593	1.585	1.555	1.525	1.536	1.561	1.556	1.498	1.333
57.2	1.280	1.397	1.520	1.565	1.585	1.583	1.577	1.566	1.550	1.508	1.451	1.301
63.6	1.261	1.377	1.456	1.477	1.494	1.491	1.487	1.465	1.407	1.341	1.298	1.184
66.8	1.210	1.276	1.327	1.335	1.355	1.365	1.361	1.333	1.286	1.209	1.178	1.083

Y \ X	66.8	70.0	73.3	76.4	82.8	89.1	95.5	101.8	108.2	114.5	120.9	127.2	133.6	136.8
28.6	1.349	1.369	1.422	1.411	1.366	1.347	1.341	1.332	1.327	1.315	1.298	1.250	1.160	1.109
31.8	1.415	1.432	1.467	1.492	1.492	1.478	1.466	1.457	1.452	1.442	1.405	1.336	1.223	1.151
38.2	1.382	1.425	1.478	1.495	1.470	1.446	1.438	1.435	1.431	1.423	1.389	1.319	1.210	1.139
41.4	1.318	1.325	1.387	1.384	1.328	1.298	1.285	1.285	1.287	1.282	1.268	1.223	1.141	1.092

W2/W1=0.32

z/Z=1.0

R=108 000

Velocity in m/s ; Location in mm.

Y \ X	3.3	6.4	12.8	19.1	25.5	31.8	38.2	44.5	50.9	57.2	63.6	66.8
3.3	1.175	1.255	1.331	1.365	1.378	1.364	1.331	1.294	1.222	1.151	1.179	1.120
6.4	1.227	1.364	1.473	1.513	1.523	1.514	1.477	1.429	1.370	1.293	1.298	1.211
12.8	1.242	1.383	1.550	1.619	1.634	1.626	1.604	1.566	1.519	1.469	1.448	1.331
19.1	1.321	1.456	1.601	1.631	1.621	1.618	1.622	1.613	1.594	1.569	1.509	1.393
25.5	1.380	1.497	1.618	1.625	1.611	1.610	1.621	1.625	1.610	1.563	1.453	1.340
31.8	1.396	1.529	1.631	1.626	1.619	1.638	1.620	1.609	1.580	1.528	1.462	1.446
38.2	1.381	1.515	1.614	1.614	1.604	1.606	1.614	1.614	1.589	1.538	1.470	1.455
44.5	1.360	1.483	1.606	1.619	1.598	1.595	1.609	1.620	1.609	1.555	1.440	1.328
50.9	1.306	1.442	1.582	1.628	1.626	1.622	1.628	1.622	1.594	1.573	1.507	1.391
57.2	1.247	1.386	1.546	1.621	1.639	1.630	1.611	1.572	1.505	1.472	1.431	1.312
63.6	1.234	1.345	1.458	1.511	1.526	1.523	1.482	1.430	1.368	1.295	1.302	1.193
66.8	1.167	1.227	1.319	1.355	1.356	1.367	1.342	1.298	1.240	1.164	1.181	1.117

Y \ X	66.8	70.0	73.3	76.4	82.8	89.1	95.5	101.8	108.2	114.5	120.9	127.[illegible]	133.6	136.8
28.6	1.361	1.390	1.442	1.436	1.394	1.371	1.355	1.345	1.325	1.304	1.270	1.218	1.164	1.097
31.8	1.433	1.449	1.490	1.518	1.507	1.485	1.469	1.456	1.447	1.419	1.390	1.344	1.235	1.130
38.2	1.399	1.434	1.486	1.500	1.469	1.442	1.427	1.420	1.397	1.380	1.351	1.296	1.214	1.118
41.4	1.326	1.337	1.384	1.379	1.328	1.306	1.285	1.283	1.270	1.262	1.228	1.180	1.129	1.076

APPENDIX C

Error Analysis

In order to place error limits on the data presented in Appendices A and B, the following error analysis was performed. All of the velocity measurements were made with a simple stagnation tube. The static portion of the total pressure was obtained from an independent measurement of static pressure. As a preamble to the actual error calculations, a general discussion of errors associated with pressure tube instruments will be given.

C.1 Pressure Tube Measurements

One source of error in pressure tube measurements is the effect of yaw angle. The tip design of the stagnation tube is quite critical in determining its sensitivity to yaw angle. The tube in this study was fabricated by cutting the tube square to form the tip. Such tip designs are more insensitive to misalignment with the flow than conical or ellipsoidal tips. For the particular probe used in this study the fluid velocity can be up to 10^{o} from the probe axis without effecting the stagnation pressure (Chue [1975]). Pitot-static combinations are much more sensitive to yaw angle because the static pressure is increased by the appropriate component of the dynamic head impacting on the side of the probe. The measurements done in this study where for a confined channel flow where the flow is strongly aligned with the channel axis. A yaw angle of 10° would require a cross flow velocity of 17% of the axial component. These velocities where probably not that strong at any of the measuring locations so this error was neglected.

A second error in the measurement would be due to the closeness of the stagnation tube to the wall. This would be important only for the near wall points. The ratio of tube diameter to distance from the wall was about two in this study. According to MacMillan [1956], no error is introduced for circular pitot tubes until this ratio drops to about 1.75. Therefore this source of error was neglected.

Another source of error for pressure tubes is the effect of turbulence. The turbulent fluctuations in the flow tend to augment the mean stagnation pressure somewhat. A stagnation tube would read as follows:

$$P_t = P_s + \frac{1}{2}\rho\overline{W} + \frac{1}{2}\rho(u^2+v^2+w^2)$$

where P_t = total or stagnation pressure .

P_s = static pressure.

ρ = fluid density.

$\overline{W}$ = mean velocity aligned with tube.

u,v,w = fluctuating components of velocity.

This error is generally considered negligible especially for turbulent intensities less than 20%. The turbulent intensity in a channel flow such as was studied here would be low enough that this source of error can be safely neglected.

In a shear flow it is known that pressure tubes do not indicate the total pressure at their geometric center but at some displaced location towards the higher velocity. An expression recommended by Sami [1967] for this displacement is given below.

$$\delta/D = 0.45\ K - 3.05\ K^3$$

where δ = apparent displacement.

D = outside diameter of tube.

K = (D/2) * U * (dU/dy)

U = velocity.

dU/dy = velocity gradient.

Sample calculations to indicate the magnitude of this error were done. Several locations with high gradients were chosen and typically it was found that K was about 0.002 which yielded a displacement error of 0.0033 mm. Since this was much smaller than the resolution of the traversing devices it was considered negligible.

C.2 Detailed Combination of Component Errors

The task of propagating the basic instrument errors through to the final reported data still remains and will be explained here. The sequence of this procedure is given below.

1. Place relative or absolute error estimates on each primary sensing device involved in the measurement.
2. Identify the sequence of calculations required to obtain the final reported values from the output of the primary sensing devices.
3. Develop an error formula based on this sequence of calculations using the definition of the total derivative.
4. Calculate final error estimates by substituting basic errors into the error formula.

C.2.1 Error Estimates for Primary Sensing Elements

There were six basic places where error was introduced into the velocity measurement. These are stated below and a relative or absolute error is assigned to them.

1) Differential Pressure Cell:
   - Foxboro Model 613HM DP Cell (0-50 cm H_2O).
   - accuracy is +/- 0.5% of full span (+/- 24 Pa).
2) Integrating Digital Voltmeter
   - Vidar Model 5330B
   - accuracy +/-0.005 Volts.
3) Preset Counter
   - Hewlett Packard 5330B.
   - accurate to within 0.001 sec.
   - this source of error neglected.

4) & 5) Two measurements on test section to locate the traversing plane wrt. static pressure taps.

- machining of taps and stagnation tube ports was within 0.127 mm.

6) Temperature of water

- Type J thermocouple.
- +/- 1 degree C.

C.2.2 Sequence of Calculations

The velocity measurement will be discussed in this error analysis since the static pressure measurements are a subset of the velocity measurements. The method of measuring velocity will be briefly reviewed to identify the series of calculations required to obtain the final velocities.

The stagnation (or total) pressure was measured with a simple stagnation tube at various locations in the test section. The pressure from the tube was measured with a differential pressure cell referenced to the nearest convenient static wall tap. Static wall taps were located every 10 cm. along the length of the test section so the closest tap just downstream of the stagnation tube's location was always used. In addition the static pressure at all of the wall taps was measured with the same differential pressure cell. These readings were referenced to a common reference tap near the outlet end of the test section. The static pressure at the stagnation tube traversing station was inferred from these measurements of static pressure at the wall. This involved a linear interpolation between the two nearest static pressure readings. The critical assumption here is that the variation of static pressure over any plane perpendicular to the channel axis is negligible. During commissioning of the test section, a static pressure probe was used to make several traverses at various axial locations and with several subchannel configurations. No variation in static pressure on any of the traversing planes could be detected. (The gravitational pressure variation on this plane is very significant but, as long as care was taken to keep all pressure lines full of water, its effect was nulled by the static head in the lines leading to the differential pressure cell.)

Although much of the fluctuation in the flow was damped out by fluid resistance and inertance in the lines, an integrating digital voltmeter (IDVM) was used to average the signal. The integrating period was automatically started and stopped by a preset counter.

The error formula to be developed from this measurement method must state the error in terms of the raw data collected. The raw data was in the form of integrated voltage readings from the IDVM front panel.

C.2.3 Development of Error Formula

The error formula required to calculate the net contribution of these errors to the velocity measurements will now be developed. The definition of the total derivative will be applied and the absolute value of each contribution will be taken to arrive at the maximum possible error in the measurement.

Since the error in both the differential pressure cell and the IDVM are absolute, the error in the integrated output from the IDVM, V_s will be absolute. The maximum error in the voltage sensed by the IDVM is the sum of the possible error in the DP cell's output (0.5% of 5 volt Full Scale reading) and the error in the IDVM (0.5 mV).

$$dV_s = 0.005(5) + 0.005 = 0.030 \text{ volts}$$

The integrated output voltage, V_t is obtained through the following conversion:

$$V_t = T_i V_s (6000). \qquad \ldots \text{C.1}$$

where V_t = integrated voltage reading on IDVM display.

T_i = integration time.

V_s = voltage sensed by IDVM.

and 6000 is an errorless conversion factor.

now, with the error in T_i being neglected,

$$dV_t = \frac{\partial V_t}{\partial V_s} dV_s \qquad \ldots \text{C.2}$$

$$dV_t = 180\ T_i \qquad \ldots \text{C.3}$$

The differential pressure, DP is obtained from this integrated reading by the following relationship:

$$DP = A \frac{V_t}{T_1} + B \qquad \ldots \text{ C.4}$$

Recall that the method for determining the static pressure at the measurement location involved a linear interpolation of nearby static pressure readings as depicted in Figure C.1.

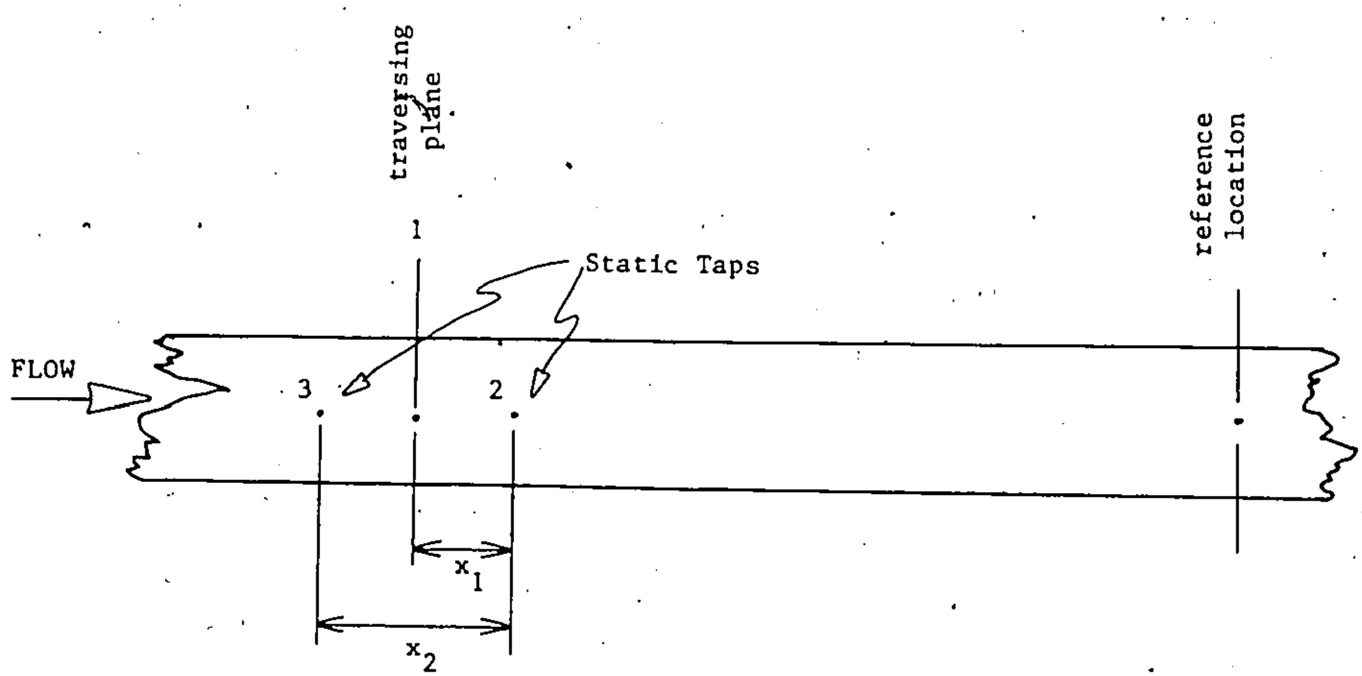

Figure C.1 Static Pressure Measurement from Wall Taps

The following three measurements with the DP (differential pressure) cell were needed to measure the velocity.

$$DP_1 = P_{t_1} - P_{s_2} \qquad \text{... C.5}$$

$$DP_2 = P_{s_2} - P_s^{ref} \qquad \text{... C.6}$$

$$DP_3 = P_{s_3} - P_s^{ref} \qquad \text{... C.7}$$

The desired pressure differential for measuring velocity is the velocity pressure, P_v defined as follows:

$$P_v = P_{t_1} - P_{s_1} \qquad \text{... C.8}$$

The static pressure at the traversing location, P_{s_1} is obtained from DP_2 and DP_3 as follows:

$$P_{s_1} = DP_2 + \frac{x_1}{x_2}(DP_3 - DP_2) + P_s^{ref} \qquad \text{... C.9}$$

so that the velocity pressure is given by,

$$P_v = DP_1 + \frac{x_1}{x_2}(DP_2 - DP_3) \qquad \text{... C.10}$$

substituting for the differential pressures gives,

$$P_v = (A\frac{V_{t_1}}{T_i} + B) + \frac{x_1}{x_2}(A\frac{V_{t_2}}{T_i} - A\frac{V_{t_3}}{T_i}) \qquad \text{... C.11}$$

and since,

$$dP_v = \left|\frac{\partial P_v}{\partial V_{t_1}}\right| dV_{t_1} + \left|\frac{\partial P_v}{\partial V_{t_1}}\right| dV_{t_1} + \left|\frac{\partial P_v}{\partial V_{t_3}}\right| dV_{t_3} + \left|\frac{\partial P_v}{\partial V_1}\right| dx_1 + \left|\frac{\partial P_v}{\partial x_2}\right| dx_2 \quad \ldots \text{C.12}$$

it follows that,

$$dP_v = \left|\frac{A}{T_i}\right| dV_{t_1} + \left|\frac{x_1}{x_2}\frac{A}{T_i}\right| dV_{t_2} + \left|\frac{x_1}{x_2}\frac{A}{T_i}\right| dV_{t_3} + \left|\frac{A}{T_i x_2}(V_{t_2}-V_{t_3})\right| dx_1 + \left|\frac{Ax_1}{x_2^2\, T_i}(V_{t_2}-V_{t_3})\right| dx_2 \quad \ldots \text{C.13}$$

Now, the following is true for all measurements:

$A = 0.2076$ (errorless conversion factor)

$T_i = 30$ sec

$dx_1 = dx_2 = 0.000127$ m

$dV_{t_1} = dV_{t_2} = dV_{t_3} = 180T_i = 5400$

$$dP_v = \left|37.37\right| + \left|\frac{x_1}{x_2}\,37.37\right| + \left|\frac{x_1}{x_2}\,37.37\right| + \left|\frac{879\text{x}10^{-9}}{x_2}(V_{t_2}-V_{t_3})\right| + \left|\frac{879\text{x}10^{-9}x_1}{x_2^2}(V_{t_2}-V_{t_3})\right| \quad \ldots \text{C.14}$$

From the velocity pressure, the fluid velocity is determined by the simplified form of Bernoulli's equation. It is as follows:

$$W = (2P_v/\rho)^{.5} \qquad \text{... C.15}$$

so,

$$dW = \left|\left(\frac{1}{2\rho P_v}\right)^{.5}\right| dP_v + \left|\left(\frac{P_v}{2\rho^3}\right)^{.5}\right| d\rho \qquad \text{... C.16}$$

The error in the density, ρ can be estimated from the error in the temperature measurement. The sensitivity of density on temperature around 30 C is about 0.3 kg/m^3 / C. Therefore;

$$d\rho = 0.3\ dT$$

$$d\rho = (0.3)(1) = 0.3\ kg/m^3$$

and so,

$$dW = \left|\left(\frac{1}{2\rho P_v}\right)^{.5}\right| dP_v + \left|\left(\frac{P_v}{2\rho^3}\right)^{.5}\right| d\rho \qquad \text{... C.17}$$

C.2.4 Example of Typical Error in Velocity Measurements

The following is a sample error calculation using the error formulae just developed. The conditions for this sample calculation are as follows:

$W = 0.947$ m/s

$x_1 = 0.05$ m

$x_2 = 0.10$ m

$T = 28^{\circ}$C

$V_{t_1} = 488815$

V_{t_2} = 204480

V_{t_3} = 213251

these give the following:

ρ = 997.95 kg/m^3

dP_v = 74.86 Pa

dW = 0.079 m/s

so that,

$$\frac{dW}{W} = 8.4\% \qquad \text{(maximum error)}$$

By looking at Eqn. C.14 one can reasonably see the general size of the error in the velocity measurements. The difference, $V_{t_2}-V_{t_3}$ does not contribute significantly to the error since it is multiplied by such a small number. Since all of the primary sensing element errors were absolute the error formula is quite simple and the error is really only a function of the x_1/x_2 ratio. The contribution of the density error is also very small. The x_1/x_2 ratio is the same as for the sample calculation everywhere but at the inlet plane where the positioning of the static taps gives x_1/x_2 = 2. this would yield an error of 16% if used in the above example (from an absolute error of 0.15 m/s).

From this it can be stated that the maximum absolute error in the velocity measurements is approximately 0.08 m/s everywhere but at the inlet plane where it is 0.15 m/s.